Hyporheic exchange inside a flat gravel bed, flume experiments and modelling.

Author: Arno Slager

Student number: 3345912

Supervisor: Marcel v.d. Perk

Study: Coastal Dynamics and Fluvial Systems

Universiteit Utrecht

Index

List of figures

List of tables

Abstract

The aim of this research is to gain more understanding on the parameters that affect hyporheic exchange. Hyporheic exchange is a diverse process, in which many different parameters affect the hyporheic flow paths and residence times. Literature research has showed that hyporheic exchange is in most cases mainly dependant on the channel morphology, the sediment characteristics of hyporheic zone and the flow velocity of the stream. Many other factors also affect hyporheic exchange, such as lateral groundwater inflows and natural obstructions. The diversity of all of these factors makes it hard to predict hyporheic exchange through models. The advective pumping model has shown that it is able to predict exchange due to bedforms well. This contributed to different studies, which allowed the prediction of vertical hyporheic exchange fluxes. But lateral hyporheic exchange fluxes still can not be predicted.

Flume experiments were conducted at the Quesnel River Research Centre (QRRC) in Likely, BC, Canada, to provide more insight on the pattern of hyporheic exchange. EC-meters were placed inside a flat gravel bed with a d50 of 25.28 mm for the top layer, and 22.90 mm for the bottom layer. Experiments were performed with different flow velocities and water levels. These experiments showed the irregularities in hyporheic exchange in a heterogeneous gravel bed and provided some insight in the pattern of hyporheic exchange. To further investigate some of the unknown variables, an advection-diffusion model was made. By means of this model, the effects of variations in flow velocity and water level were studied.

The following conclusion were made:

- An increase in flow velocity results in smaller residence times, and an increase in water level results in larger residence times.
- Water level has a relatively large impact on the reach of the hyporheic exchange into a flat gravel bed.

1. Introduction

In many streams, significant amounts of water are exchanged between water-saturated sediments surrounding the open channel (the hyporheic zone) and the channel itself (Findlay, 1995). These exchanges are so-called hyporheic exchange flows (fig. 1). They create a zone of pronounced biogeochemical gradients, where various key processes occur, which are of concern to hydrologists, ecologists, and biogeochemists (Cardenas, 2009). These key processes include river metabolism (Battin et al., 2008), fate and uptake of contaminants (Ren and Packman, 2005), distribution of microfauna (Feris et al., 2003) and macrofauna (Arscott et al., 2005), and heat transport (Cardenas and Wilson, 2007; Burkholder et al., 2008; from Cardenas, 2009). Hence, it is important to understand the mechanisms of hyporheic exchange in order to analyse the transport and fate of environmentally important substances such as nutrients, carbon, and toxic contaminants in watersheds (Wörman et al., 2002). Currently, there is still uncertainty about the relationship between stream conditions, hyporheic exchange fluxes, and the overall transport of ecologically relevant substances (Jones & Mulholland, 2000; Hall et al., 2002). Numerous studies investigated the basic hydrodynamic processes that are responsible for hyporheic exchange (Packman and Salehin, 2003) to get a better understanding of hyporheic exchange.

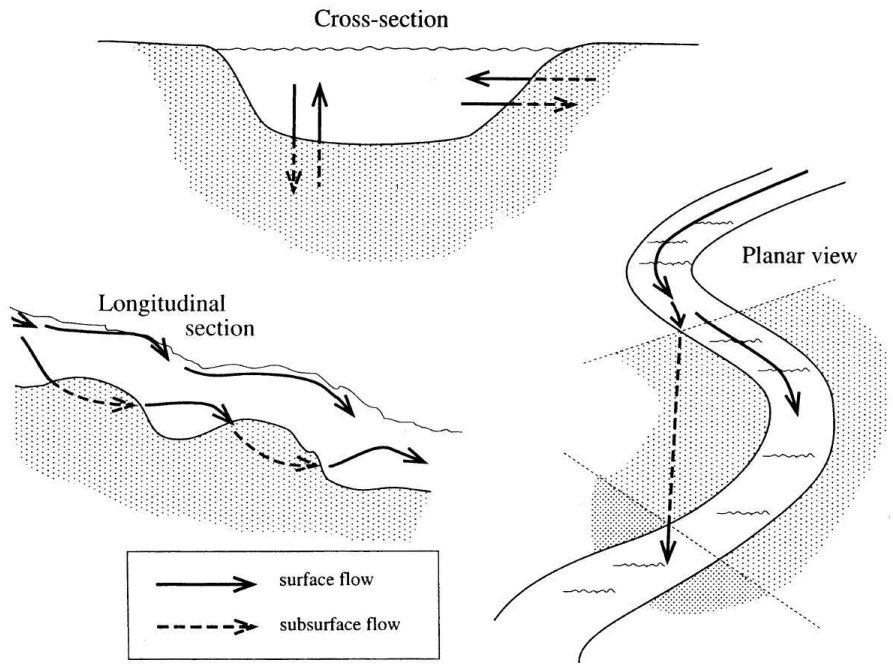

Figure 1, most common pathways of hyporheic exchange flow (Findlay, 1995).

The aim of this study is to gain more understanding on the impact of changes in flow velocity and water depth on the rate of hyporheic exchange.
The main research question is:

- What is the effect of changes in water depth and flow velocity on the residence times of hyporheic exchange in a flat gravel bed?

To obtain more knowledge about hyporheic exchange, first a literature research was carried out. In chapter 2, the parameters which affect hyporheic exchange are presented. Second, various models will be evaluated to determine if there are appropriate models that simulate hyporheic exchange (chapter 3).

To further investigate hyporheic exchange, controlled flume experiments were carried out, which were subsequently simulated using an advection- diffusion model. In chapter 4 the experimental and model setup are presented. In chapter 5 the experimental and model results are presented and discussed and residence time analyses of the results are presented and discussed. In chapter 6 the main conclusions are summarized.

2. Hyporheic exchange factors

While determining which parameters influence the hyporheic exchange flow, recent studies evaluated numerous parameters, such as discharge, flow velocity, morphology and sediment characteristics. All of these parameters affect the hyporheic exchange flow, but how large the effect of the parameters is on hyporheic exchange flows differs for each channel. Also relative differences between parameter values change the effect of the parameters on the hyporheic exchange flow. To get a better understanding of the factors that affect hyporheic exchange flows, the main findings of previous studies are discussed below.

2.1 Discharge

The discharge of a stream is a parameter which can either be, very important, irrelevant or something in between, for hyporheic exchange. The degree of importance of discharge to hyporheic exchange, depends on the characteristics of the channel through which the discharge flows. Wondzell (2006) has three mechanistic explanations for this:
- Changes in pressure field
- Changing patterns of groundwater inflows to the river channel
- Changes in the effective morphology of the stream channel

2.1.1 Changes in pressure field

Laboratory experiments (Thibodeaux and Boyle, 1987; Elliot and Brooks, 1997a; Packman and Bencala, 2000; Vollmer et al., 2002) show that the distance to which stream water penetrates into the streambed and the amounts of hyporheic exchange flow increase when the discharge increases. This is caused by changes in pressure differences between regions of high and low pressure (Wondzell, 2006). When the discharge increases, flow velocity increases, thereby increasing the pressure differences between regions of high and low pressure. This results in increased hyporheic exchange. The problem with these findings is the application to real-world systems, since the flow conditions in flumes with sand and gravel beds are different from the flow conditions in for example headwater mountain streams with cobble and boulder beds (Wondzell, 2006). However, an increase in discharge will most likely still increase the flow velocity, thereby increasing the hyporheic exchange.

2.1.2 Changes in lateral groundwater inflows to the river channel

Rates of lateral groundwater inflows are controlled by soil moisture content, precipitation (or snowmelt) inputs, and area of the hillslope draining directly to the valley floor (Wondzell, 2006). When the rates of lateral groundwater inflows increase, the water table rises and cross-valley gradients increase, turning flows more laterally across the floodplain (Wondzell and Swanson, 1996; Storey et al., 2003; Shibata et al., 2004). This causes an increase in cross-sectional area of the channel, which slightly increases the amount of lateral groundwater inflow again. Increases in lateral groundwater inflows can significantly alter the slope of the water table, forcing exchange flow paths closer to the stream or even eliminate them, as reported by Harvey and Bencala (1993) for St Kevin Gulch, by Wroblicky et al. (1998) for Rio Calaveras and Aspen Creek, and by Shibata et al. (2004) for the Karuushinai River (Wondzell, 2006). An increase in lateral groundwater inflows also increases the discharge, since more water is flowing through the channel. But the relative influence of the lateral groundwater inflows to the hyporheic exchange flow depends on the amount of groundwater inflow relative to the magnitude of the discharge. When the lateral groundwater inflow is relatively small compared to the discharge, the influence of the lateral groundwater inflow will be small, and when the lateral groundwater inflow is relatively large compared to the discharge, the influence of the lateral groundwater inflow will be large.

2.1.3 Changes in morphology of the stream channel

Changes in stream discharge alter the sediment dynamics in a stream. If this happens in a way that the morphology of the channel changes, a change in discharge can alter the hyporheic exchange flows. For example, a flat gravel bed river has a constant discharge, which is not able to move sediment. When the discharge increases in such a way that it can start to move sediment and form bedforms, this creates pressure differences in the stream, which can enhance hyporheic flow. This process will be discussed in further detail in chapter 2.3.

2.2 Sediment characteristics

Hyporheic exchange experiments have been used to study the hyporheic exchange flow in various environments, using different sediments sizes, combined with either homogeneous or heterogeneous hyporheic zones. In general, the main factor of influence concerning the sediment bed is the hydraulic conductivity of the alluvium which surrounds the water in the

channel. Storey et al. (2003) studied hyporheic exchange flows on a riffle-scale, and determined that hyporheic exchange flows are only possible when the materials surrounding the stream channel are highly permeable ($K > 10^{-5}$ m/s). In a catchment with moderate- to low-permeability ($K = 10^{-6}$ to 10^{-8} m/s), hyporheic exchange flows can also exist, but only when the stream is surrounded by a zone of alluvial deposits. A heterogeneous bed has a varying hydraulic conductivity, which causes additional variability in flux across the stream-subsurface interface and the development of preferential subsurface flow paths (Salehin et al., 2004). Salehin et al. (2004) also determined that heterogeneity (compared to homogeneity) produces greater average interfacial water flux, less vertical solute penetration, and a shorter mean hyporheic residence time. These effects should generally be seen in natural streams, since most natural streams are heterogeneous.

2.3 Morphology

Laboratory experiments on hyporheic exchange flow are often carried out in straight flumes, and sometimes even with a flat sediment bed. In reality however, stream channels have all kinds of shapes and forms. This so-called channel morphology is controlled by the balance between sediment supply and sediment transport capacities in the channel (Montgomery and Buffington, 1997). Morphology plays an important role in controlling hyporheic exchange flow (Kasahara and Wondzell, 2003). The first signs for this, were identified when studies began to use numerical groundwater flow models (Kasahara and Wondzell, 2003; Cardenas et al., 2004; Gooseff et al., 2006) to calculate hyporheic exchange.

Kasahara and Wondzell (2003) found that the control of surface-visible valley-floor and channel morphologic features on hyporheic exchange flow differed significantly with stream size and channel constraint (in the mountain stream reaches they examined). These differences reflected the dissimilarity of channel morphology among the streams they examined, that control both the amount and residence time of hyporheic exchange flows (Kasahara and Wondzell, 2003).

Cardenas et al. (2004) studied the effects of heterogeneity, bed form configuration, and river bends on hyporheic flow. They found that these factors all have a significant influence on

subchannel hyporheic processes, in particular on hyporheic zone geometry, fluxes, and residence time. Since the relative importance of these factors is dynamic, insight in these factors is important for a good understanding of hyporheic exchange.

Gooseff et al. (2006) found that longitudinal stream geomorphologic bedform scaling and channel unit sequence both control hyporheic exchange patterns along the river continuum, which corroborated with the results of Kasahara and Wondzell (2003).

A more recent study by Tonina and Buffington (2007) used a different approach. They presented a three-dimensional modification of the pumping exchange model of Elliott and Brooks (1997b) to predict the hyporheic flow in gravel pool-riffle channels, in which bed topography variations are captured and the observed pressure profile at the bed surface drives hyporheic flow. The modelled results showed agreement with the measurements, suggesting that hyporheic exchange is predominantly driven by bed form-induced advection, which is influenced by discharge and relative submergence of the bed form into the bed. Bed forms affect both the near-bed pressure and the surface area which is available for hyporheic exchange at a certain flow. However, the primary finding of Tonina and Buffington (2007) was that bed form-induced was not dominating hyporheic exchange, but that there is a complex interaction between discharge and bed form topography that drives flow regime and the consequent magnitude and pattern of hyporheic exchange.

3. Hyporheic exchange models

A variety of models have been developed and applied to analyse hyporheic exchange. The most commonly used model is the Transient Storage Model of Bencala and Walters (1983), where hyporheic exchange is formulated as a first-order mass transfer with the exchange defined by two parameters: an exchange coefficient and a storage zone depth or area (Wörman et al., 2002). The Transient Storage Model yields an exponential probability density function of the return times of the exchanged solute mass from the storage zone and conveniently represents the "tailing" in concentration seen after the passage of a solute pulse (Wörman et al., 2002). The mass transfer exchange rate coefficient (units of inverse time) represents the timescale of the transient storage. However, since there is often natural

variability in hyporheic exchange, the model usually has to include multiple exchange rates (Choi et al., 2000).

It is now known that transient storage is largely controlled by advection into and out of the hyporheic zone (Wörman et al., 2002). These advective flows induced by irregularities on the bed surface create local vertical exchange (Thibodeaux and Boyle, 1987; Elliott and Brooks, 1997a). Fundamental exchange models based on this so called "pumping process" have successfully predicted the hyporheic exchange observed in laboratory flume experiments, such as those of Elliott and Brooks (1997b) and Packman et al. (2000a). Wörman et al. (2002) developed a model that uses advective pumping theory to analyse solute transport in natural streams. This model was successfully applied to improve the interpretation of the results of recent field tracer experiments (Johansson et al., 2000; Jonsson and Wörman, 2000; Salehin et al., 2003). Recent studies can even predict the vertical hyporheic fluxes and residence times (Cardenas and Wilson, 2007; Wörman et al., 2007), but lateral hyporheic fluxes, typically induced by channel sinuosity (Boano et al., 2006; Cardenas, 2008), still can not be predicted (Cardenas 2009).

There are several papers which describe the theory of hyporheic exchange models. Most use groundwater models to describe the flow paths through the hyporheic zones. The pumping process exchange model of Elliott and Brooks (1997a) was one of the first models to succesfully predict hyporheic exchange, based on the principle of advective flows, induced by bedforms. Wörman et al. (2002) adapted the model of Elliott and Brooks, by suggesting a formulation for the residence time of solutes in the hyporheic zone that is based on knowledge of hyporheic flow dynamics. This created a better understanding of hyporheic exchange flows, hereby allowing generalization of experimental results. So the theory of hyporheic exchange as described by Wörman et al. (2002) is presented here to obtain a better understanding of the hyporheic exchange flows.

Wörman et al. (2002) tested different solute residence time distributions, since there are several processes and conditions that can induce a hyporheic exchange flow. These different processes and conditions are expected to produce different distributions of subsurface retention times. For example, hyporheic exchange flows can occur in streams with spatially varying slope (Harvey and Bencala, 1993; Castro and Hornberger, 1991) or in a meandering river that has different flow direction in relation to that of the groundwater flow (Wroblicky et al., 1998). Irregularities on the bed surface can also induce hyporheic exchange flow, due to pressure variations along the bed surface. The most common irregularities are bedforms. Additional irregularities can be formed by obstacles like tree branches or stones, or even by biotic processes (Huettel et al., 1996). All of these irregularities create pressure differences at the channel bed, bringing about hyporheic flow paths. Generally these obstructions will produce a high-pressure region on the upstream side of the obstruction, where the water and solutes enter the bed, and a low pressure region on the downstream side of the obstruction, where the water and solutes exit the bed and enter the stream. This process is known as the pumping process.

All of the hyporheic exchange flows discussed above are similarly defined, since they are defined by a distribution of travel times that is caused by a spatially periodic variation of hydraulic head along the stream boundary (Wörman et al., 2002). The subsurface flows follow the continuity equation, and when the permeability of the hyporheic zone is low enough, Darcy's Law. These equations can be solved by using the exact boundary conditions of specific cases, but Wörman et al. (2002) used a general approximation, which assumed that the bed surface is flat, the sediment is homogeneous, and the distribution of pressure head along the bed is sinusoidal. The assumption of a flat bed surface and a sinusoidal distribution of pressure head seems a bit contradictory, since a sinusoidal distribution of pressure head is only present in streams with certain bed forms. The sinusoidal distribution can be accepted since the particles on the bed create enough pressure differences for a sinusoidal distribution to exist. The smaller the particles, the smaller the scale of such a distribution will be.

Advective pumping exchange is characterized by a pore water velocity field V(x, y). The infiltration velocity into the bed in the direction of the streamlines is given by $V_z(T, \tau)|_{t=0}$ (m/s) and the exfiltration velocity out of the bed in the direction of the streamlines is given by $V_z(T, \tau)|_{\tau=T}$ (m/s), where z denotes a curve-linear coordinate along the hyporheic flow path. These velocities are defined as Darcy velocities (the product of the pore water velocity and

bed porosity), and the exfiltration is defined by a residence time, τ(s) ($0 < \tau < T$), where T (s) is the total residence time due to transport along an individual hyporheic exchange flow path. The dissolved solute exchange rate per unit bed surface area is the product of the component of the hyporheic exchange velocity perpendicular to the bed surface and the dissolved solute concentration in the stream water , c_d (kg/m^3).

With this framework, the net solute mass flux (kg) in the dissolved phase in the stream water can be found by integrating over the distribution of transport pathways:

$$J_s = 1/2 \int_0^\infty f(T)\, \xi\, P/A\, (- V_z(\tau, T)|_{\tau=0}\, c_d + |V_z(\tau, T)\, g_d)|_{\tau=T})\, dT \qquad (1)$$

where g is solute mass per unit volume of water in the hyporheic zone (kg m^{-3}), f (T) is the probability density function (PDF) of T weighted by the velocity component normal to the bed surface, V_n (m/s), P (m) is the wetted perimeter, A (m^2) is the cross-sectional area of the stream, and ξ is an area reduction factor equal to V_n/V_z that accounts for the fact that the streamlines are not necessarily always perpendicular to the bed surface. The introduction of V_z and ξ simplifies the forthcoming analysis because $\int_0^\infty V_n(T)/V_z(T) f(T\, dT$ has been found to be close to constant and V_z varies only little along the bed. Hence, V_z and ξ are both treated as constants. The first term of the right-hand side of (1) is due to the flow of solute into the bed, and the second term represents the flow of solute out of the bed. The factor 1/2 in the flux expression is introduced because half of the bed is subjected to infiltration and the other half to exfiltration. The term Vz/2 can be interpreted as an effective exchange velocity. Solute transport in the stream can be coupled with the hyporheic exchange flux by writing a mass balance for solute in the stream:

$$\partial c_d/(\partial t) + 1/A_T\, \partial(AUc_d)/(\partial x) - E\, \partial^2 c_d/(\partial x^2) = J_s \qquad (2)$$

where A_T (m^2) is the cross-sectional area of the main stream including side pockets, A (m^2) is the cross-sectional area of the main stream excluding side pockets, U is the flow velocity in the main stream (m/s) ($Q = UA$), Q is the discharge (m^3/s), and E is the main stream dispersion coefficient (m^2/s). The effective flow velocity in the main stream channel corrected for side pockets with stagnant water is given by $U_e = Q/A_T$ (Wörman, 1998).

With equations (1) and (2) solute breakthrough curves in the stream can be calculated from in-stream transport parameters and the residence time distribution of solutes in the subsurface. These two equations essentially define the overall hyporheic exchange model. But this model is not applicable to all cases, due to the general approximation, which assumed that the bed surface is flat, the sediment is homogeneous, and the distribution of pressure head along the bed is sinusoidal. However, the assumptions of a flat surface and sinusoidal pressure variation can be used to derive important insights into the relationship between state variables, exchange velocities, and the residence time distribution. With the scale variables suggested by Elliot and Brooks (1997b) and Packman et al. (2000b) where the dimensionless velocity $V_z^* = (V_z\lambda)/(2\pi K h_m)$, the dimensionless time $t^* = 4\pi^2 (tKh_m)/\lambda^2$, and the streambed depth is scaled with the bed form wavelength, we can express the flow field as a unique function of two parameters, d_b/λ and u^*_{adv}/V_z^* ($x = 0$, $z = 0$), where λ (m) is the wavelength of the pumping pressure distribution, K is the hydraulic conductivity (m/s), h_m (m) is the maximum pressure head due to pumping, d_b (m) is the mean depth of the hyporheic zone (corresponding with the location of an impermeable boundary), and u_{adv} (m/s) is the longitudinal velocity of the underlying groundwater flow. Wörman et al. (2002) calculated the probability density function for the residence time distribution (T-PDF) of a solute as a function of d_b/λ, by employing both numerical ‘‘particle tracking’’ simulations and the pumping exchange model (fig. 2).

Wörman et al. (2002), used this residence time distribution to show that hyporheic zones of increasing depth are dominated by larger residence times, until $d_b/\lambda > 1.0$. Also the longitudinal groundwater flow induced by the mean stream slope does not have a significant effect on the residence times for typical stream conditions [Packman et al., 2000a]. This could be used to create a good approximation for the residence time in the range of $0.3 < d_b/\lambda < 1.0$:

$$\int_0^\infty f(T)\, T^*\, dT = 4\pi^2 \int_0^\infty f(T)\, T\, dT\, Kh_m/\lambda^2 = 21\, d_b/\lambda \qquad (3)$$

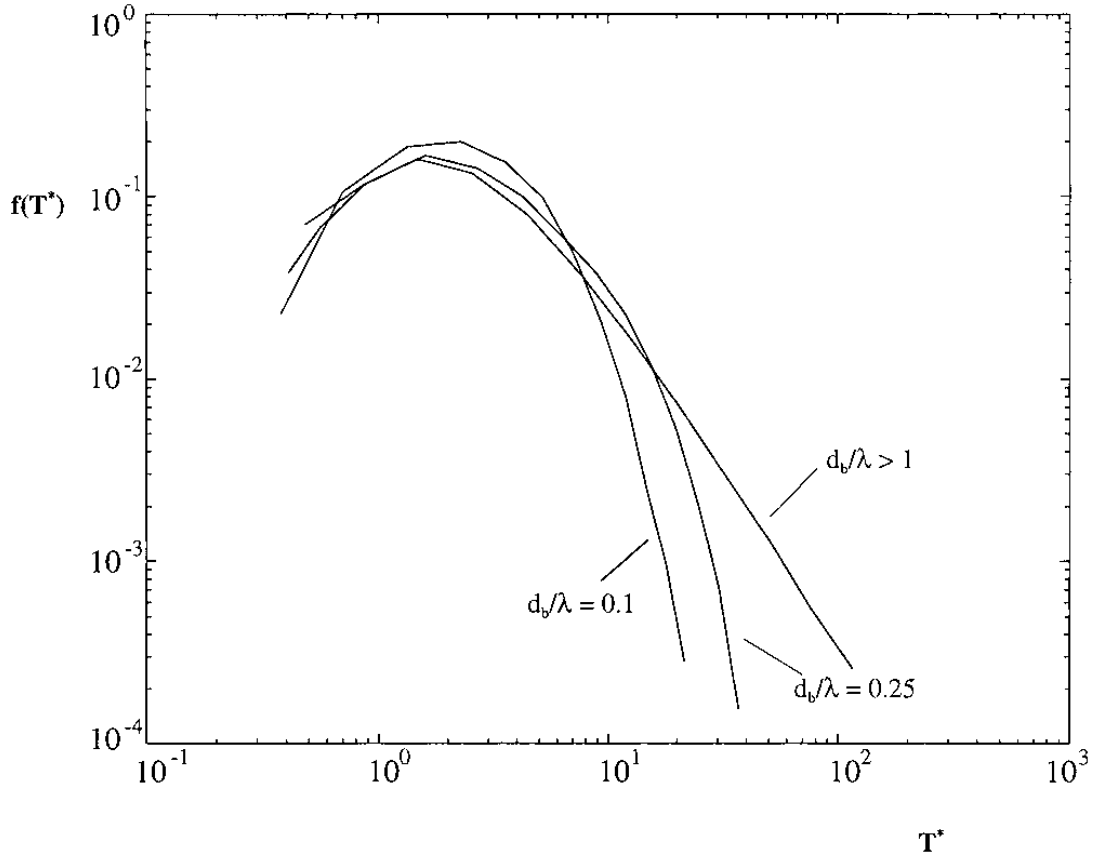

Figure 2, residence time PDF's associated with the flat boundary approximation and a sinusoidal pressure variation. The probability density function is weighted by discharge (Wörman et al., 2002).

For larger values of d_b/λ the dimensionless residence time is approximately constant, ${}_0\int^{\infty} f(T)\, T\, dT \approx 25$. The exchange velocity normalized in the form $E[V_z|_{z=0} / \max(V_z|_{z=0})]$ was found to be practically constant along the bed; for stagnant groundwater the exchange velocity value varied from 0.84 when $d_b/\lambda = 0.1$, to 0.98 when $d_b/\lambda = 2.0$. A good approximation of the exchange velocity is given by:

$${}_0\int^{\infty} f(T)\, V_z\, dT|_{z=0} = (2\pi K h_m)/\lambda \qquad (4)$$

The corresponding area reduction factor ξ was evaluated as ${}_0\int^{\infty} f(T)\, V_n/V_z\, dT$ and was found to be fairly constant, $\xi \approx 0.79$ for $0.3 < d_b/\lambda$.

The variation of the velocity along the travel paths was quantified in terms of $E[V_z|_{mid}/V_z|_{z=0}]$, where the subscript ‘‘mid’’ indicates a position exactly in the middle of the travel path. If the groundwater advection is zero, this ratio assumes a lowest value slightly below 0.7 for db/l > 0.5 and approaches unity as d_b/λ decreases below 0.5.

The residence time PDF of the pumping exchange model resembled a log-normal distribution. Although multiple residence time functions were tested by Wörman et al. (2002), the log normal PDF was determined as the best approximation. It provided the best representation of the observed breakthrough curves and the residence time distribution of solute in the storage zone.

The residence time distribution of solutes in the hyporheic zone does not uniquely define the rate of solute mass exchange between the stream and the hyporheic zone, since the exchange rate also depends on the accumulation capacity of the hyporheic zone or on the magnitude of the hyporheic exchange velocity (Wörman et al. 2002). The exchange velocity was introduced in (1), which was used for the transport equations of the hyporheic zone. For a nonreactive solute, mass conservation arguments yield:

$$\partial g_d n/(\partial t) + 1/A_t \, \partial A_t V_z g_d/(\partial z) = 0 \qquad (5)$$

where n is the porosity, $1/A_t \, \partial A_t/(\partial x)$ reflects a relative divergence (m^{-1}) of an imaginary flow tube with a cross-sectional area At (m^2), and g is the dissolved solute mass in the bed per unit volume of pore water (kg/m^3). As boundary condition at inflow locations, the dissolved phase concentration is continuous at the streambed interface:

$$g_d \, (z = 0, t) = c_d \, (x, t) \qquad (6)$$

Consideration of advective transport along hyporheic flow paths allowed Wörman et al. (2002) to analyse the effect of different types of T-PDFs on solute breakthrough in the stream. When only a single residence time is used, the solute that enter the hyporheic zone will travel along the hyporheic flow paths for a definite time $_0\int^\infty f\,(T)\,T\,dT$ and give rise to a series of peaks with a period $_0\int^\infty f\,(T)\,T\,dT$. When a uniform or exponential distribution of travel times is used, the peaks are smoothed out.

This causes the solute breakthrough in the stream to be strongly dependent on the form of the T-PDF for hyporheic exchange. Also observed breakthrough curves can provide information about the residence time distribution of solutes in the hyporheic zone and the underlying exchange processes.

Wörman et al. (2002) also created methods to solve the Advective-Storage-Path (ASP) model: All parameters except discharge are assumed to be constants along subreaches of the stream. The volumetric rate, Q = UA, is assumed to vary linearly along each subreach according to $Q/Q_0 = (1 + \theta x)$, where Q_0 is the upstream flow rate, Q is the downstream flow rate and θ is a proportionality coefficient. For such a discharge variation the problem could be solved in the Laplace domain, following similar steps as those of Maloszewski and Zuber (1990) as showed by Forsman (2000).

On the assumption that there is a symmetric flow field in the sediment bed, the variation of At and Vz along the travel path is not important to the concentration at the end of the path (i.e., at t = T). So the solution to (5) and (6) becomes: $avg(g_d) = avg(c_d(x)) \exp(-st)$, where a Laplace transform of an arbitrary function u is defined as $avg(u) = {}_0\int^\infty ue^{-st}\, dt$, s is an arbitrary real number, and $\tau = z/(V_z/n)$. This gives the source/sink expressed by (1) in a simple manner that allows inclusion of additional diagenetic processes if required. Provided a unit Dirac pulse at the upstream boundary, zero initial concentration elsewhere ($g_d(t = 0) = c_d(t = 0) = 0$), and an infinite stream, the solution $avg(S_D)$ to (1) and (2) becomes:

$$avg(S_D) = avg(c_T)/(M/Q) = (1 + \theta x)^{-1} \exp [x(Q/(2EA_T) - ((Q/(2EA_T))^2 + s/E - {}_0\int^\infty f(T)\, 1/2 \xi PV_z/(AE)\, (e^{-sT} - 1)\, dT)^{1/2})] \quad (7)$$

where M is the total solute mass injected at x = 0. Since the transport along each travel path in the hyporheic zone are assumed to be independent, the averaging ${}_0\int^\infty f(T) \ldots dT$ reflected by the integral in (1) is readily performed for any know form of f (T) after the derivation of (7). Since S_D is the solution at a section x due to a unit Dirac pulse introduced at the boundary, the concentration at a section x for a temporal variation of the boundary concentration, G_{BC} (kg/m^3), is given by the following convolution operation:

$$G_x(t) = {}_0\int^t S_D(t-\tau)\, G_{BC}(\tau)\, d\tau \quad (8)$$

If the Peclet number (ux)/E is sufficiently large, the solution can be used as a boundary condition for the next downstream reach. So the solution can be found stepwise, by substituting $G_{BC} = G_x$ before (8) is used to calculate a new G_x for the next reach.

Since the Laplace transform is a moment-generating function, the temporal moments of the breakthrough curve can be easily derived by repeated derivation of (8) with respect to sand evaluating the result for s = 0 (Wörman, 2000).

Although the theory of Wörman et al. (2002) is applicable to the most typical cases, for some cases this is a theory which will not result in a good approximation of the measurements. Packman and Salehin (2003) found that the exchange in a gravel bed can be significantly enhanced relative to that in a sand bed due to turbulent interactions, direct coupling of stream and pore water flows can produce significant exchange in gravel bed sediments (Nagaoka and Ohgaki, 1990). Packman and Salehin (2003) compared hyporheic exchange in gravel beds with and without bedforms, and found that net exchange would often be the result of both advective and diffusive processes. Advective flow patterns were observed even when the bed was flat. The small variations on the bed surface most likely created pressure variations on the bed surface, which created advective flow patterns. But hyporheic exchange flow in gravel stream beds is so complex, that no theory that can predict hyporheic exchange in terms of stream and bed parameters in gravel stream beds exists. Zhou and Mendoza (1993) theorized that the larger pore spaces in gravel admits the penetration of considerable stream-driven turbulence into the bed, which causes a non-Darcy slip velocity at the bed surface and an exponentially decreasing flow in the bed. But without a good theory, the bulk solute exchange can only be modelled with an effective diffusion coefficient. When there is initially a tracer concentration C_0 (kg/m^3) in the stream and no tracer in the subsurface, this exchange flux is given by:

$$J = C_0/\pi(D_{eff}/t)^{1/2} \qquad (9)$$

where D_{eff} is the effective diffusion coefficient (cm^2/s) (Packman and Salehin, 2003).

4. Methods

4.1 Experimental setup

A series of flume experiments was carried out at the Quesnel River Research Centre (QRRC) in Likely, BC, Canada. The QRRC is a research centre of the University of Northern British Columbia (UNBC). The flume was approximately 80 m long, but only 39.25 m of this length was used. The width of the flume was 2.005 m. The flume was filled with approximately 30.0 cm of gravel with a D50 of 25.28 mm for the top layer, and a D50 of 22.90 mm for the lower layer. The D50 was calculated after measuring the width, length and height of about 200 stones for the top layer, and 200 stones for the bottom layer. Near the concrete bottom of the flume a layer of course sand was present of approximately 0.5 cm, which could not be flushed out. A flat bed was used, and the slope of the concrete floor of the flume was approximately 1%. To raise the water level during the experiments, a weir was used. A small weir and a large weir were used. The heights of these weirs were 63.5 cm for the large weir and 46.7 cm for the small weir. For experiment 1 and 2 the large weir was used, and for experiment 3-8 the small weir was used. Pumped up groundwater was used for the experiments, which was first aerated in the local pump house, to add oxygen to the groundwater. The maximum discharge was 75 L/s or 0.075 m^3/s, which could be lowered with a valve. The discharge was determined by the amount of time it took for a bucket of 52.2 L to fill up. The average flow velocity was calculated with the discharge, $u = Q/A$ in which u = flow velocity (m/s), Q = discharge (m^3/s), and A = area (m^2). To determine the EC-value during the experiments, an EC-meter was used with 4 boxes, which had 4 probes each. The probes measured the EC-value every 10 seconds, and stored this data on the laptop they were connected to. The four boxes were placed in a longitudinal line, and for each box the four probes were placed in a vertical line (table 1). The first probe was placed approximately 5.0 cm above the sediment, and last three probes were placed respectively 5.0 cm 15.0 cm and 25.0 cm beneath the sediment bed.

In total, 4 sets of experiments were used for this study. Each set of experiments contained a flush out experiment followed by an injection experiment. The setup for these 4 sets of experiments is given in table 2. At the injection experiment, first the valve was opened, then after a steady flow condition was reached, a bucket filled with salt water was emptied into the

flowing water at the most upstream part of the flume, after which the EC-meter measured the changes in EC-value. For the flush out experiments the flume was filled with water. After the flume was filled with groundwater, the EC was raised to a value of 800-1200 µS/cm, by distributing buckets with salt water and mixing the water to ensure the salt was homogeneously distributed in the entire flume. The valve was then opened and the EC-values were measured by the EC-meter, until they were back to their original value. Since the temperature changed throughout the experiments, a reference temperature of 25 °C was used. The EC-values were corrected to values that correspond with a temperature of 25 °C.

$$Cref = C/(1+(Tcc/100)*(T-Tref)) \quad (10)$$

$$Tcc = (1/Cref)*((C-Cref)/(T-Tref))*100 \quad (11)$$

In which, T is the measured temperature (°C); Tref is the reference temperature (°C); C is the measured electrical conductivity (µS/cm); Cref (µS/cm) is the electrical conductivity of the water at Tref; and Tcc is the Temperature correction coefficient, which was calculated from lab data.

Table 1, probe placement at the outdoor flume

Distance from water pump	**14 m**	**18.5 m**	**23 m**	**27.5 m**	
					Distance from sediment bed
Probes	**Distance from concrete bottom flume**				
1	36.cm	34.0 cm	34.0 cm	35.0 cm	+ 5.0 cm
2	26.0 cm	24.0 cm	24.0 cm	25.0 cm	- 5.0 cm
3	16.0 cm	14.0 cm	14.0 cm	15.0 cm	- 5.0 cm
4	6.0 cm	4.0 cm	4.0 cm	5.0 cm	- 5.0 cm

Table 2, experimental characteristics during the flush out and injection experiments

Experiments	**Discharge (m3/s)**	**Avg. flow velocity (m/s)**	**Avg. water level (m)**
1 & 2	0.0738	0.1207	0.305
3 & 4	0.0729	0.1817	0.200
5 & 6	0.0443	0.1263	0.175
7 & 8	0.0097	0.0275	0.140

4.2 Model setup

It is generally assumed that Fickian diffusion theory can be applied to the dispersion processes in rivers (Csernuszenko, 1987). Following this assumption, an advection diffusion equation was used for the base of the model, since advection and dispersion are the two driving processes in hyporheic flow.
The general advection diffusion equation states:

$$\partial C/\partial t = D_x * \partial^2 C/\partial x^2 + D_y * \partial^2 C/\partial y^2 - u_x * \partial C/\partial x - u_y * \partial C/\partial y \quad (12)$$

In which, D_x = longitudinal diffusion coefficient (m^2/s), D_y = vertical diffusion coefficient (m^2/s), u_x = average flow velocity in the x-direction (m/s), u_y = average flow velocity in the y-direction (m/s) and C = concentration of a solute (kg/m^3). For this model, only the x component of the flow velocity (u_x) was used, to avoid the complexity of the mass balance equation, which will be incorrect if both u_x and u_y would be used.
The vertical dispersion was calculated with a vertical dispersion coefficient, which was assumed to decrease exponentially with depth, just like flow velocity in gravel beds in turbulent streams (Zhou and Mendoza, 1993; Habel et al., 2002). The formula for this vertical dispersion coefficient (vdc) is:

vdc(yn) = vdc0*(exp(-b*(7-yn))) (Van der Perk et al., 2011), (13)

in which, b (beta) is a variable, 7-yn represents the depth in the sediment and vdc0 represent the vertical dispersion coefficient at the bed. The vertical dispersion coefficient at the sediment bed was determined by Jobson and Sayre (1970) as vdc0 = 0.067*0.3*u_{sh}*0.5, in which u_{sh} = shear velocity (m/s). Since this dispersion coefficient was too high for the experiments that were carried out, z (zeta) was introduced to simulate the effect of a change in the vertical dispersion coefficient at the sediment bed:

vdc0 = 10^(-z)*0.067*0.3* u_{sh}*0,5 (14)

in which, z (zeta) is a variable, and u_{sh} (shear velocity) = $(g*h*I)^{0,5}$; in which, g is the gravitational acceleration coefficient (m/s^2), h is the water depth (m), and I is the gradient.

For the longitudinal dispersion coefficient (ldc) in the sediment, beta was used to reduce the longitudinal dispersion when getting deeper into the sediment:

$ldc(yn) = ldc_w*(exp(-b*(7-yn)))$ (Van der Perk et al. 2011), (15)

in which ldc_w = the longitudinal dispersion coefficient in the water column, as described by Fischer et al. (1979):

$ldc_w = 0.11*u^{2.0} * w^{2.0}/(h*u_{sh})$ (16)

in which u = flow velocity (m/s), w = width (m), h = water depth (m) and u_{sh} = shear velocity.

A similar formula as formula 13 is used for u_{sed} (flow velocity in the sediment; m/s):

$u_{sed}(yn) = u_{sed}0*(exp(-b*(7-yn)))$ (Van der Perk et al. 2011), (17)

in which, $u_{sed}0$ = phi*u; in which phi is a constant of approximately 0.5625; Phi was derived from the findings of Zeng and Li (2012).

For the water column the vertical dispersion coefficient was set to 0.
A grid was designed to represent the flume. The yn ranges from 1-13, where each ystep represented 0.0504 m. The xn ranged from 1-61, where each x-step represented 0.50 m. This represented a 30 m long and 0.605 m deep flume. The flat gravel bed was represented with yn = 1-7, and xn = 1-61. The water column was represented with yn = 8-13, and xn = 1-61. The concentration in the water was assumed to be approximately the same for the entire water column. Because of this assumption, this grid was used for all the experiments. To account for the fact that the water column changes in size for the different experiments, the variable water depth was changed for every experiment, instead of changing the entire grid. This simplified the modelling considerably, while keeping the variables which changed with water level correct.
The initial concentration was set to 1.0 at the start of the model. After 1 second the concentrations at xn = 1 were set to 0.0 for the entire model run. This represented the fresh water flowing into the flume. For every timestep, and at every coordinate (x, y), the new concentration was calculated. To calculate the concentration for a next timestep, first the x-

contribution of the dispersion was added to the concentration of the current timestep, secondly the y-contribution of dispersion was added, and finally the x-contribution of the flow was subtracted (equation 12).

The flow paths make turns inside the sediment to pass the gravel, and the water can only flow through the pores, which results in a reduction in flow velocity and dispersion when getting deeper into the sediment (Zhou and Mendoza, 1993; Habel et al., 2002). To account for this reduction, the flow velocity and dispersion coefficients in the x- and y-direction are all dependent on their distance beneath the bed as shown in formula's 13,15 and 17. The variable "beta" in these formulas accounts for the rate of decline in dispersion and flow velocity with depth.

For an example of the model script, see appendix 3.

4.3 Model calibration

To study the effects of changes in water level and flow velocity on the residence times of hyporheic exchange in the model, the variables "zeta" and "beta" were varied. After a sensitivity analysis, to determine the effects of changes in these variables, a best estimate was determined by using least squares fitting.

4.3.1 Sensitivity analysis

Zeta and beta were changed several times to analyse the sensitivity of the model results to the variables zeta and beta. First, zeta was analysed for all four flush out experiments. Second, beta was analysed for all four flush out experiment. The values that were picked to analyse the sensitivity of the model were a relatively high value, an average value and a relatively low value for both zeta and beta, while keeping the other variable at an average value. For example, when analysing the sensitivity of zeta, the variable beta was kept at an average value of 1.0, while zeta was set on 1.0, 2.0, and 3.0.

4.3.2 Best estimate

After the sensitivity analysis, a best estimate was calculated. To find the best estimate the "least squares fit" (lsf) method was used by minimising the following objective function lsf(zeta, beta):

$$lsf(zeta, beta) = (ModelResult-ExpResult)^2. \quad (18)$$

But before such a method could be used, the data from the flush out experiments and the model were standardised for easy comparison between modelling and experimental data (chapter 5.2):

$$Ct = (ECt-ECmin)/(ECmax-ECmin) \text{ (Van der Perk et al., 2011)} \quad (19)$$

Where Ct is the standardised concentration at time t; ECt is the measured EC at time t; ECmin is the minimum measured EC; and ECmax is the maximum measured EC.
After standardising, the maximum EC is represented as 1.0 and the minimum EC is represented as 0.0.

At the lsf method, the lowest sum of differences provides the best estimate. For the best estimate in this research, the sum of all 4 flush out experiments was taken:

$$LsfSum = LsfSumExp1+LsfSumExp3+LsfSumExp5+LsfSumExp7 \quad (20)$$

By using trial and error, in which the knowledge from the sensitivity analysis was used, the values of zeta and beta were changed numerous times. Hence, the best estimate of all the model runs was found.

4.4 Residence time analysis

To provide a good summary of the experimental and model results, residence time analyses were performed. From the figures, the time till a certain concentration was reached was estimated for every experiment, at every measuring point, and at every measuring node. For the injection experiments, the time till max EC, and the max EC value were estimated, and for the flush out experiments, the time till 0.5 * max EC was estimated. The residence times of the experimental results were compared with the residence times of the model results of the best estimate.

5. Results and discussion

To create a better understanding of the flow patterns in the hyporheic zone, experiments were carried out, which were compared to modelling data, made by an advection diffusion model. To analyse parameters separately, the experiments were carried out in a controlled environment (outdoor flume).

5.1 Experimental results

First the injection experiments will be discussed (experiment 2, 4, 6 and 8), followed by the flush out experiments (experiment 1, 3, 5 and 7), since the injection experiments reveal some hyporheic flow patterns. The injection experiments are not standardised or corrected for temperature. The experimental results of the flush out experiments are corrected for temperature, but are presented without standardising. This is mainly due to time it takes for the experiments to be finished. Injection experiments are carried out much quicker than flush out experiments, and experience minimal temperature differences.

5.1.1 Injection experiments

At the injection experiments (appendix 1, figures 23-38), a peak can be seen in the EC value at the measuring points after the injection. This peak is usually measured first by the measuring points most upstream (table 3). Also the peak is measured earlier by the measuring points in the water than the measuring points inside the sediment (table 3). The measuring points that are 25 cm beneath the sediment bed are the last to measure the peak in EC value. It is also shown that at experiment 4 (fig. 27-30), the peaks are being measured faster than at the other experiments. This is caused by the flow velocity, which is highest at experiment 4. This results in faster distribution of the dissolved salt. Experiments 2 and 6 have approximately the same flow velocity, but the water level in experiment 2 is higher than the water level in experiment 6. In figures 23 and 31 it can be seen that this causes a noticeable difference in time it takes to measure the peak. Since there is more water available in the flume for experiment 2, the salt is spread out more, which results in a less pronounced peak and causes the peaks in concentration to take longer to reach the measuring points (fig. 23, 31; table 4).

Experiment 8 is the experiment with the smallest flow velocity. Figures 36-38 show that the peaks do not reach as far into the sediment and are all less pronounced as for the other experiments, which have a higher flow velocity (table 3, 4). At 15 cm beneath the bed (fig. 37), there is only a small peak in EC value measured, and at 25 cm beneath the bed (fig. 38), there is no peak in EC value measured.

Table 3, residence time analysis of injection experiments showing time till max EC values

	Time till max EC (s)				**Distance from sediment bed (cm)**	**Flow velocity (m/s)**	**Water level (m)**
Distance from water pump	***14 m***	***18.5 m***	***23 m***	***27.5 m***			
Experiment 2	170	220	300	340	5	0.1207	0.305
	190	380	1080	640	-5	0.1207	0.305
	480	1120	790	840	-15	0.1207	0.305
	#	#	#	#	-25	0.1207	0.305
Experiment 4	60	70	100	130	5	0.1817	0.2
	80	90	110	220	-5	0.1817	0.2
	210	230	170	320	-15	0.1817	0.2
	250	260	310	1680	-25	0.1817	0.2
Experiment 6	60	110	150	190	5	0.1263	0.175
	90	170	170	190	-5	0.1263	0.175
	240	360	340	350	-15	0.1263	0.175
	290	330	590	#	-25	0.1263	0.175
Experiment 8	300	440	550	740	5	0.0275	0.14
	380	640	1350	1020	-5	0.0275	0.14
	1220	2020	1380	#	-15	0.0275	0.14
	#	#	#	#	-25	0.0275	0.14

Table 4, residence time analysis of injection experiments showing max EC values

	max EC value				**Distance from sediment bed (cm)**	**Flow velocity (m/s)**	**Water level (m)**
Distance from water pump	***14 m***	***18.5 m***	***23 m***	***27.5 m***			
Experiment 2	0.459	0.319	0.336	0.286	5	0.1207	0.305
	0.723	0.264	0.134	0.183	-5	0.1207	0.305
	0.159	0.147	0.142	0.146	-15	0.1207	0.305
	#	#	#	#	-25	0.1207	0.305
Experiment 4	1.131	0.93	0.957	0.751	5	0.1817	0.2
	0.943	0.932	0.695	0.706	-5	0.1817	0.2
	0.518	0.352	0.635	0.209	-15	0.1817	0.2
	0.229	0.968	0.264	0.105	-25	0.1817	0.2
Experiment 6	0.879	0.671	0.738	0.598	5	0.1263	0.175
	0.546	0.882	1.483	0.678	-5	0.1263	0.175
	0.849	0.264	0.234	0.221	-15	0.1263	0.175
	0.45	0.516	0.201	#	-25	0.1263	0.175
Experiment 8	0.267	0.26	0.294	0.26	5	0.0275	0.14
	0.202	0.173	0.2	0.186	-5	0.0275	0.14
	0.135	0.128	0.12	#	-15	0.0275	0.14
	#	#	#	#	-25	0.0275	0.14

5.1.2 Flush out experiments

For the flush out experiments a pattern is expected which follows the results from the injection experiment. In general it is expected that the EC values will be flushed out from upstream to downstream. Meaning that at 14m a drop in the EC values will be seen faster than at the more downstream measuring points. This mechanism is also expected vertically. In general the deeper into the sediment the measurement point is, the longer it will take for the EC value to return to the EC value of the groundwater which is pumped in. A decrease in water level will result in smaller residence times, and a decrease in flow velocity will result in larger residence times. Also for experiment 8 it is expected that the measuring point at 25 cm beneath the bed barely shows a decline. Any disruptions to these patterns will be discussed.

The EC measurements of experiment 1 are seen in figures 3, 4, 5 and 6.

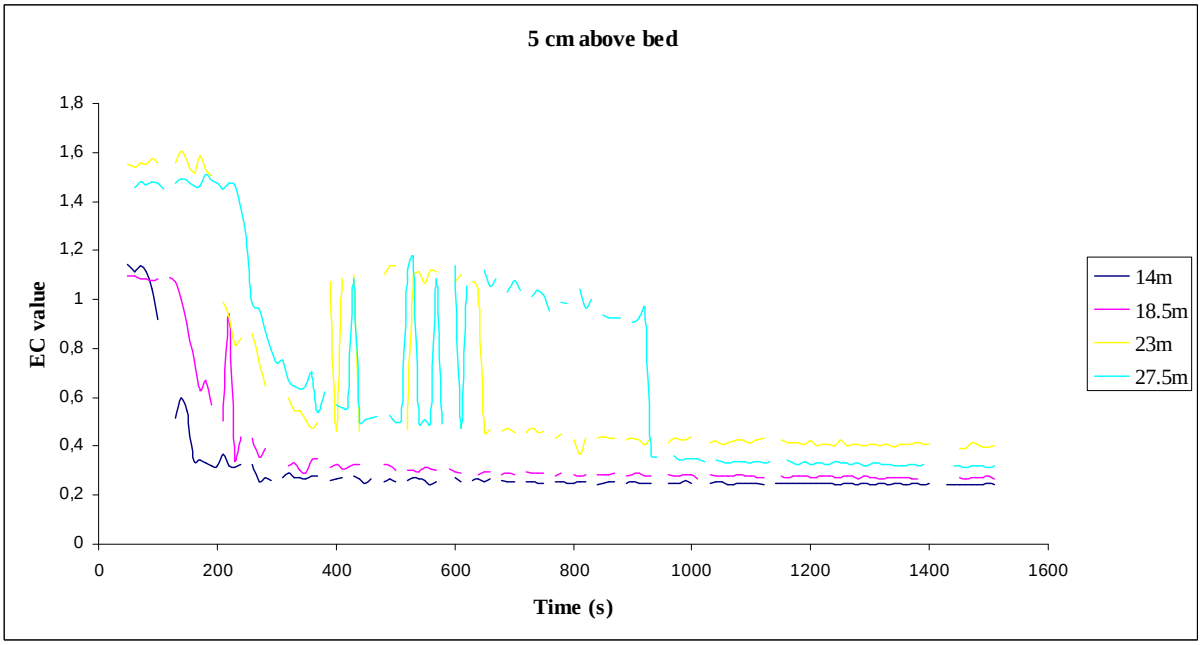

Figure 3, EC measurements for all probes 5 cm above the bed for experiment 1.

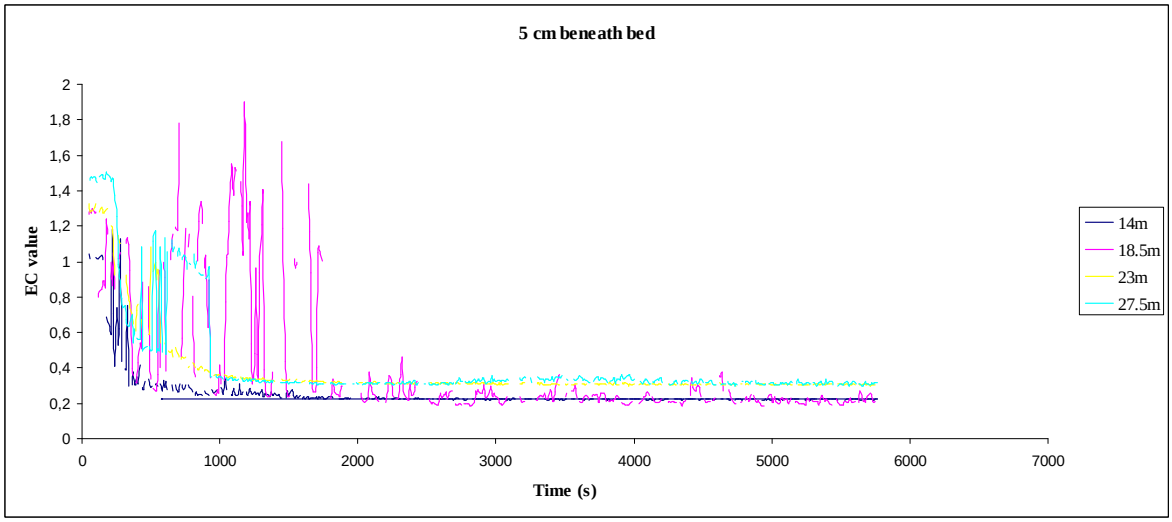

Figure 4, EC measurements for all probes 5 cm beneath the bed for experiment 1.

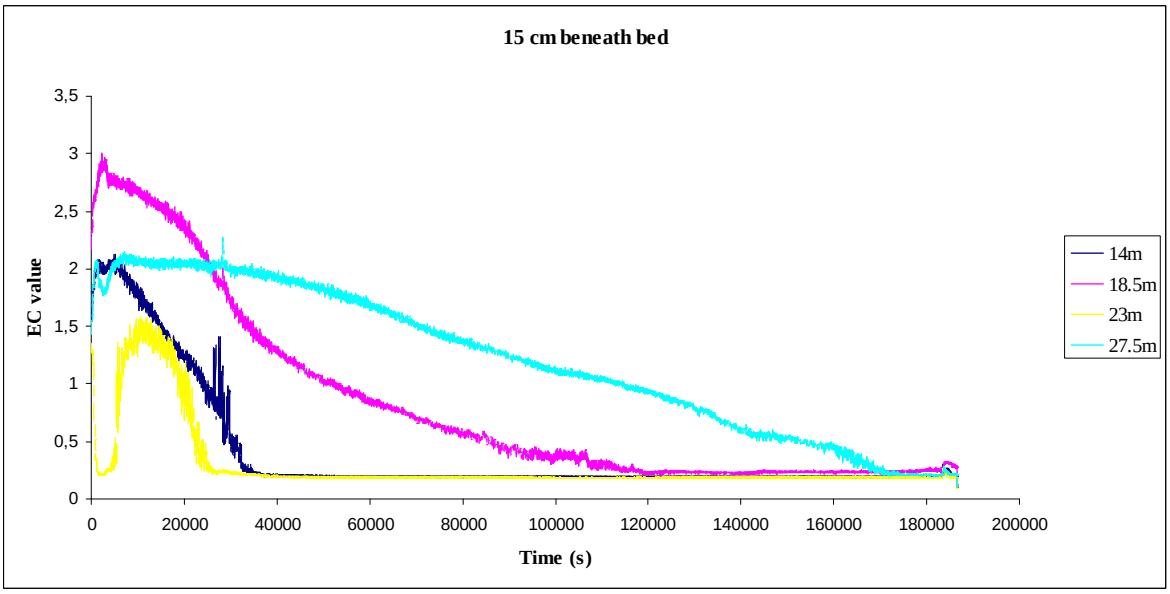

Figure 5, EC measurements for all probes 15 cm beneath the bed for experiment 1.

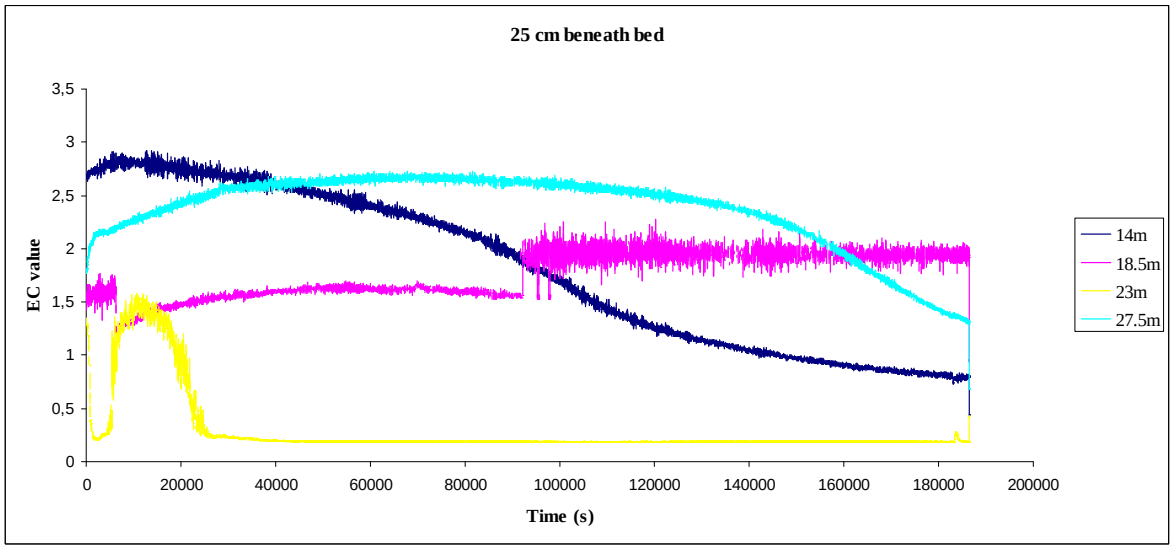

Figure 6, EC measurements for all probes 25 cm beneath the bed for experiment 1.

In figure 5, the EC value at 23 m declines fastest. The quick decline might be caused by a small bedform or a specific sorting of sediment, resulting in such a pressure distribution that the exchange rate is increased at the measuring point, ultimately resulting in the quick decline in EC value compared to the other measuring points at 15 cm beneath the bed. In figure 6, it is shown that the EC value at measuring point 18,5 m measures a nearly constant EC value. It seems, this measuring point shows no decline at all. The EC values in the other three points eventually decline to the EC value of the fresh groundwater. This most likely means that the stream flow of fresh groundwater is not able to reach the measuring point 25 cm beneath the bed at 18,5 m, resulting in a constant EC value, which is higher than the EC of the fresh groundwater, as shown in figure 6. In figure 3 and 4 there is some noise in the measurements. This is most likely caused by water from deeper in de sediment, flowing past the measuring point with higher concentrations of salt from deeper in the sediment. After some time, the high concentrations were flushed out, and only small concentrations were flushed out, causing the noise in the measurements to disappear.

The EC measurements of experiment 3 are seen in figures 7, 8, 9 and 10.

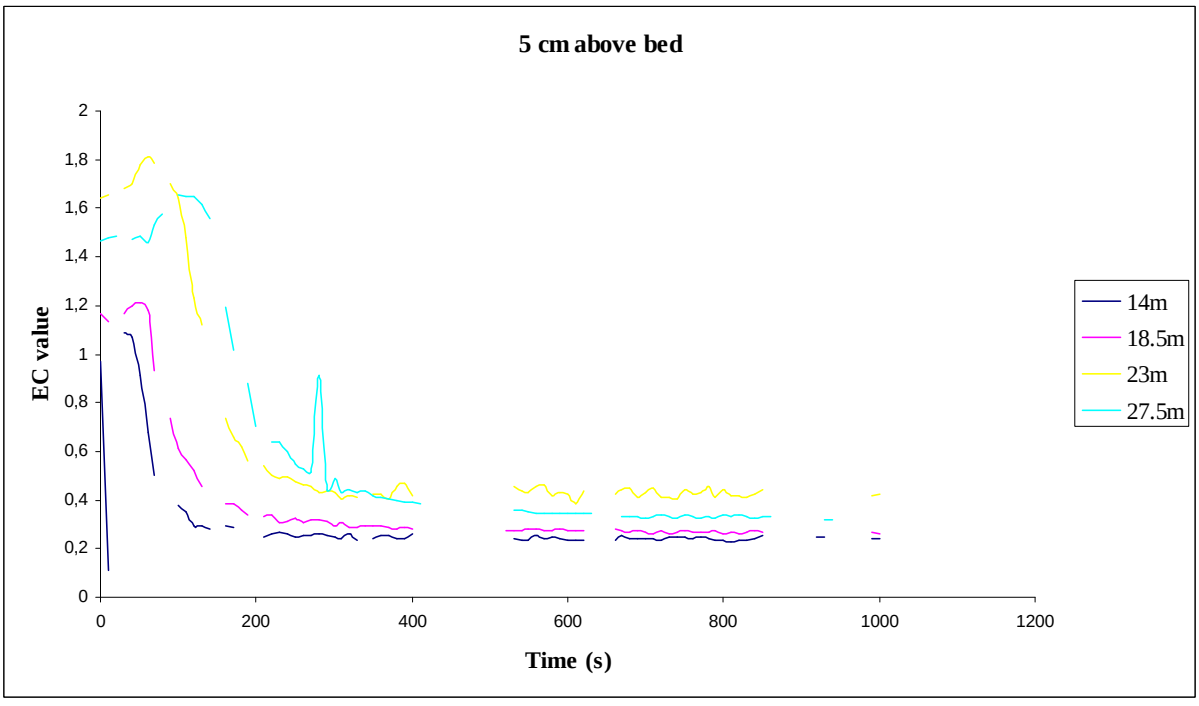

Figure 7, EC measurements for all probes 5 cm above the bed for experiment 3.

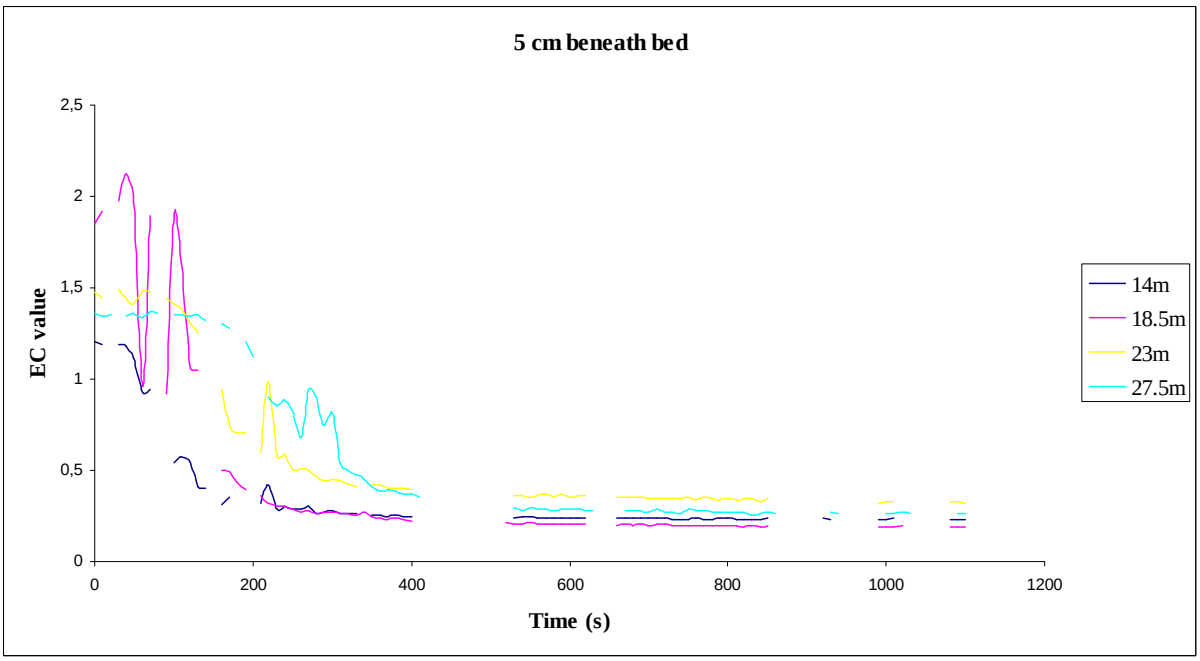

Figure 8, EC measurements for all probes 5 cm beneath the bed for experiment 3.

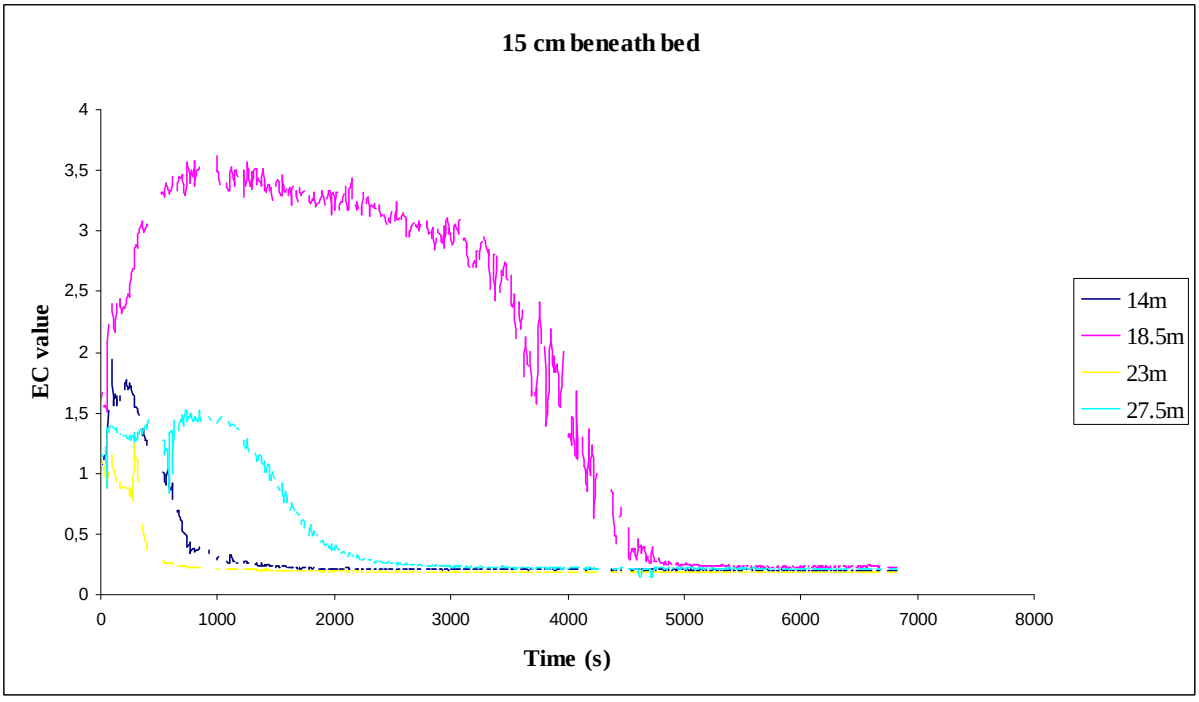

Figure 9, EC measurements for all probes 15 cm beneath the bed for experiment 3.

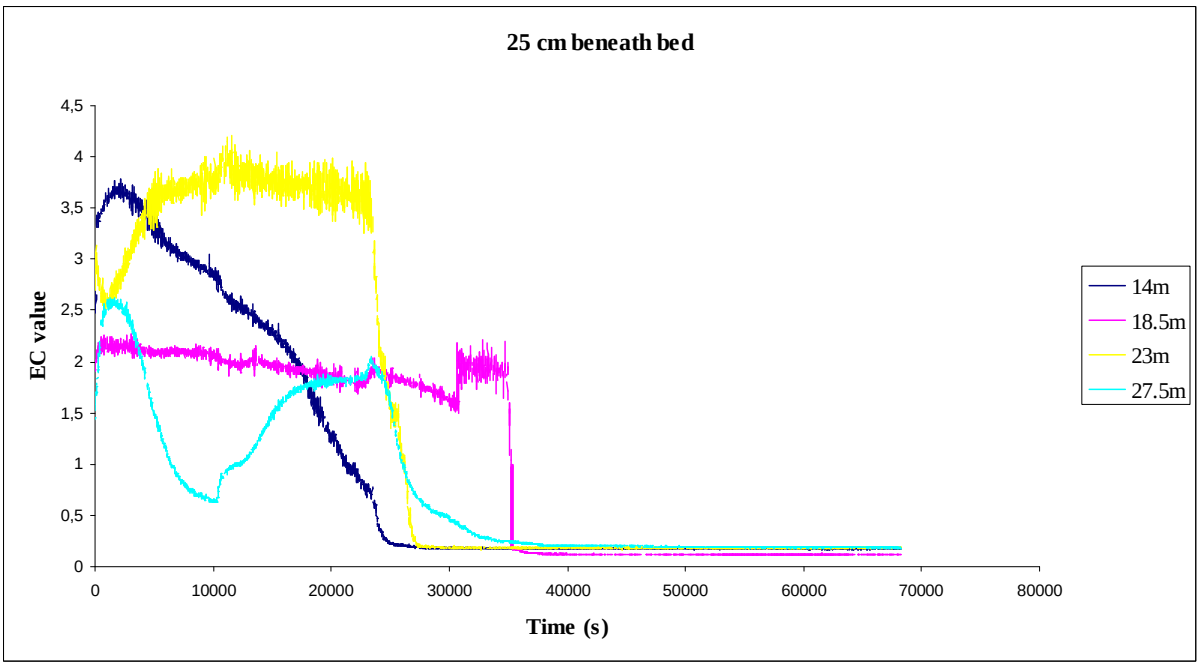

Figure 10, EC measurements for all probes 25 cm beneath the bed for experiment 3.

Figure 7 and 8 show the expected results, but figure 9 and 10 show some variations to the expected patterns. In figure 9 the measuring point at 23 m shows the fastest decline, and the measuring point at 18.5 m takes much longer to be reduced to the EC value of the aerated groundwater than the other measuring points located 15 cm beneath the bed. Figure 5 and 9 both show the same fast decline for the measuring point at 23 m. So this is more likely the result of a small bedform or a specific sorting of sediment than some random disturbance. The relatively long decline of the EC value at measuring point 18.5 m in figure 25 might be a result of the high starting value at this measuring point. In figure 10 the standard pattern is seen again, but instead of measuring point 18.5 m being the second measuring point to be flushed out, the 18.5 m measuring point is the last to be flushed out.

Also it is shown in figure 10 that the EC value at measuring point 27.5m shows a relatively fast decline at first, but the EC value increases again. At the start of the increase in EC value at 10.000 seconds, the measuring point further upstream (23 m) is still at an EC value of approximately 0.65. The salt water from this measuring point lying further upstream might have been flowing through the sediment slowly, eventually reaching the measuring point at 27.5 m after 10.000 seconds. To verify this hypothesis the distance of 4.5 m was divided by 10.000 seconds. This would result in a hydraulic conductivity of $4.5*10^{-2}$ cm/s, which is a good estimate of hydraulic conductivity through gravel/sand (Fitts, 2002).

The EC measurements of experiment 5 are seen in figures 11, 12, 13 and 14.

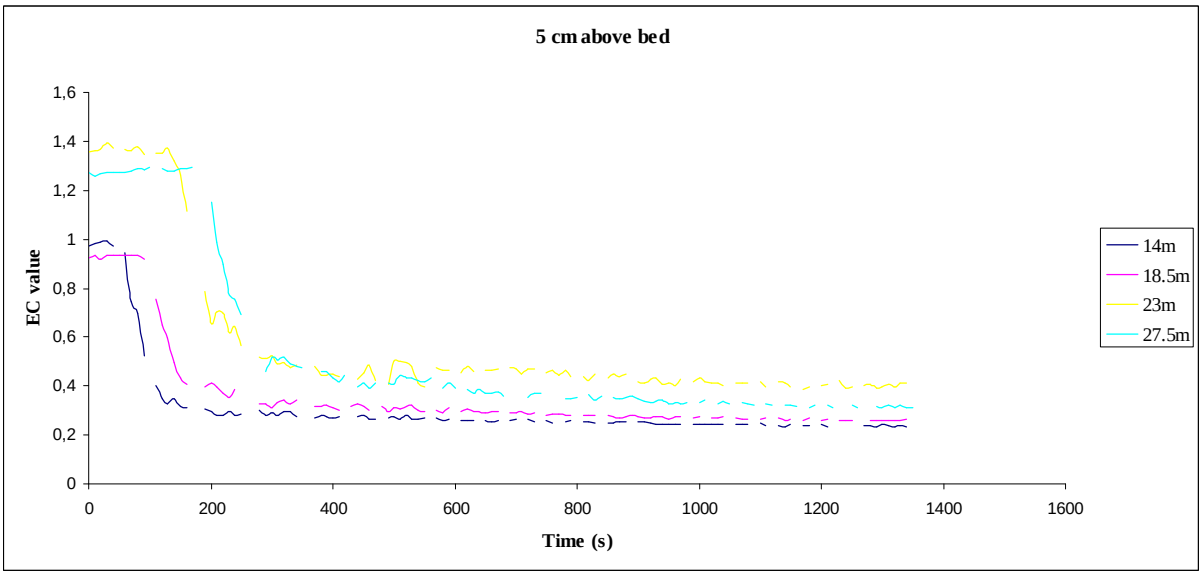

Figure 11, EC measurements for all probes 5 cm above the bed for experiment 5.

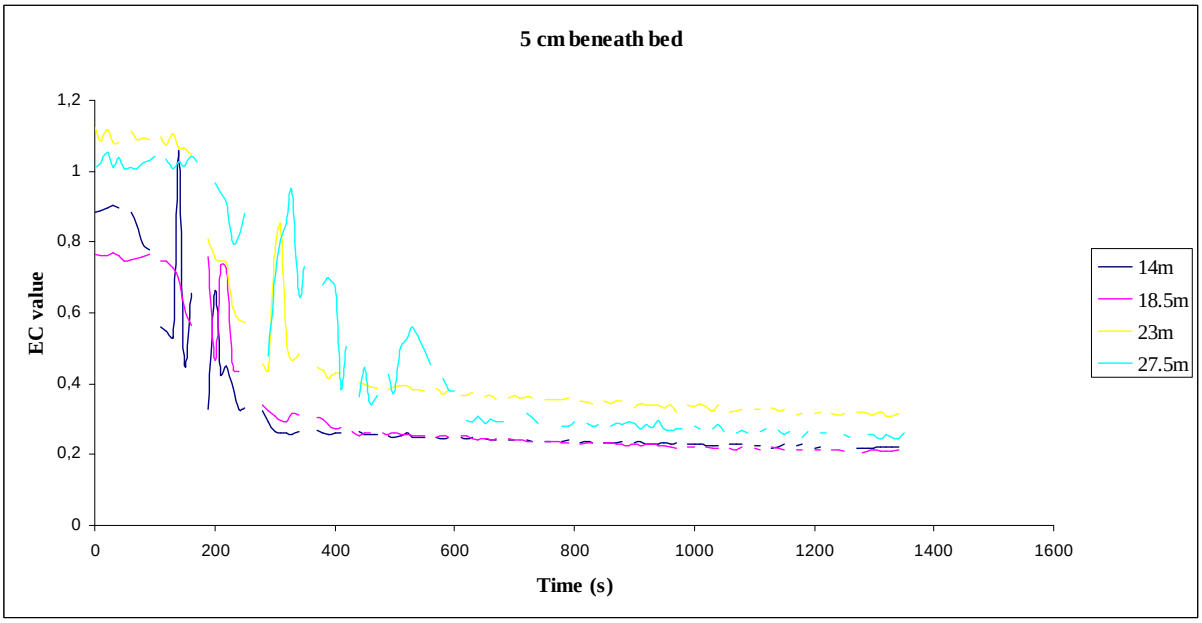

Figure 12, EC measurements for all probes 5 cm beneath the bed for experiment 5.

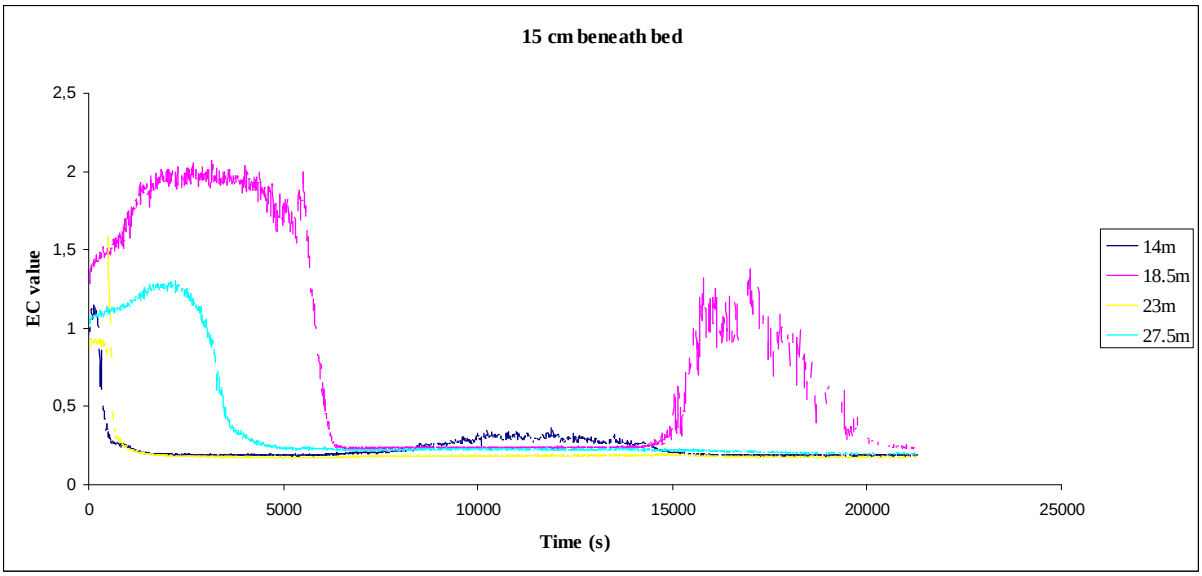

Figure 13, EC measurements for all probes 15 cm beneath the bed for experiment 5.

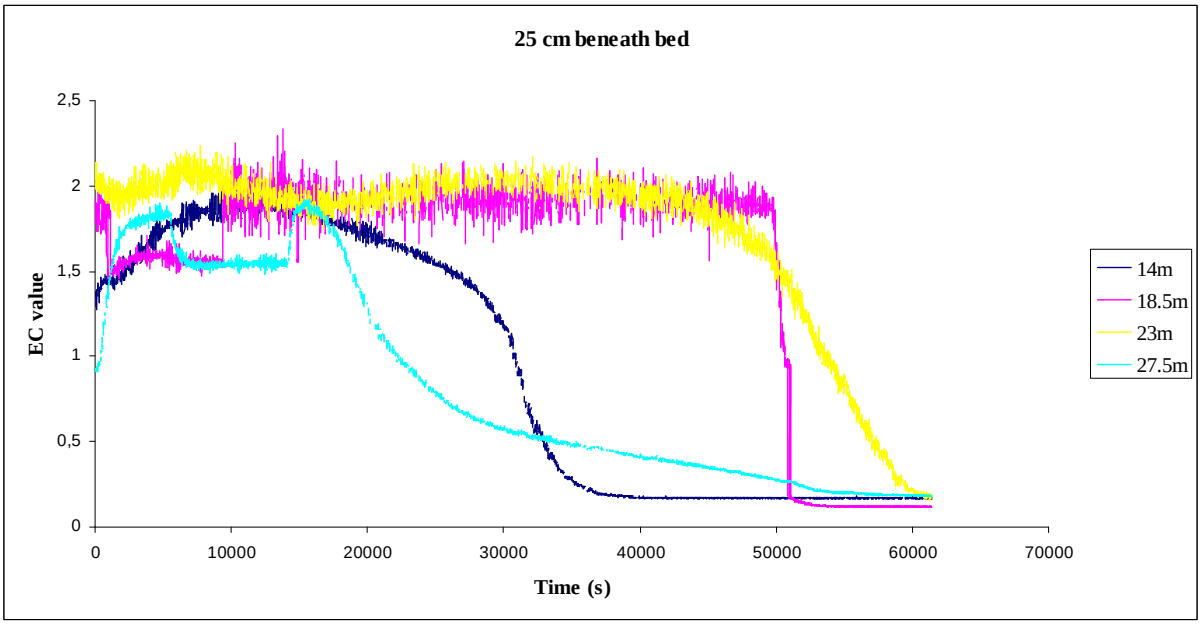

Figure 14, EC measurements for all probes 25 cm beneath the bed for experiment 5.

The figures 11-14 mainly show the expected pattern, but in figure 13 a spike in the EC values is seen for the measuring points at 14 m and at 18.5 m. The spike at 18.5 m is more pronounced. These spikes might be caused by a hyporheic flow path travelling from the sediment below the measuring points, which transported water with higher EC values to the measuring points, since the measuring points at 25 cm beneath the bed are still relatively high at that moment in time.

The EC measurements of experiment 7 are seen in figures 15, 16, 17 and 18.

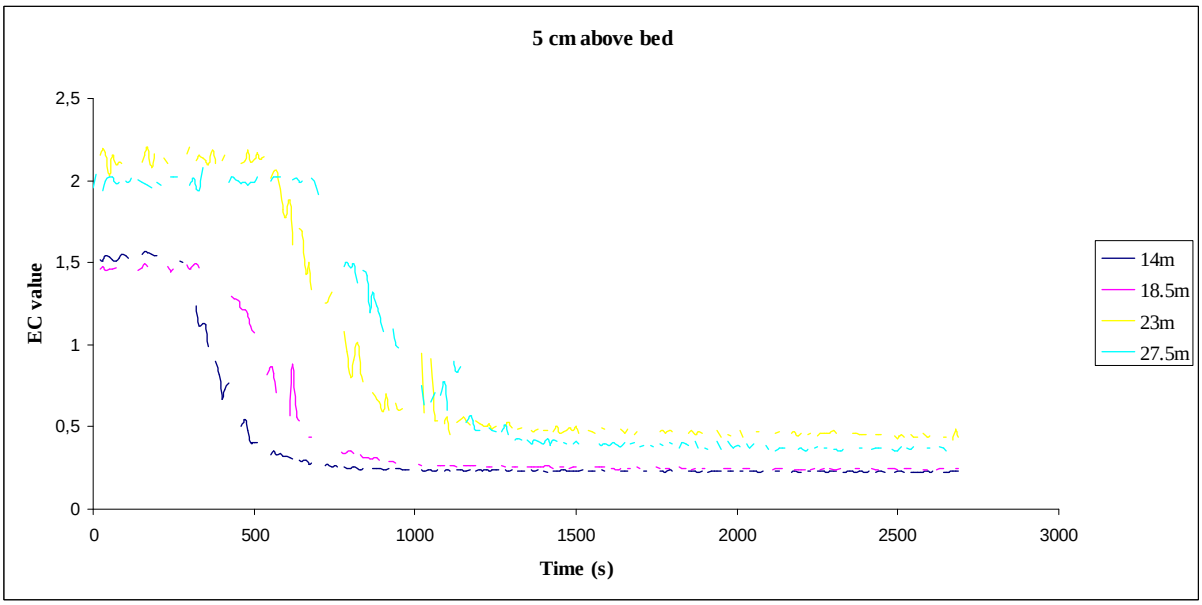

Figure 15, EC measurements for all probes 5 cm above the bed for experiment 7.

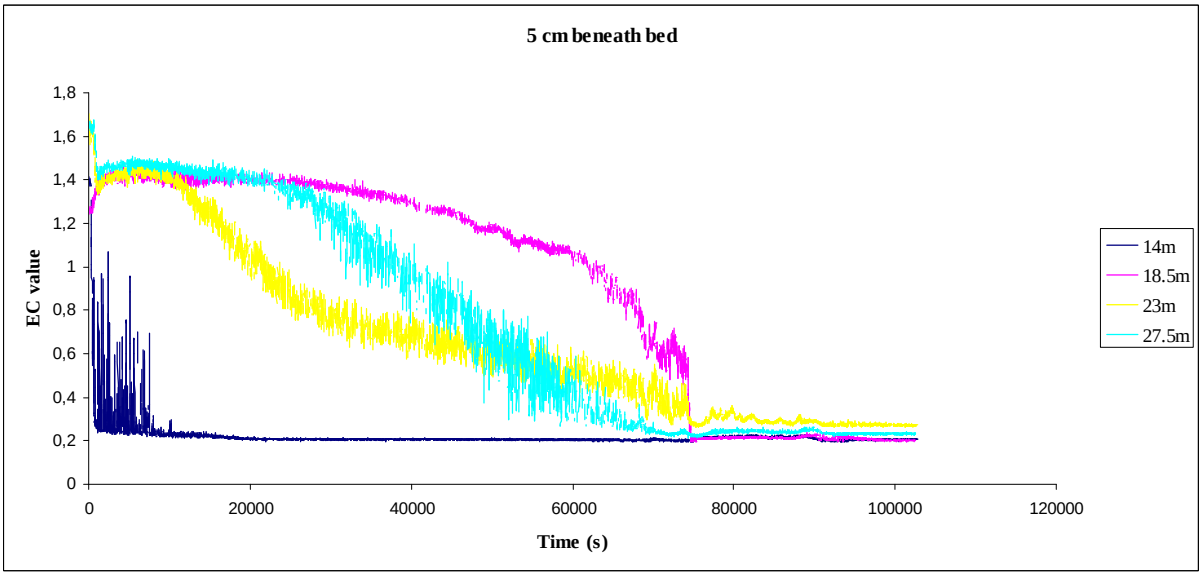

Figure 16, EC measurements for all probes 5 cm beneath the bed for experiment 7.

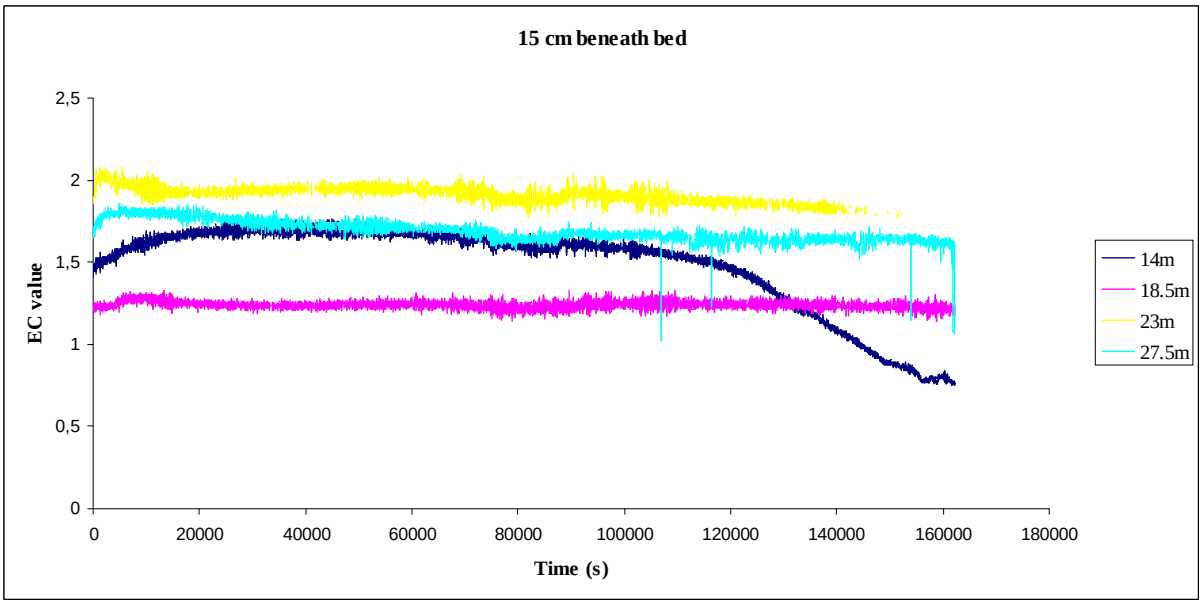

Figure 17, EC measurements for all probes 15 cm beneath the bed for experiment 7.

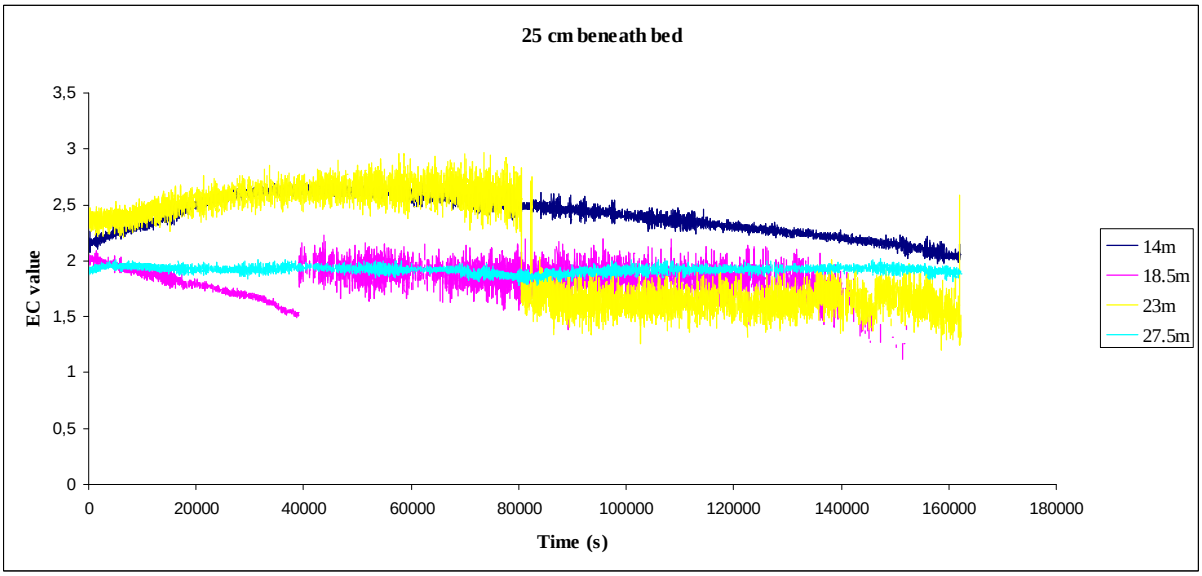

Figure 18, EC measurements for all probes 25 cm beneath the bed for experiment 7.

In the figures 15-18 it is shown that all EC values gradually decline, but since the flow velocity is so low, it takes a long time. The water column itself already takes 1500 seconds to be flushed out completely, and 5 cm beneath the bed this takes 75.000 seconds. Since there was no pronounced change in EC values at the measuring points deeper in the sediment, the experiment was stopped after approximately two and a half days. Figures 17 and 18 show a small decrease at some of the measuring points over this period of two and a half days.

5.2 Model results

5.2.1 Sensitivity analysis

5.2.1.1 Zeta

It appears that zeta only affects the vertical dispersion coefficient at the sediment bed as seen in formula 14, but the vertical dispersion coefficient at the sediment bed is also a factor in formula 13, which calculates the vertical dispersion coefficient in the sediment. For the sensitivity analysis of zeta, zeta was set to a value of 1.0; 2.0; and 3.0; while beta was set to a constant value of 1.0. Experiment 1 is shown in figures 39-41, experiment 3 is shown in figures 42-44, experiment 5 is shown in figures 45-47, and experiment 7 is shown in figures 48-50. A summary of the results at 27.5 m is provided in table 5. Only the results of 27.5 m are presented for both zeta and beta, since the results of the other measuring points show the same pattern, only with larger residence times.

Table 5, data for residence time analysis at 27.5 m for different values of zeta

	Time till 0.5 * max EC at 27.5 m (s)					
Distance from water pump	***Zeta 1.0 Beta 1.0***	***Zeta 2.0 Beta 1.0***	***Zeta 3.0 Beta 1.0***	**Distance from sediment bed (cm)**	**Flow velocity (m/s)**	**Water level (m)**
Experiment 1	210	210	210	5	0.1207	0.305
	500	1200	1100	-5	0.1207	0.305
	15000	10000	9000	-15	0.1207	0.305
	35000	65000	60000	-25	0.1207	0.305
Experiment 3	140	140	140	5	0.1817	0.2
	470	750	700	-5	0.1817	0.2
	12000	6000	5500	-15	0.1817	0.2
	30000	42000	38000	-25	0.1817	0.2
Experiment 5	200	200	200	5	0.1263	0.175
	520	1120	1000	-5	0.1263	0.175
	16000	7500	7000	-15	0.1263	0.175
	38000	62000	55500	-25	0.1263	0.175
Experiment 7	800	800	800	5	0.0275	0.14
	2500	5000	3750	-5	0.0275	0.14
	40000	50000	25000	-15	0.0275	0.14
	60000	210000	205000	-25	0.0275	0.14

When zeta is increased, the vertical dispersion coefficient is decreased, and when zeta is decreased, the vertical dispersion coefficient is increased.
At experiment 1, 3 and 5, the measuring point 15 cm beneath the bed is flushed out quicker when zeta is increased. The measuring points 5 cm and 25 cm beneath the bed are flushed out slower when zeta is increased to 2.0, but they are flushed out slightly quicker when zeta is increased to 3.0. In this model, the vertical dispersion starts influencing the flush out process when the concentration in the water column drops below the concentration in the sediment. This occurs after 60-780 seconds at the flush out experiments (table 8). When zeta is high, the dispersion process is slow, and when zeta is low, the dispersion process is faster. Hence, the flushing out process starts with a slow decline when zeta is high and a fast decline when zeta is low.
The setup of this model simulates an upward concentration transport. A high dispersion coefficient will result in a relatively fast upward transport, and a low dispersion coefficient will result in a relatively slow upward transport. For the measuring points at 25.0 cm beneath the bed this causes a faster decline in concentration when the dispersion coefficient is increased. The concentration transported upwards delays the flushing out at the measuring points 5.0 cm and 15.0 cm beneath the bed, since the upward concentration transport increases the concentration of these layers during the flush out process. If the dispersion coefficient is reduced, the amount of delay is reduced, and the residence times of the salt at the measuring points 5.0 cm and 15.0 cm beneath the bed are decreased. The horizontal dispersion and advection cause a reduction in concentration. The balance between horizontal and vertical flush out processes can change the general flush out pattern. When changing zeta, the ratio between horizontal and vertical flush out processes changes, as can be seen in figures 35-46 and table 5.

5.2.1.2 Beta

Beta is used in three formulas; Formula 13, 15 and 17. These formulas affect the flow velocity in the sediment, the longitudinal dispersion in the sediment and the vertical dispersion in the sediment. If beta is increased, this results in an increase in the rate of reduction in flow velocity and dispersion over depth, and when beta is decreased, this results in a decrease in the rate of reduction in flow velocity and dispersion over depth. If beta is increased, the residence time of the salt water in the sediment will increase, and if beta is decreased, the residence time of salt water in the sediment will decrease. Deeper into the sediment this effect is more pronounced.

For the sensitivity analysis of beta, beta was set to a value of 0.5; 1.0; and 1.5; while zeta was set to a constant value of 2.0. The figures of the sensitivity analysis of beta are shown in appendix 2. Experiment 1 is shown in figures 51-53, experiment 3 is shown in figures 54-56, experiment 5 is shown in figures 57-59, and experiment 7 is shown in figures 60-62. A summary of the results is presented in table 6. Table 5 and 6 show that the variable "beta" is relatively more sensitive to change than the variable "zeta", and the effect of changes in beta are more easily described.

Table 6, data for residence time analysis at 27.5 m for different values of beta

	Time till 0.5 * max EC at 27.5 m (s)					
Distance from water pump	***Zeta 2.0 Beta 0.5***	***Zeta 2.0 Beta 1.0***	***Zeta 2.0 Beta 1.5***	**Distance from sediment bed (cm)**	**Flow velocity (m/s)**	**Water level (m)**
Experiment 1	210	210	210	5	0.1207	0.305
	600	1200	2500	-5	0.1207	0.305
	1500	10000	60000	-15	0.1207	0.305
	5000	65000	300000	-25	0.1207	0.305
Experiment 3	140	140	140	5	0.1817	0.2
	420	750	1380	-5	0.1817	0.2
	1000	6000	27500	-15	0.1817	0.2
	3000	42000	170000	-25	0.1817	0.2
Experiment 5	200	200	200	5	0.1263	0.175
	640	1120	2200	-5	0.1263	0.175
	1000	7500	50000	-15	0.1263	0.175
	4500	62000	210000	-25	0.1263	0.175
Experiment 7	800	800	800	5	0.0275	0.14
	2000	5000	8000	-5	0.0275	0.14
	7500	50000	380000	-15	0.0275	0.14
	15000	210000	900000	-25	0.0275	0.14

5.2.2 Best estimate

The best estimate was found at a zeta of 1.8 and a beta of 1.13. The model results and experimental results are shown in figures 19-22. The straight lines are the model results. Comparison between the model results and experimental results are presented in chapter 5.3.

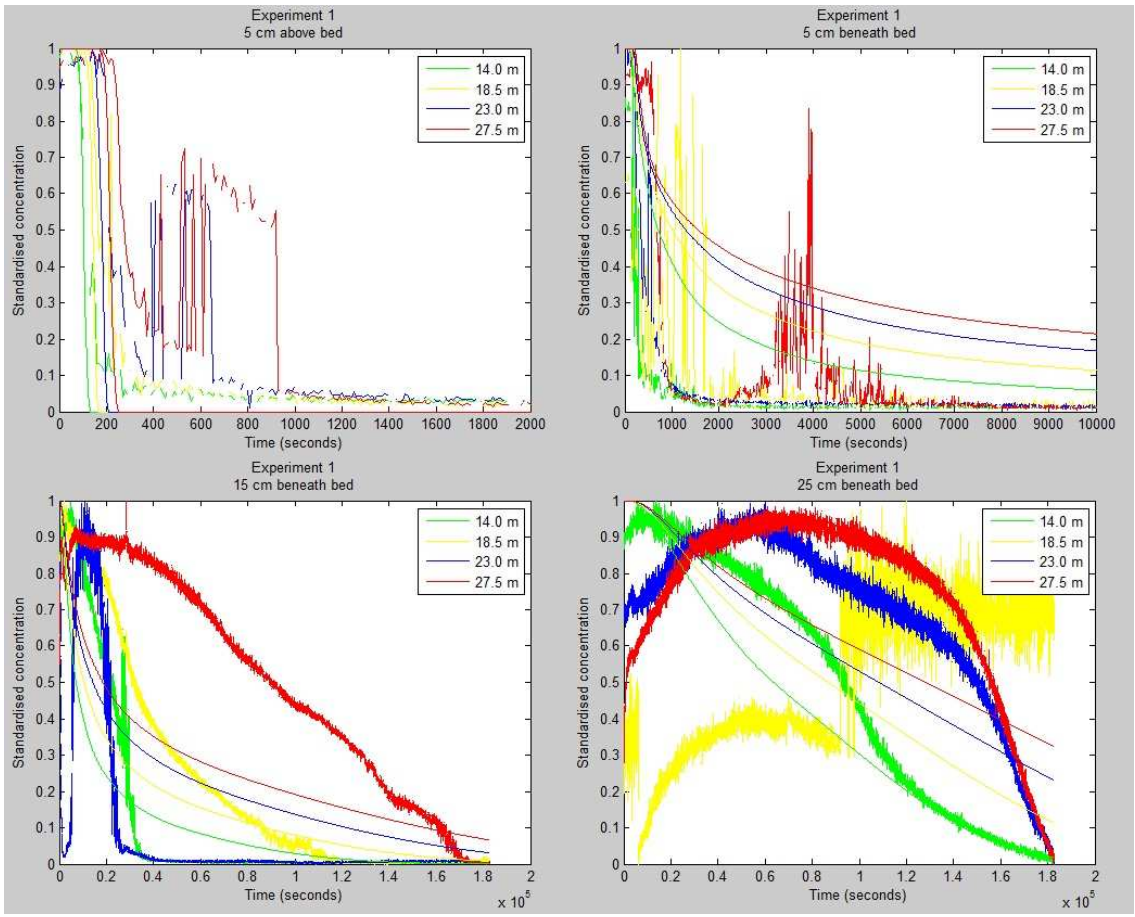

Figure 19, model results of experiment 1, with beta = 1.13 and zeta = 1.8.

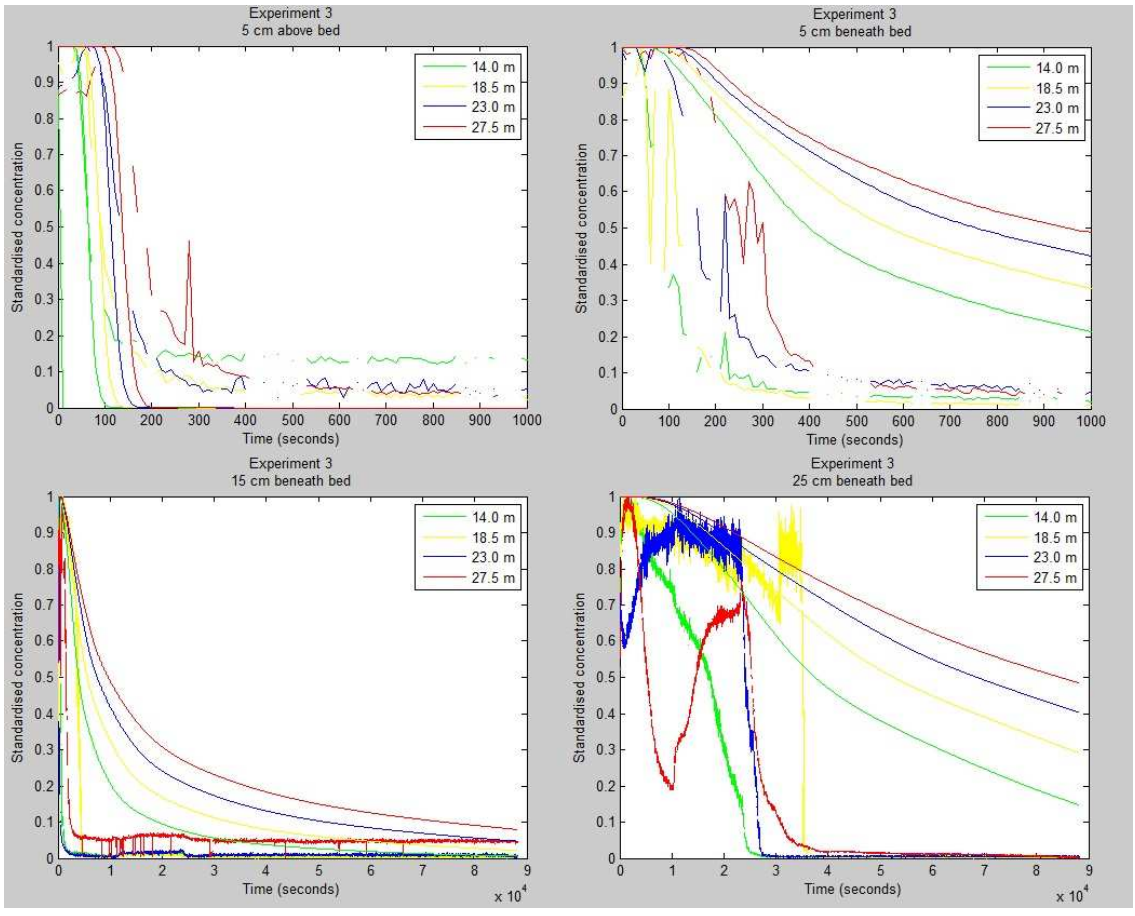

Figure 20, model results of experiment 3, with beta = 1.13 and zeta = 1.8.

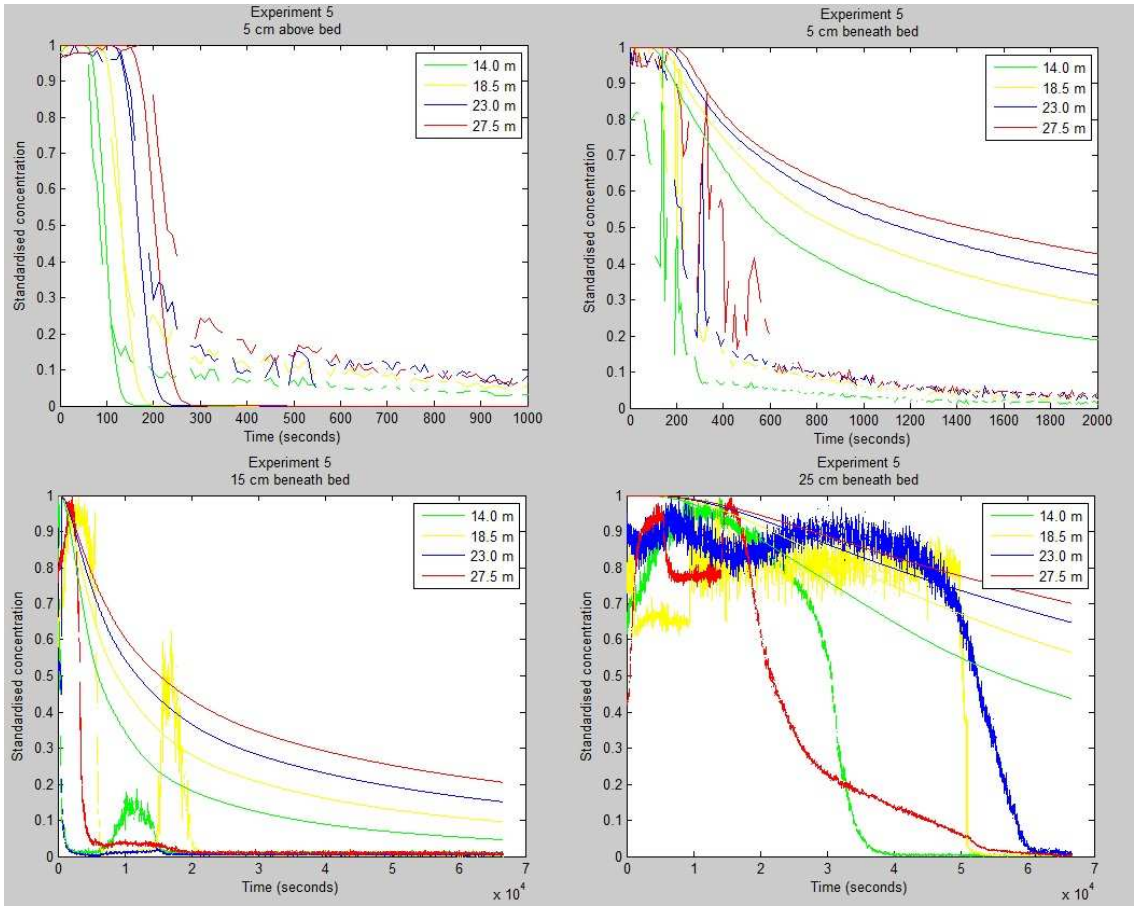

Figure 21, model results of experiment 5, with beta = 1.13 and zeta = 1.8.

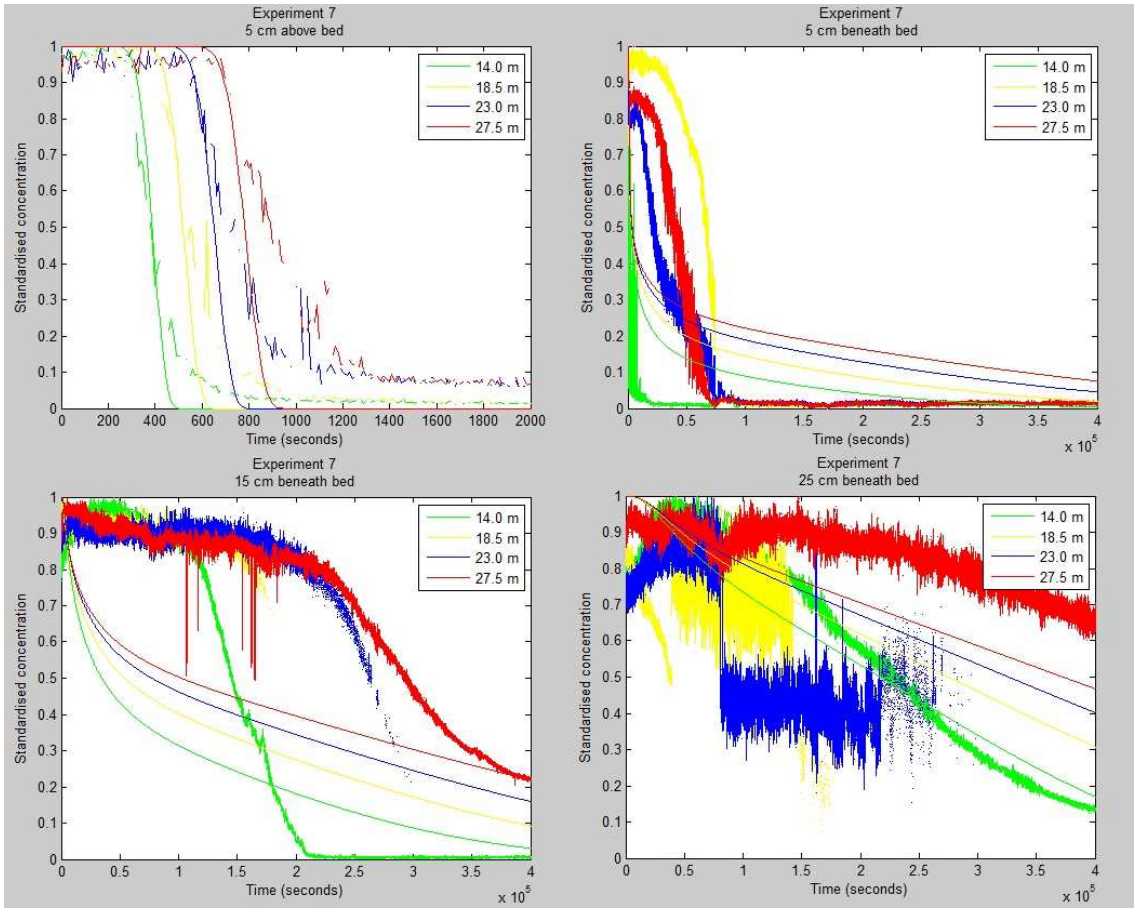

Figure 22, model results of experiment 7, with beta = 1.13 and zeta = 1.8.

5.3 Residence time analysis

To determine the influence of flow velocity and water level on the residence times of hyporheic exchange in a flat gravel bed, a statistical analysis on the residence times of a salt concentration in a flat gravel bed was carried out. For each measuring point at every experiment, the time until EC values reduced to half of their maximum values was determined. This provides a representation of the time it takes to flush out half of the salt concentration. The analyses presented here were carried out on the best estimate of the model results and on the experimental results (table 7, 8). By analysing and comparing these values, some conclusions can be made about the influence of flow velocity and water level. Hence, to compare both residence time analyses, the residence times of the model results were subtracted from the residence times of the experimental results (table 9).

5.3.1 Experimental results

Table 7, data for residence time analysis of experimental results; # represents the measuring points for which the time till 0.5 * max EC could not be determined

	Time till 0.5 * max EC (s)				**Distance from sediment bed (cm)**	**Flow velocity (m/s)**	**Water level (m)**
Distance from water pump	***14 m***	***18.5 m***	***23 m***	***27.5 m***			
Experiment 1	100	200	250	300	5	0.1207	0.305
	200	350	350	350	-5	0.1207	0.305
	24000	31000	20000	120000	-15	0.1207	0.305
	92000	#	20000	180000	-25	0.1207	0.305
Experiment 3	65	100	150	200	5	0.1817	0.2
	100	150	180	300	-5	0.1817	0.2
	550	3800	350	1600	-15	0.1817	0.2
	18000	35000	24000	5000	-25	0.1817	0.2
Experiment 5	90	135	195	255	5	0.1263	0.175
	205	260	300	400	-5	0.1263	0.175
	360	5850	600	3400	-15	0.1263	0.175
	30800	50600	53800	23500	-25	0.1263	0.175
Experiment 7	400	570	780	950	5	0.0275	0.14
	4000	69000	27000	46000	-5	0.0275	0.14
	152500	#	#	#	-15	0.0275	0.14
	#	#	#	#	-25	0.0275	0.14

Experiment 1 and experiment 5 have approximately the same flow velocity, but the water level in experiment 5 is nearly half of the water level in experiment 1. Table 7 shows that the residence times are generally larger at experiment 1 than at experiment 5. Deeper in the sediment (15 cm and 25 cm beneath bed) this difference in residence times becomes apparent. Hence, a higher water level results in larger residence times and a lower water level results in smaller residence times, especially deeper into the sediment (15 cm and 25 cm beneath the bed).

The main difference between experiment 3 and experiment 5 is flow velocity. Water level is only 15% larger at experiment 3, while flow velocity is 50% larger. Residence times are larger for experiment 5. Since the difference between experiment 1 and experiment 5 showed that a decrease in water level reduces the residence times, the difference in residence times between experiment 3 and experiment 5 shows that a decrease in flow velocity increases the residence time. Hence, a larger flow velocity results in smaller residence times and a smaller flow velocity results in larger residence times.

5.3.2 Model results

Table 8, data for residence time analysis of model results; # represents the measuring points for which the time till 0.5 * max EC could not be determined

	Time till 0.5 * max EC (s)				**Distance from sediment bed (cm)**	**Flow velocity (m/s)**	**Water level (m)**
Distance from water pump	***14 m***	***18.5 m***	***23 m***	***27.5 m***			
Experiment 1	100	140	180	220	5	0.1207	0.305
	710	1010	1300	1560	-5	0.1207	0.305
	7140	10530	14280	18480	-15	0.1207	0.305
	63800	87130	108530	128260	-25	0.1207	0.305
Experiment 3	60	90	110	140	5	0.1817	0.2
	400	570	750	950	-5	0.1817	0.2
	3950	5620	7520	9630	-15	0.1817	0.2
	37580	52680	68640	84630	-25	0.1817	0.2
Experiment 5	100	130	170	200	5	0.1263	0.175
	610	880	1160	1440	-5	0.1263	0.175
	6040	8840	11960	15330	-15	0.1263	0.175
	56630	#	#	#	-25	0.1263	0.175
Experiment 7	390	520	650	780	5	0.0275	0.14
	2630	3190	3490	3670	-5	0.0275	0.14
	34640	54380	77600	102920	-15	0.0275	0.14
	217440	275490	326890	373210	-25	0.0275	0.14

Table 8 shows the residence time analysis of the best estimate of the model results. Experiment 1 and 5 show nearly the same results, while the water level is much higher in experiment 1, which should result in larger residence times at experiment 1 or smaller residence times at experiment 5. Experiment 3 and experiment 5 do show the expected results, with larger residence times at experiment 5, which has smaller flow velocity. The water level is most likely not incorporated properly in the model. In the model script, the water level is not incorporated in the flow velocity in the sediment, but it is in the vertical dispersion and longitudinal dispersion. Most likely, the water level should be incorporated in the formula for flow velocity in the sediment, since water level clearly has a more pronounced role in the flush out process than expected.

5.3.3 Difference between model and experimental results

Table 9, data for residence time analysis of difference between model and experimental results; # represents the differences that could not be determined

	Time till 0.5 * max EC (s)				**Distance from sediment bed (cm)**	**Flow velocity (m/s)**	**Water level (m)**
Distance from water pump	***14 m***	***18.5 m***	***23 m***	***27.5 m***			
Experiment 1	0	-60	-70	-80	5	0.1207	0.305
	510	660	950	1210	-5	0.1207	0.305
	-16860	-20470	-5720	-101520	-15	0.1207	0.305
	-28200	#	88530	-51740	-25	0.1207	0.305
Experiment 3	-5	-10	-40	-60	5	0.1817	0.2
	300	420	570	650	-5	0.1817	0.2
	3400	1820	7170	8030	-15	0.1817	0.2
	19580	17680	44640	61130	-25	0.1817	0.2
Experiment 5	10	-5	-25	-55	5	0.1263	0.175
	405	620	860	1040	-5	0.1263	0.175
	5680	2990	11360	11930	-15	0.1263	0.175
	25830	#	#	#	-25	0.1263	0.175
Experiment 7	-10	-50	-130	-170	5	0.0275	0.14
	-1370	-65810	-23510	-42330	-5	0.0275	0.14
	-117860	#	#	#	-15	0.0275	0.14
	#	#	#	#	-25	0.0275	0.14

Due to the calculation method of the model, in which timesteps were used, the residence times of the model are larger than they could be with a more efficient timestep of for example 0.1 second. Hence, if the model represents the experimental data correctly, the calculations with a timestep of 1.0 second should be higher than the experimental results. Thus, the difference between model and experimental results should be positive.
For experiment 3 and 5 this is mainly true, but experiment 7 shows only negative values. This shows that the model was not able to correctly calculate the slow hyporheic exchange at experiment 7. The water level at experiment 7 was very low, and since water level was not incorporated correctly within the model, this is probably the main cause for the negative values at experiment 7. A reduction in water level should have had a more pronounced impact on the residence times of the model, since a decrease in water level resulted in relatively smaller residence times at the experimental results than at the model. Deeper into the sediment (15 cm and 25 cm beneath the bed) this difference became more apparent. If the model would properly represent the effect of a reduction in water level, this would have resulted in smaller residence times for the model results of experiment 7, and hereby reduced the difference between the model results and the experimental results.
At experiment 1, the water level was significantly higher than the water level at experiment 3 and 5. This should have caused larger residence times for the model results, especially deeper into the sediment, which would have created a better representation of the experimental results.
Water level seems to have a relatively large impact on the reach of the hyporheic exchange into the sediment bed, since a decrease in water level can cause the hyporheic exchange to reach deeper into the sediment bed more easily, resulting in smaller residence times deeper into the sediment.

6. Conclusions

6.1 Flow velocity

A decrease in flow velocity resulted in larger residence times. Changes in the flow velocity between different experiments revealed the sensitivity of hyporheic flow to flow velocity. This partly clarified why the flume experiments show irregularities. Due to the heterogeneous character of the sediment, small differences in flow velocity occur inside the sediment, and since flow velocity has a major impact on the residence time, even small differences in flow velocity can create irregularities between different measuring points.

6.2 Water level

A decrease in water level resulted in smaller residence times, especially deeper into the sediment (15 cm and 25 cm beneath the bed). Comparison between model and experimental results showed that water level has a larger influence than expected for the water levels that were used. Water level has a relatively large impact on the reach of the hyporheic exchange into a flat gravel bed. To adjust the model for such an influence, the effect of water level on the reach of hyporheic exchange should be incorporated in the advection diffusion model.

Acknowledgements

This research was carried out as part of the MSc programme Coastal Dynamics and Fluvial Systems at Utrecht University, the Netherlands under supervision of M. van der Perk (Utrecht University). I want to thank M. van der Perk for supervising my MSc research and for all his help during my study. I want to thank E.L. Petticrew, and P.N. Owens (University of Northern British Columbia, Prince George BC, Canada) for discussing their thoughts on the research with me. Utrecht University and Marcel van der Perk provided funding for this Master research. The flume at the Quesnel River Research Center was made available by the University of Northern British Columbia. Flume construction was made possible by Ben Anderson Millington and Adam Simons. I also want to thank Laszlo Enyedy for technical support at the QRRC.

References

Arscott D.B., Tockner K., Ward J.V., 2005. Lateral organization of aquatic invertebrates along the corridor of a braided floodplain river. Journal of the North American Benthological Society, vol. 24, no. 4, pp. 934-954.

Battin T.J., Kaplan L.A., Findlay S., Hopkinson C.S., Marti E., Packman A.I., Newbold J.D., Sabater F., 2008. Biophysical controls on organic carbon fluxes in fluvial networks. Nature Geoscience, vol. 1, no.2, pp. 95–100.

Bencala K.E., Walters R.A., 1983. Simulation of solute transport in a mountain pool-and-riffle stream: a transient storage model. Water Resources Research, vol. 19, no. 3, pp. 718– 724.

Boano F., Camporeale C., Revelli R., Ridolfi L., 2006. Sinuosity-driven hyporheic exchange in meandering rivers. Geophysical Research Letters, vol. 33.

Burkholder B.K., Grant G.E., Haggerty R., Khangaonkar T., Wampler P.J., 2008. Influence of hyporheic flow and geomorphology on temperature of a large, gravel-bed river, Clackamas River, Oregon, USA. Hydrological Processes, vol. 22, pp. 941–953.

Cardenas M.B., Wilson J.L., Zlotnik V.A., 2004. Impact of heterogeneity, bed forms, and stream curvature on subchannel hyporheic exchange. Water Resources Research, vol. 40.

Cardenas M.B., Wilson J.L., 2007. Effects of current–bed form induced fluid flow on the thermal regime of sediments. Water Resources Research, vol. 43.

Cardenas M.B., 2008. Surface water– groundwater interface geomorphology leads to scaling of residence times. Geophysical Research Letters, vol. 35.

Cardenas M.B., 2009. A model for lateral hyporheic flow based on valley slope and channel sinuosity. Water Resources Research, vol. 45.

Castro N.M., Hornberger G.H., 1991. Surface-subsurface water interactions in an alluviated mountain stream channel. Water Resources Research, vol. 27, no. 7, pp. 1613–1621.

Choi J., Harvey J.W., Conklin M.H., 2000. Characterizing multiple timescales and storage zone interaction that affect solute fate and transport in drainage basins. Water Resources Research, vol. 36, no. 6, pp. 1511 –1518.

Csernuszenko W., 1987. Dispersion of pollutants in rivers. Hydrological Sciences, vol. 32, no. 1, pp. 59-67.

Elliott A.H., Brooks N.H., 1997a. Transfer of non-sorbing solutes to a streambed with bed forms: laboratory experiments. Water Resources Research, vol. 33, no. 1, pp. 137–151.

Elliott A.H., Brooks N.H., 1997b. Transfer of non-sorbing solutes to a streambed with bed forms: theory. Water Resources Research, vol. 33, no. 1, pp. 123-136.

Feris K., Ramsey P., Frazar C., Moore J.N., Gannon J.E., Holben W.E., 2003. Differences in hyporheic-zone microbial community structure along a heavy-metal contamination gradient. Applied and Environmental Microbiology, vol. 69, no. 9, pp. 5563–5573.

Findlay S., 1995. Importance of surface-subsurface exchange in stream ecosystems: The hyporheic zone. Limnology and Oceanography, vol. 40, no. 1, pp. 159-164

Fischer H.B., List E.J., Koh R.C.Y., Imberger J., Brooks N.H., 1979. Mixing in Inland and Coastal Waters. Academic Press, New York.

Fitts C.R., 2002. Groundwater Schience. Elsevier Science Publications, The Netherlands.

Forsman J., 2000. Contaminant transport in non-uniform streams and streambeds, Ph.D. thesis, Uppsala University, Uppsala, Sweden.

Gooseff M.N., Anderson J.K., Wondzell S.M., LaNier J., Haggerty R., 2006. A modelling study of hyporheic exchange pattern and the sequence, size, and spacing of stream bedforms in mountain stream networks, Oregon, USA. Hydrological Processes, vol. 20, pp. 2443-2457.

Hall R.O. Jr., Bernhardt E.S., Likens G.E., 2002. Relating nutrient uptake with transient storage in forested mountain streams. Limnology and Oceanography, vol. 47, pp. 255–265.

Habel F., Mendoza C., Bagtzoglou A. C., 2002. Solute transport in open channel flows and porous streambeds. Advances in Water Resources, vol. 25, pp. 455–469.

Harvey J., Bencala K.E., 1993. Effect of streambed topography on surface-subsurface water exchange in mountain catchments. Water Resources Research, vol. 29, no. 1, pp. 89– 98.

Huettel M., Ziebis W., Forster S., 1996. Flow-induced uptake of particulate matter in permeable sediments. Limnology and Oceanography, vol. 41, no. 2, pp. 309 – 322.

Jobson, H.E., Sayre W.W., 1970. Vertical transfer in open channel flow. Journal of the hydraulics division, Proceedings of the American society of civil engineers, vol. 96, pp. 703-724.

Johansson H., Jonsson K., Forsman J., Wörman A., 2000. Retention of conservative and sorptive solutes in rivers-simultaneous tracer experiments. Science of the Total Environment, vol. 266, pp. 229– 238.

Jones J.B., Mulholland P.J., 2000. Streams and Ground Waters. Academic Press.Ecological Society Journal of Ecology, vol. 88, pp. 728-729.

Jonsson K., Wörman A., 2000. Effect of sorption kinetics on the transport of solutes in streams. Science of the Total Environment, vol. 266, pp. 239– 247.

Kasahara T., Wondzell S.M., 2003. Geomorphic controls on hyporheic exchange flow in mountain streams. Water Resources Research, vol. 39, no. 1.

Maloszewski P. Zuber A., 1990. Mathematical modelling of tracer behavior in short-term experiments in fissured rocks. Water Resources Research, vol. 26, no. 7, pp. 1517– 1528.

Montgomery D.R., Buffington J.M., 1997. Channel–reach morphology in mountain drainage basins. Geological Society of America Bulletin, vol. 109, pp. 596–611.

Nagaoka H,. Ohgaki A.J., 1990. Mass transfer mechanism in a porous riverbed. Water Resources Research, vol. 24, pp. 417–425.

Packman A.I., Bencala K.E., 2000. Modeling surface–subsurface hydrologic interactions. In Streams and Ground Waters, Jones J.A., Mulholland P.J. (eds). Academic Press: San Diego, CA; pp. 45–80.

Packman A.I., Brooks N.H., Morgan J.J., 2000a. Kaolinite exchange between a stream and streambed: Laboratory experiments and validation of a colloid transport model. Water Resources Research, vol. 36, no. 8, pp. 2363– 2372.

Packman A.I., Brooks N.H., Morgan J.J., 2000b. A physicochemical model for colloid exchange between a stream and a sand streambed with bed forms. Water Resources Research, vol. 36, no. 8, pp. 2351– 2361.

Packman A.I., Salehin M., 2003. Relative roles of stream flow and sedimentary conditions in controlling hyporheic exchange. Hydrobiologia, vol. 494, pp. 291–297.

Perk M., Petticrew E.L., Owens P.N., Bierkens M.F.P., Hulsman R., Wubben L., 2011. Estimation of hyporheic exchange rates and transit time distributions in gravel-bed sediments from salt-tracer experiments. Not published.

Ren J.H., Packman A.I., 2005. Coupled stream-subsurface exchange of colloidal hematite and dissolved zinc, copper, and phosphate.
Environmental Science & Technology, vol. 39, no.17, pp. 6387– 6394.

Salehin M., Packman A.I., Wörman A., 2003. Comparison of hyporheic exchange in vegetated and unvegetated reaches of a small agricultural stream in Sweden: Seasonal variation and anthropogenic manipulation. Advances in Water Resources, vol. 26, no. 9, pp. 951– 964.

Salehin M., Packman A.I., Paradis M., 2004. Hyporheic exchange with heterogeneous streambeds: Laboratory experiments and modeling. Water Resources Research, vol. 40.

Shibata H., Sugawara O., Toyoshima H., Wondzell S.M., Nakamura F., Kasahara T., Swanson F.J., Sasa K., 2004. Nitrogen dynamics in the hyporheic zone of a forested stream during a small storm, Hokkaido, Japan. Biogeochemistry, vol. 69, pp. 83–104.

Storey R.G., Howard K.W.F., Williams D.D., 2003. Factors controlling riffle-scale hyporheic exchange flows and their seasonal changes in a gaining stream: A three-dimensional groundwater flow model. Water Resources Research vol. 39, no. 2, pp. 1034.

Thibodeaux L.J., Boyle J.O., 1987. Bed-form generated convective transport in bottom sediment. Nature, vol. 325, pp. 341–343.

Tonina D., Buffington J.M., 2007. Hyporheic exchange in gravel bed rivers with pool-riffle morphology: Laboratory experiments and three-dimensional modelling. Water Resources Research, vol. 43

Vollmer S., de los Santos Ramos F., Daebel H., Kuhn G., 2002. Micro scale exchange processes between surface and subsurface water. Journal of Hydrology, vol. 269, pp. 3–10.

Wondzell S.M., Swanson F.J., 1996. Seasonal and storm dynamics of the hyporheic zone of a 4th-order mountain stream. I: hydrologic processes. Journal of the North American Benthological Society, vol. 15, pp. 1–19.

Wondzell S.M., 2006. Effect of morphology and discharge on hyporheic exchange flows in two small streams in the Cascade Mountains of Oregon, USA. Hydrological Processes, vol. 20, pp. 267–287.

Wörman A., 1998. Analytical solution and timescale for transport of reactive solutes in rivers and streams. Water Resources Research, vol. 34, no. 10, pp. 2703–2716.

Wörman A., 2000. Comparison of models for transient storage in small streams. Water Resources Research, vol. 36, no. 2, pp. 455–468.

Wörman, A., Packman A.I., Johansson H., Jonsson K., 2002. Effect of flow-induced exchange in hyporheic zones on longitudinal transport of solutes in streams and rivers. Water Resources Research, vol. 38, no.1, pp. 1001.

Wörman A., Packman A.I., Marklund L., Harvey J.W., Stone S.H., 2007. Fractal topography and subsurface water flows from fluvial bedforms to the continental shield. Geophysical Research Letters, vol. 34.

Wroblicky G.J., 1998. Seasonal variation in surface-subsurface water exchange and lateral hyporheic area of two stream-aquifer systems. Water Resources Research, vol. 34, no. 3, pp. 317–328.

Wroblicky G.J., Campana M.E., Valett H.M., Dahm C.N., 1998. Seasonal variation in surface–subsurface water exchange and lateral hyporheic area of two stream–aquifer systems. Water Resources Research, vol. 34, pp. 317–328.

Zeng C., Li C.W., 2012. Modeling flows over gravel beds by a drag force method and a modified S–A turbulence closure. Advances in Water Resources, vol. 46, pp. 84–95.

Zhou D., Mendoza C., 1993. Flow through porous bed of turbulent stream. Journal of Engineering Mechanics, vol. 119, pp. 365–383.

Appendices

Appendix 1: Injection experiments

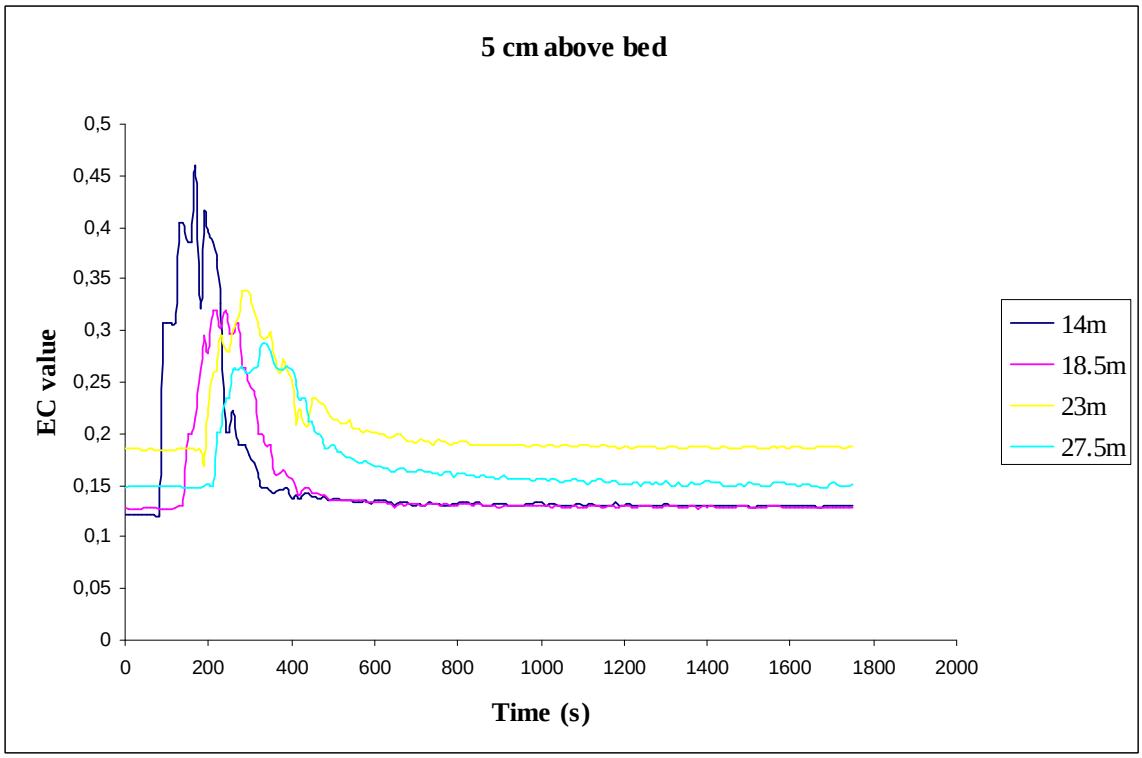

Figure 23, EC measurements for all nodes 5 cm above the bed for experiment 2.

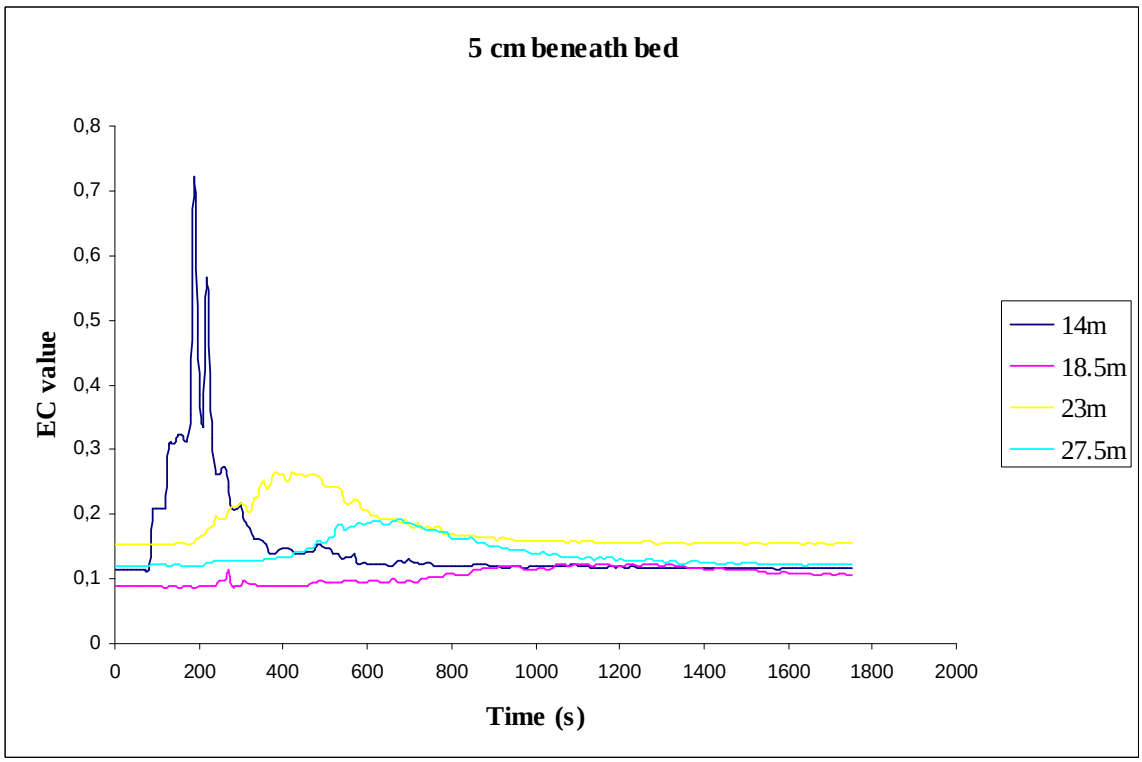

Figure 24, EC measurements for all nodes 5 cm beneath the bed for experiment 2.

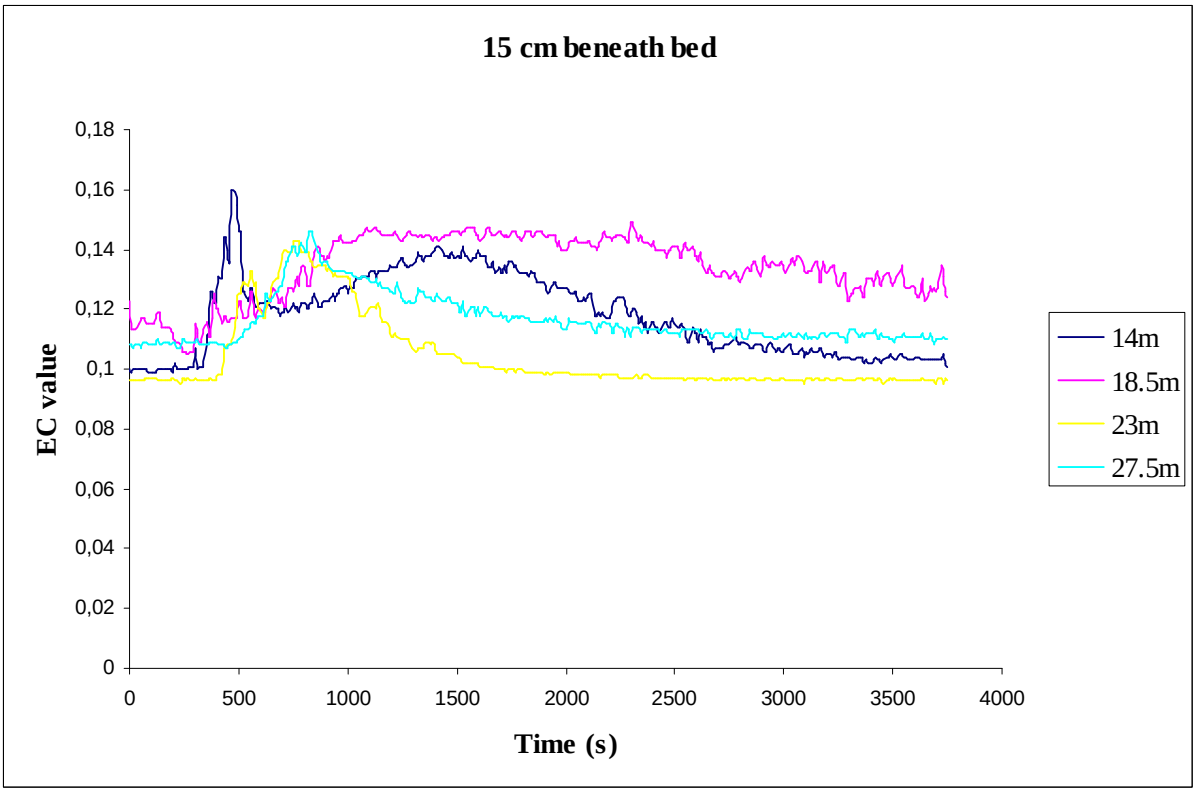

Figure 25, EC measurements for all nodes 15 cm beneath the bed for experiment 2.

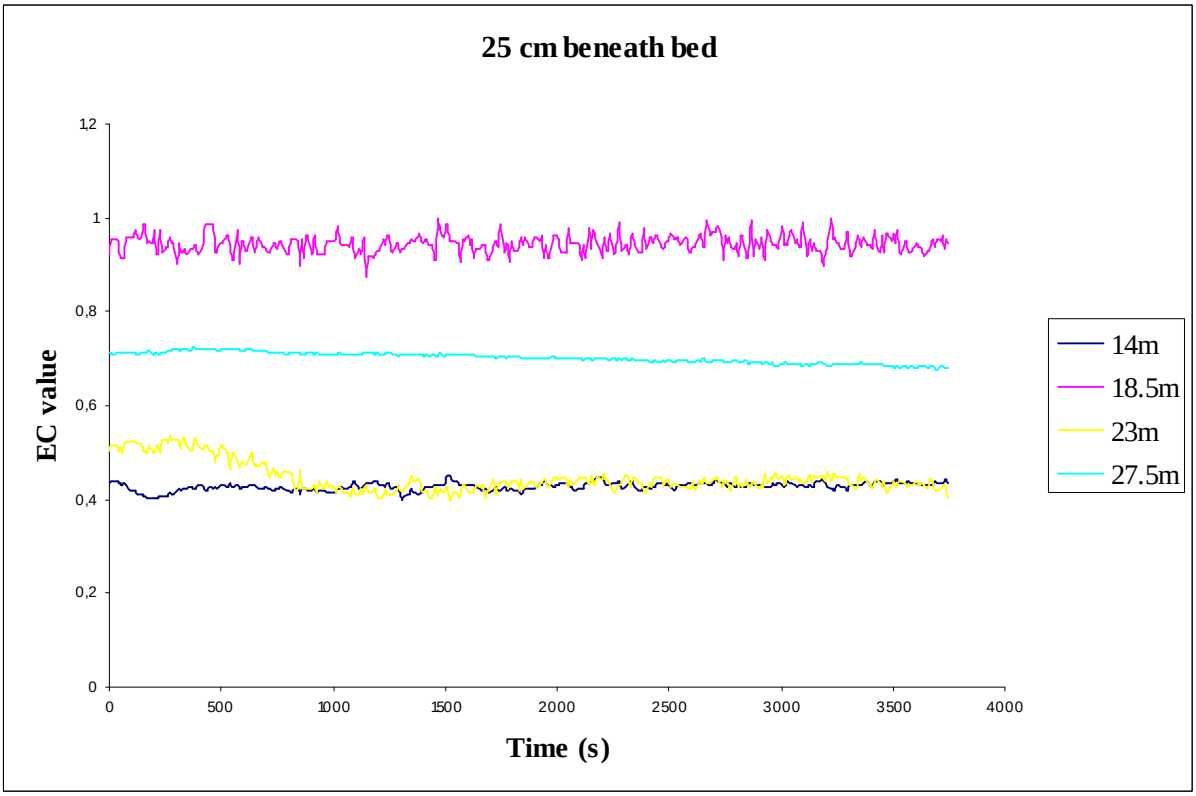

Figure 26, EC measurements for all nodes 25 cm beneath the bed for experiment 2.

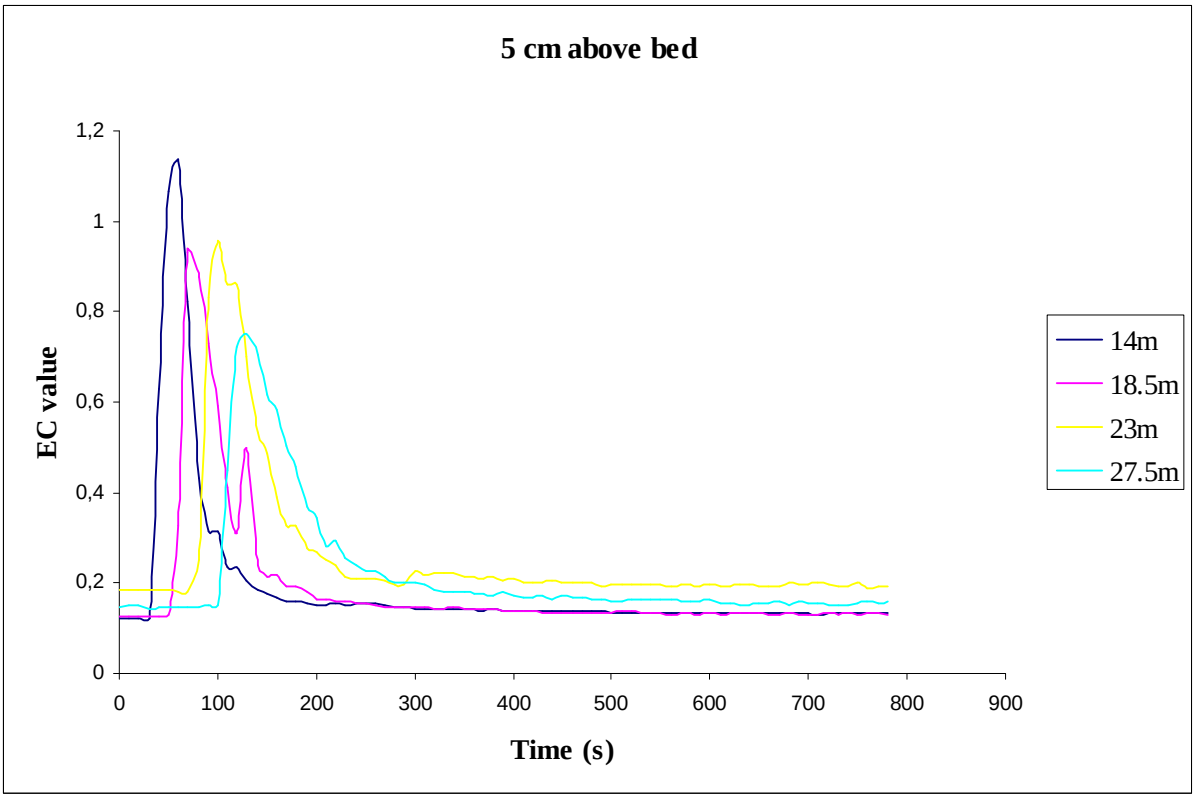

Figure 27, EC measurements for all nodes 5 cm above the bed for experiment 4.

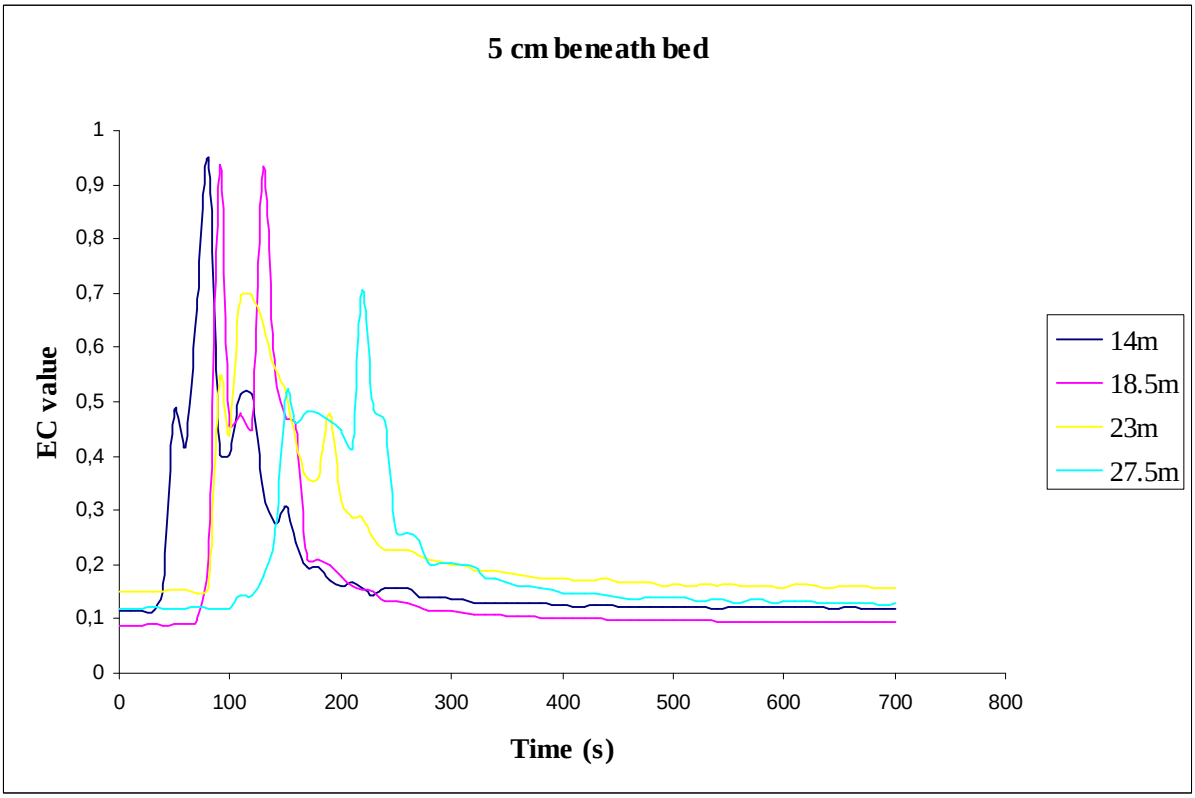

Figure 28, EC measurements for all nodes 5 cm beneath the bed for experiment 4.

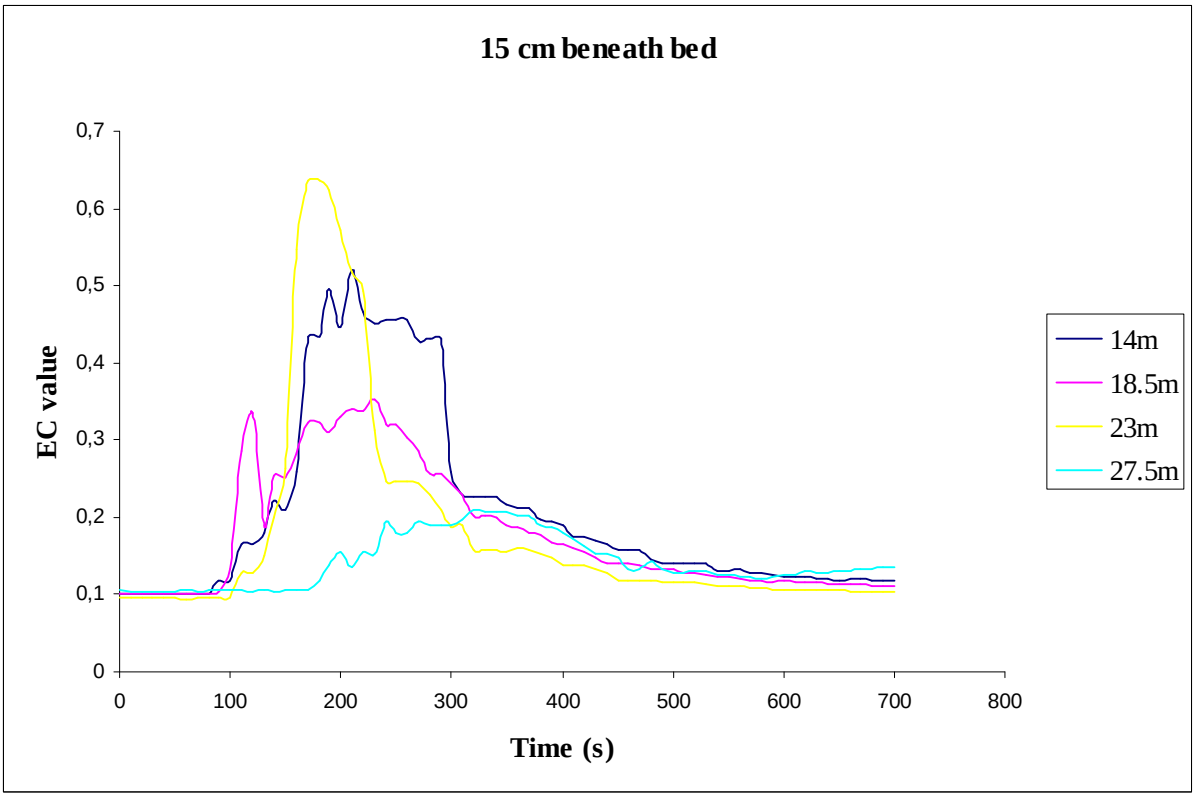

Figure 29, EC measurements for all nodes 15 cm beneath the bed for experiment 4.

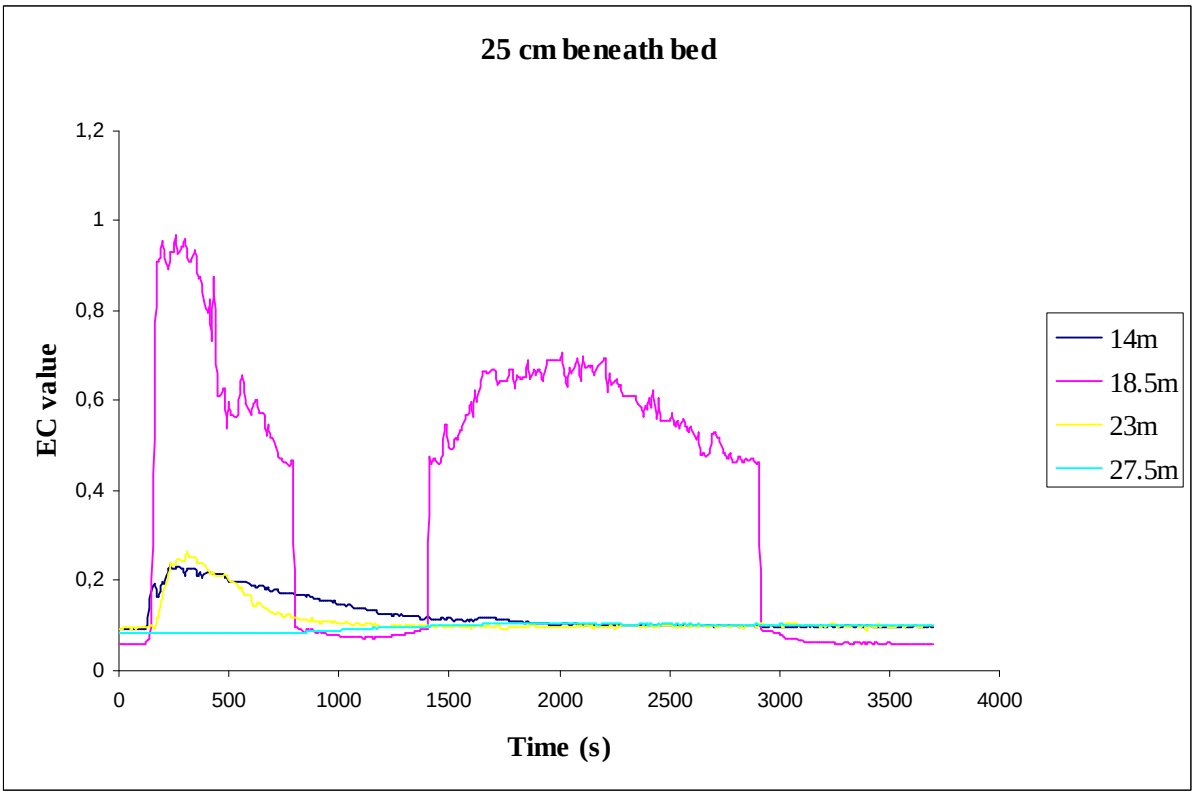

Figure 30, EC measurements for all nodes 25 cm beneath the bed for experiment 4.

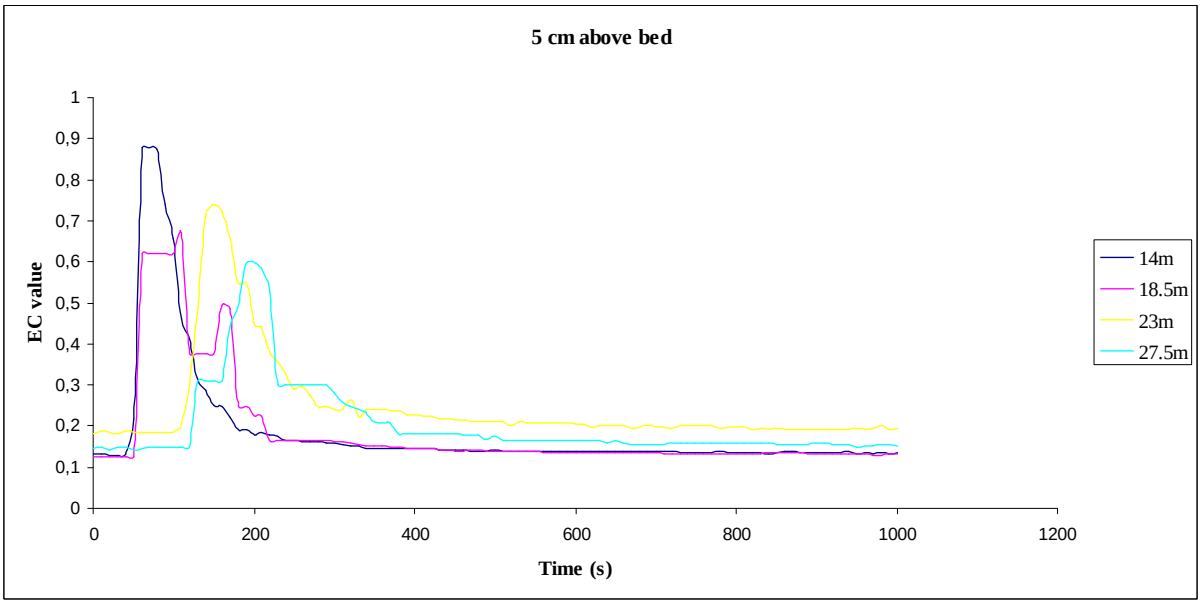

Figure 31, EC measurements for all nodes 5 cm above the bed for experiment 6.

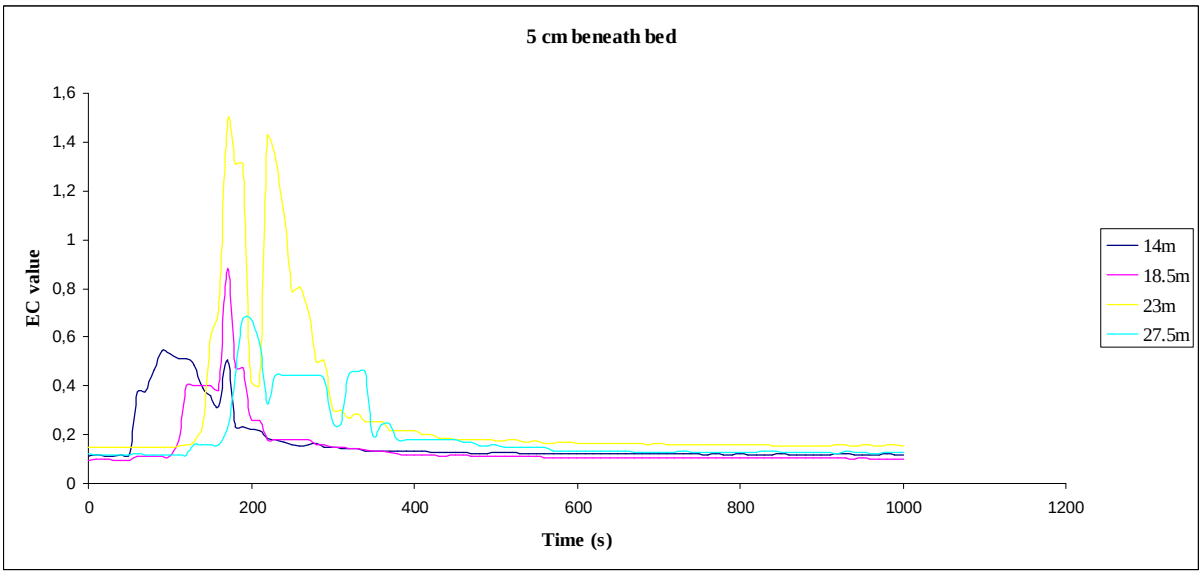

Figure 32, EC measurements for all nodes 5 cm beneath the bed for experiment 6.

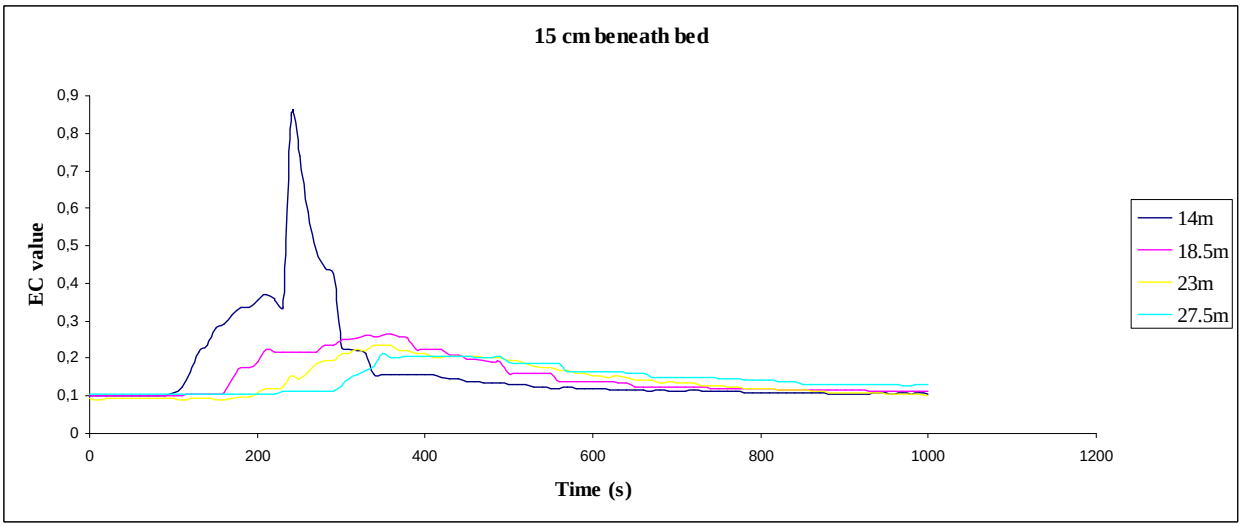

Figure 33, EC measurements for all nodes 15 cm beneath the bed for experiment 6.

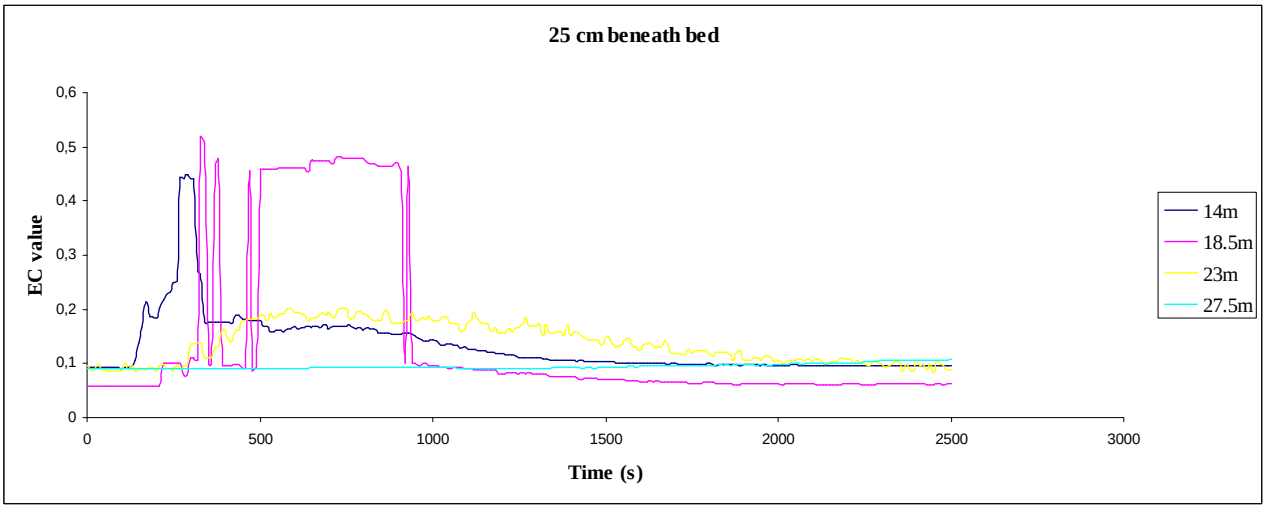

Figure 34, EC measurements for all nodes 25 cm beneath the bed for experiment 6.

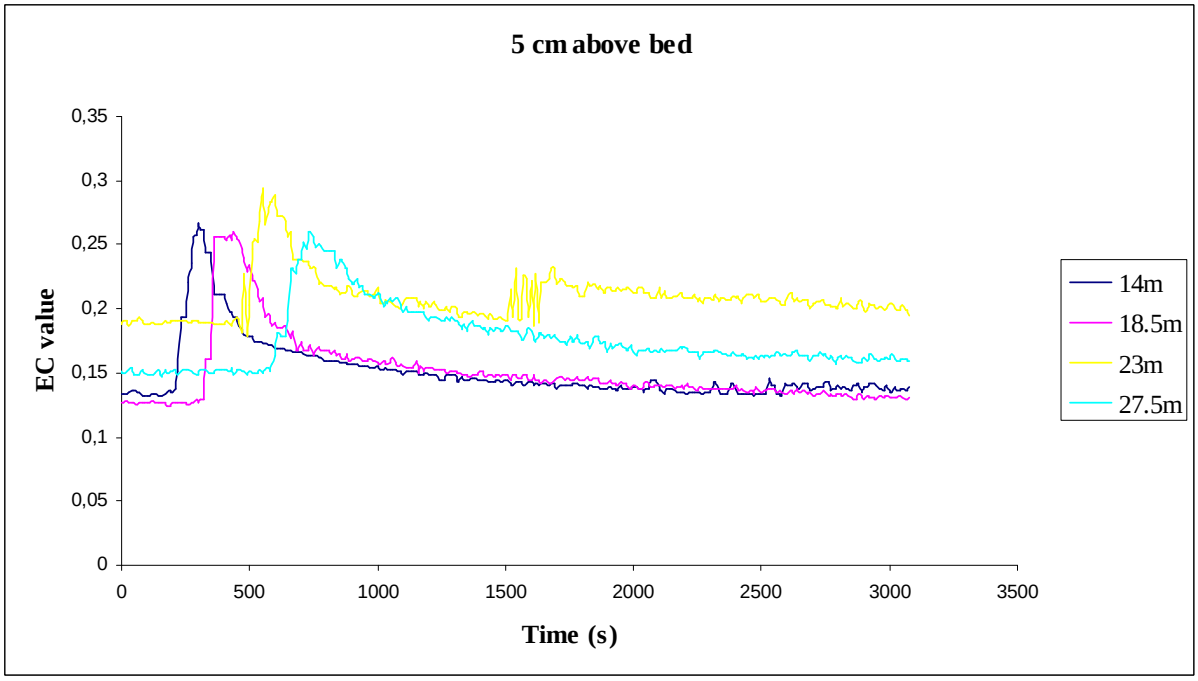

Figure 35, EC measurements for all nodes 5 cm above the bed for experiment 8.

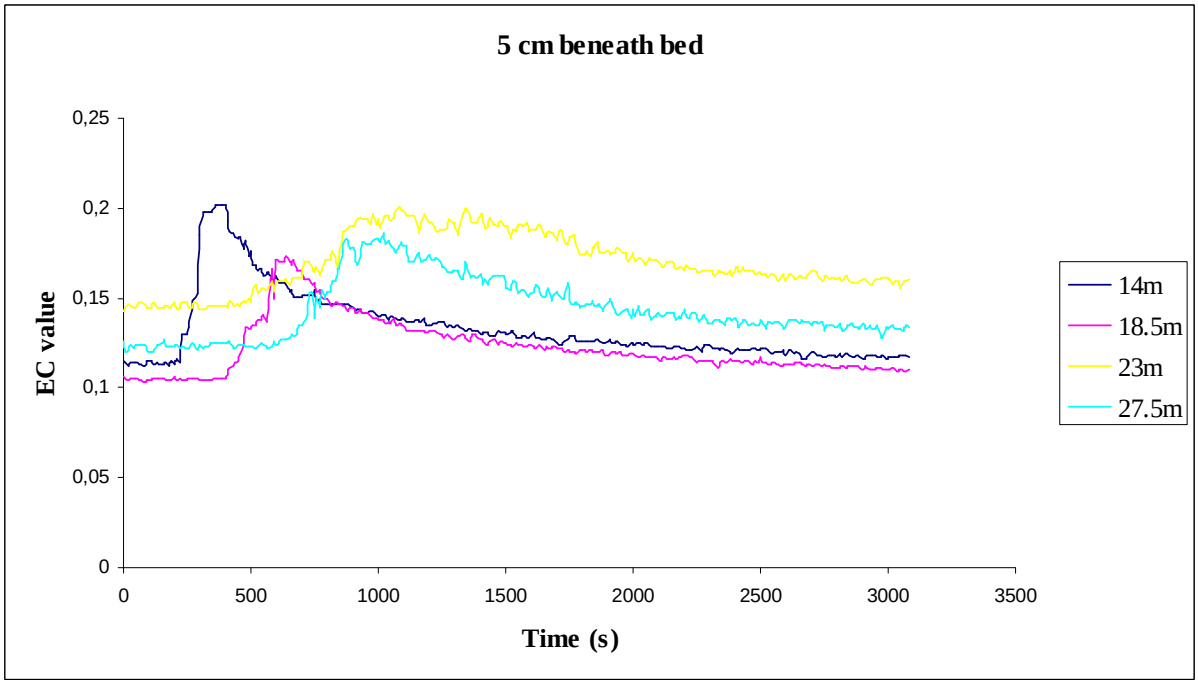

Figure 36, EC measurements for all nodes 5 cm beneath the bed for experiment 8.

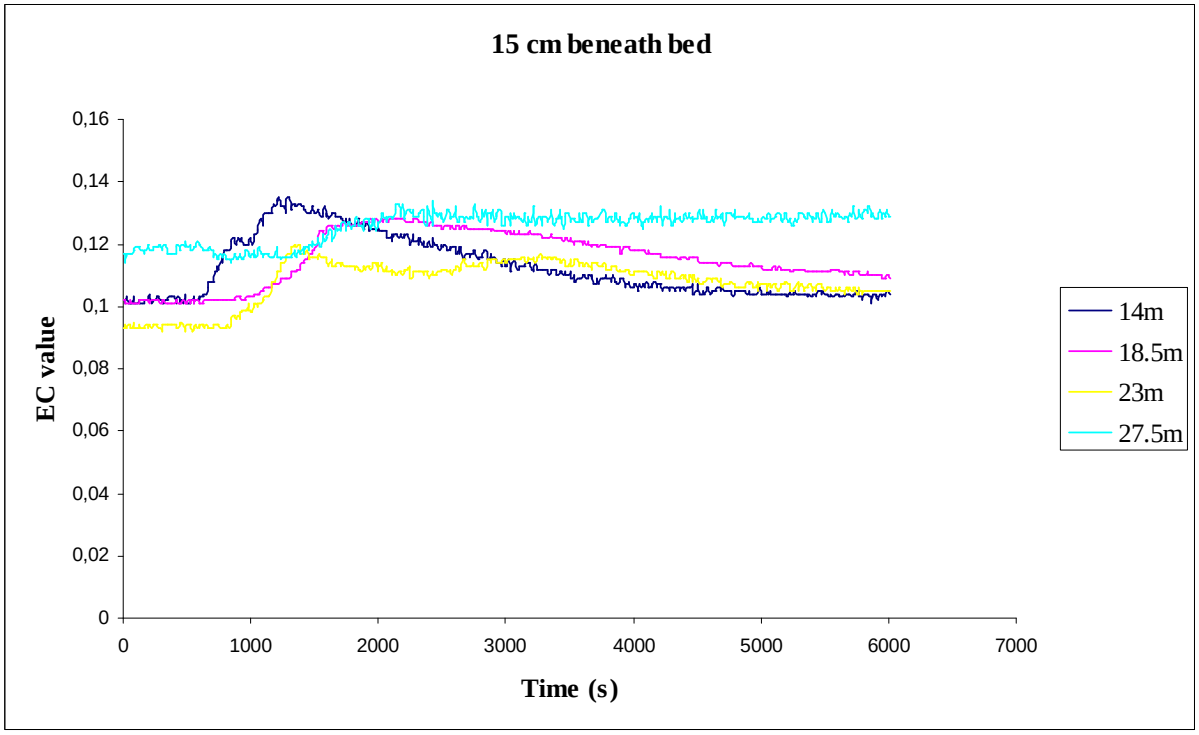

Figure 37, EC measurements for all nodes 15 cm beneath the bed for experiment 8.

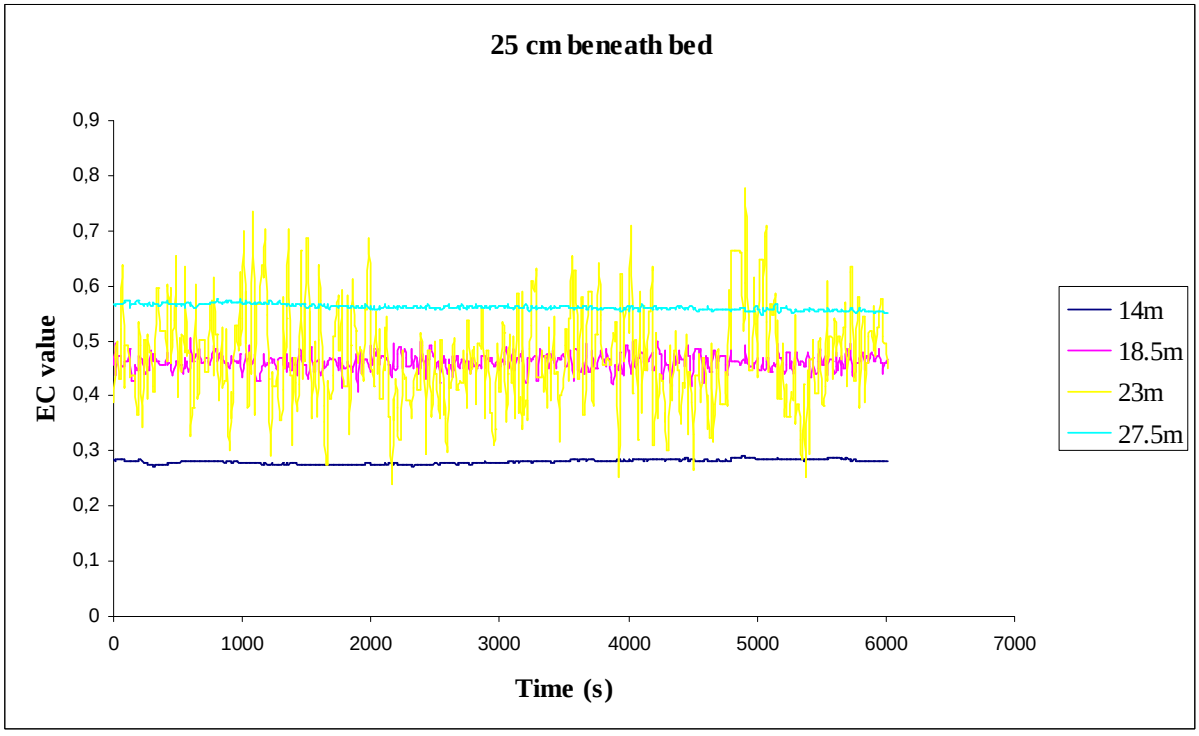

Figure 38, EC measurements for all nodes 25 cm beneath the bed for experiment 8.

Appendix 2 : Sensitivity analysis

Zeta

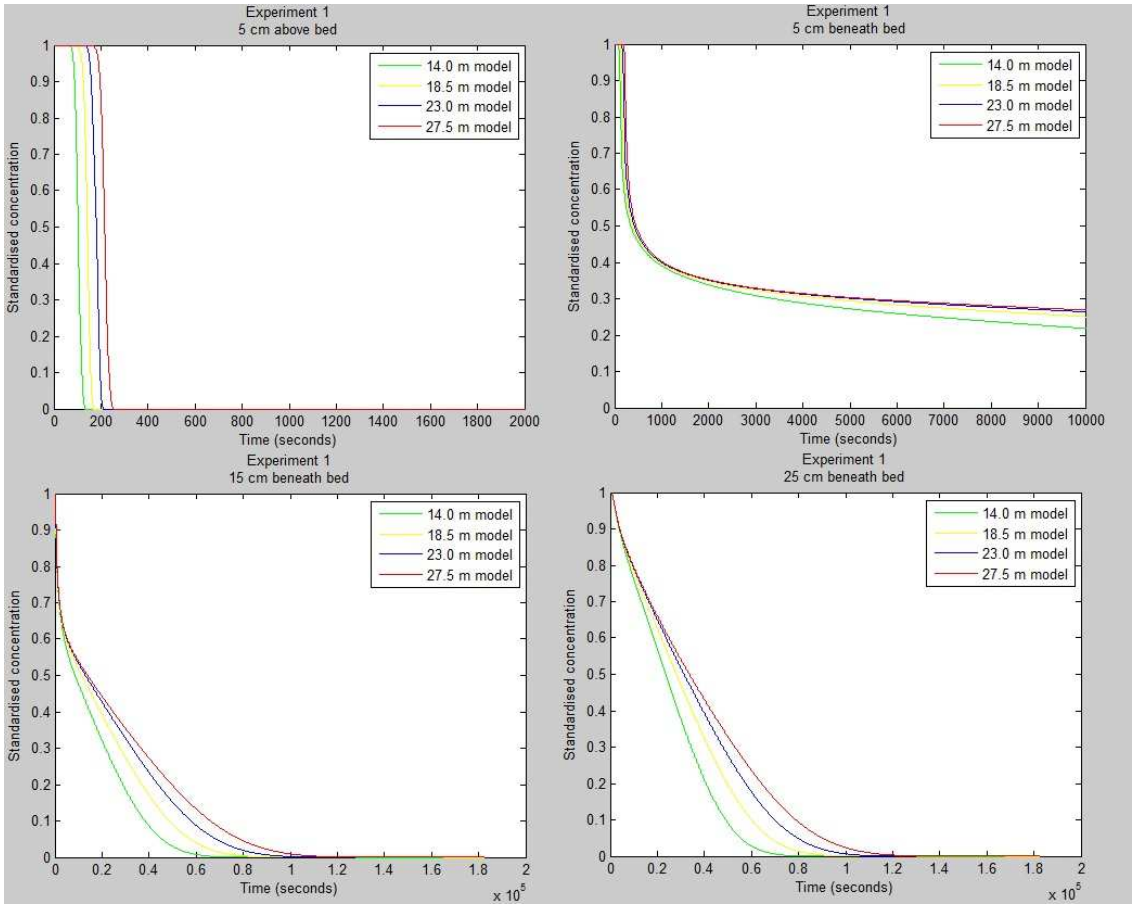

Figure 39, model results of experiment 1, with zeta = 1.0 and beta = 1.0.

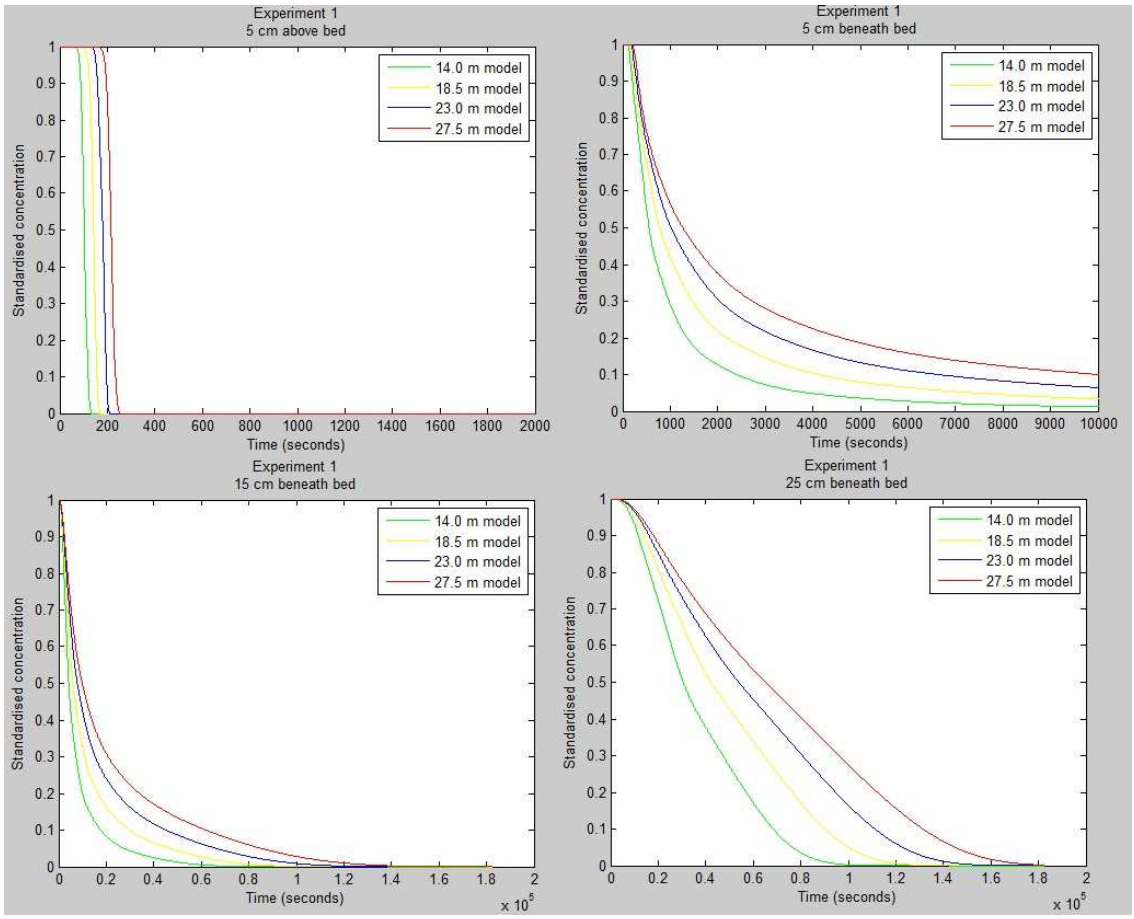

Figure 40, model results of experiment 1, with zeta = 2.0 and beta = 1.0.

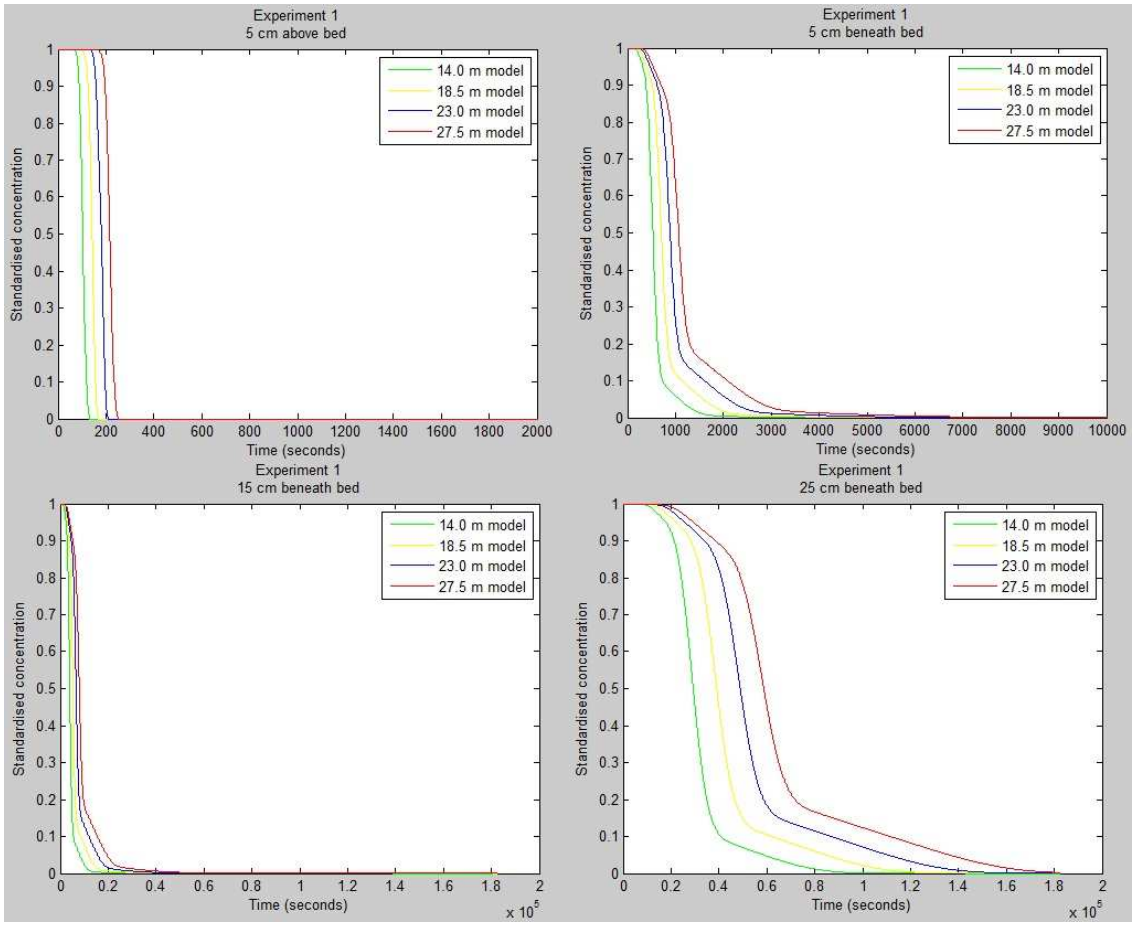

Figure 41, model results of experiment 1, with zeta = 3.0 and beta = 1.0.

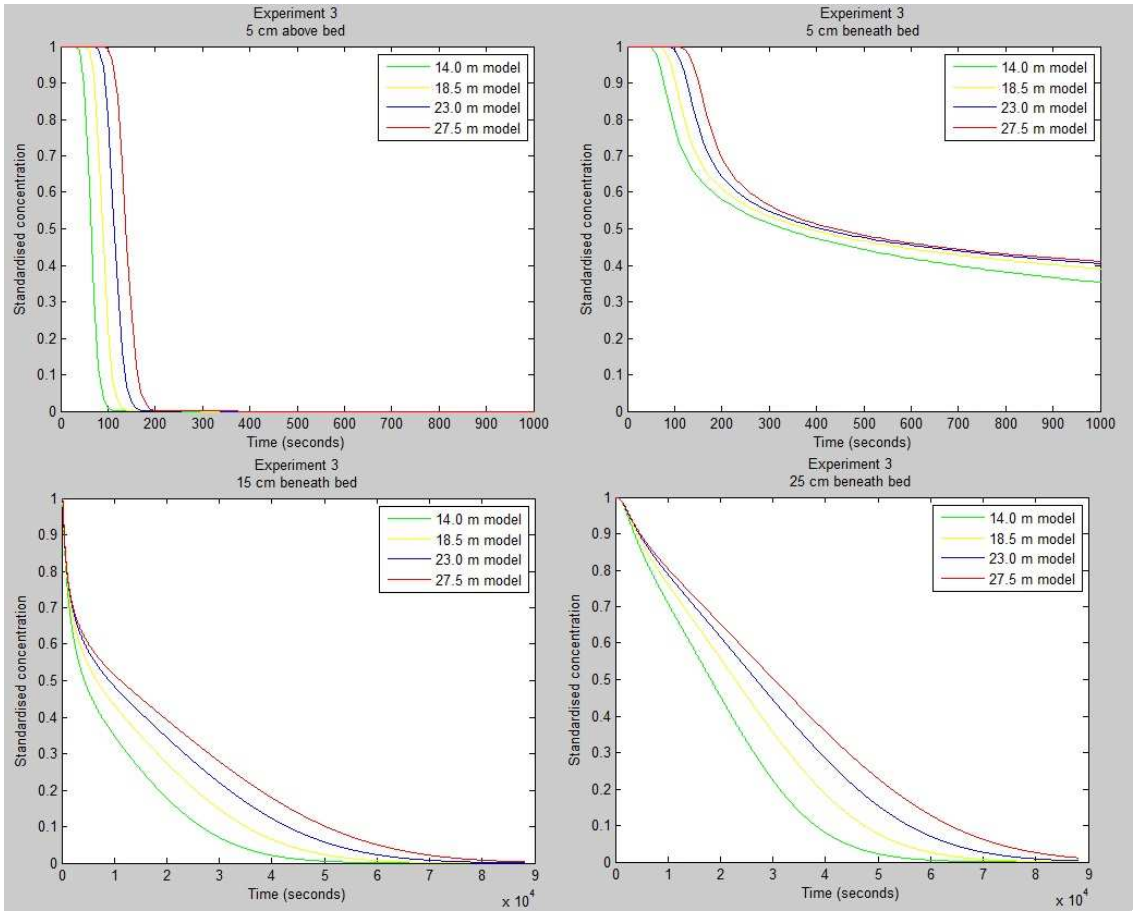

Figure 42, model results of experiment 3, with zeta = 1.0 and beta = 1.0.

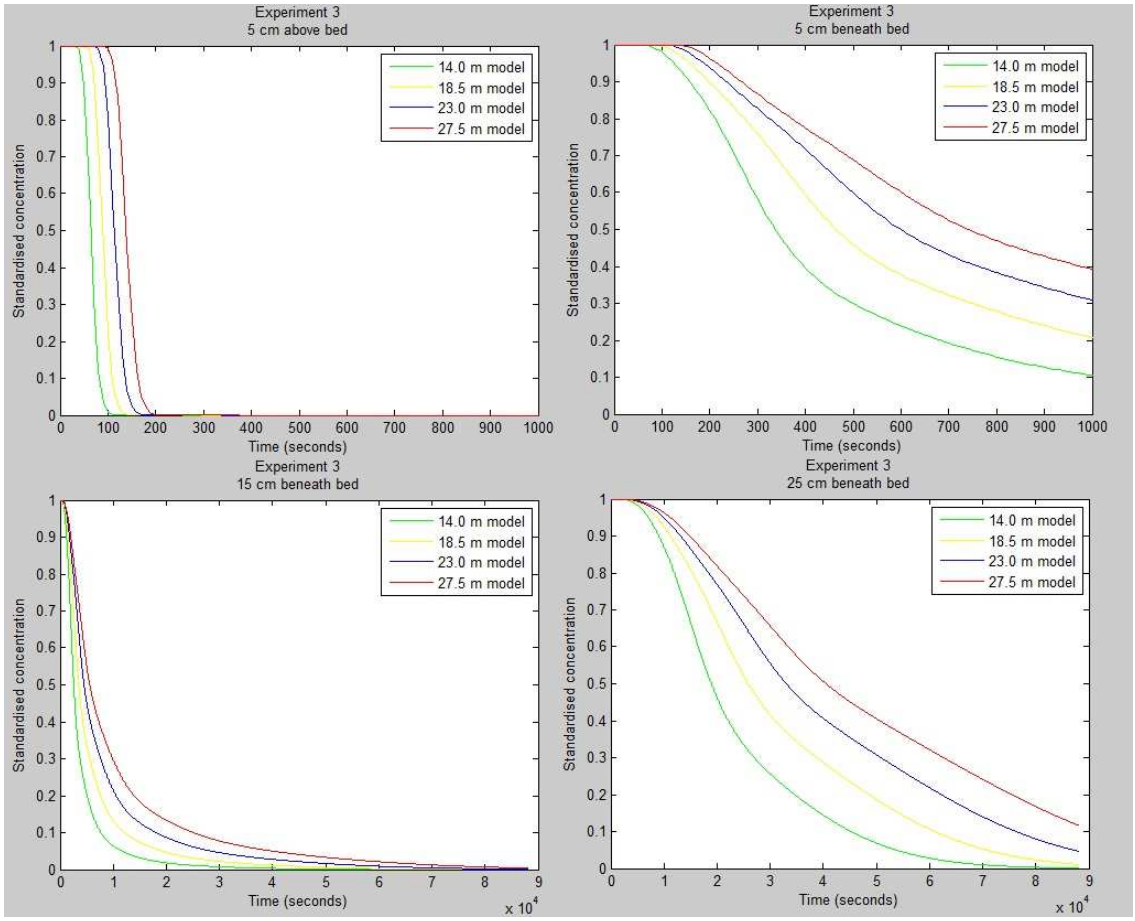

Figure 43, model results of experiment 3, with zeta = 2.0 and beta = 1.0.

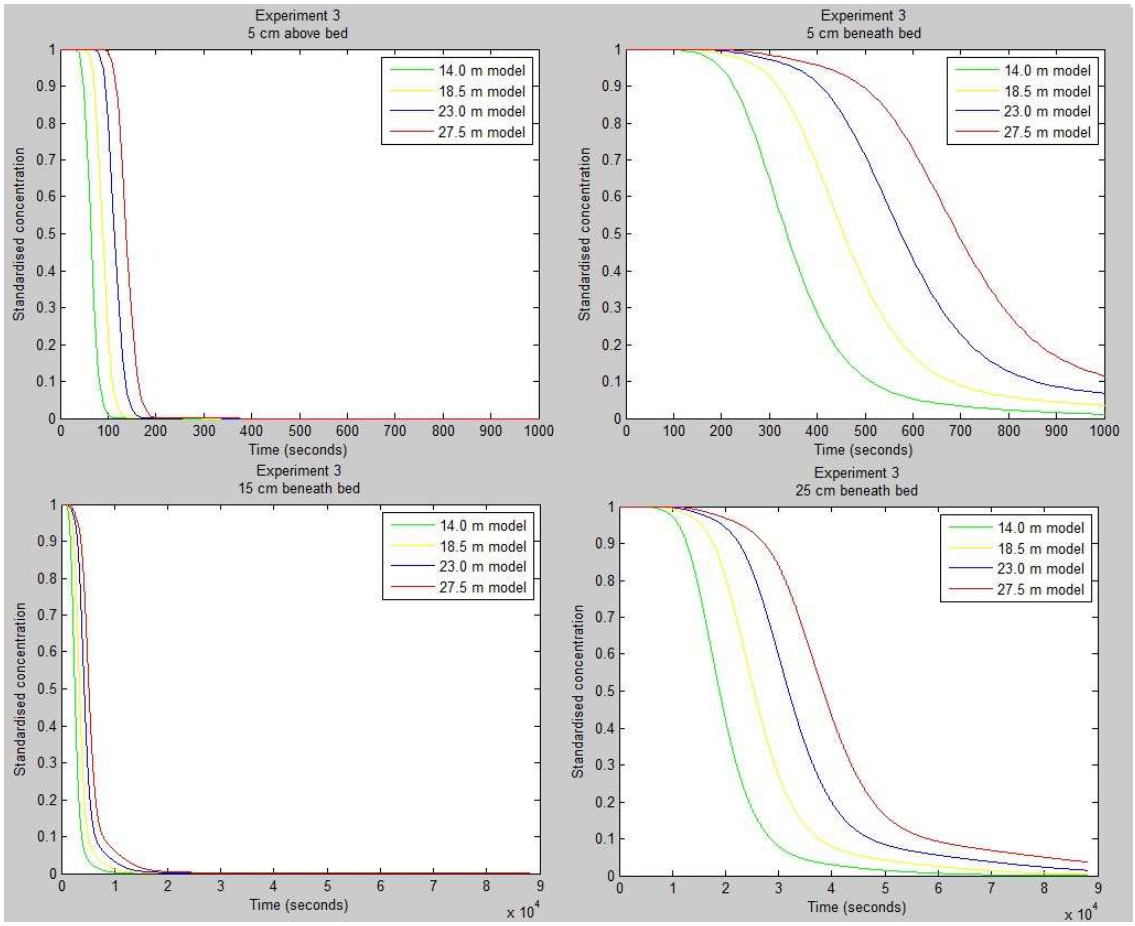

Figure 44, model results of experiment 3, with zeta = 3.0 and beta = 1.0.

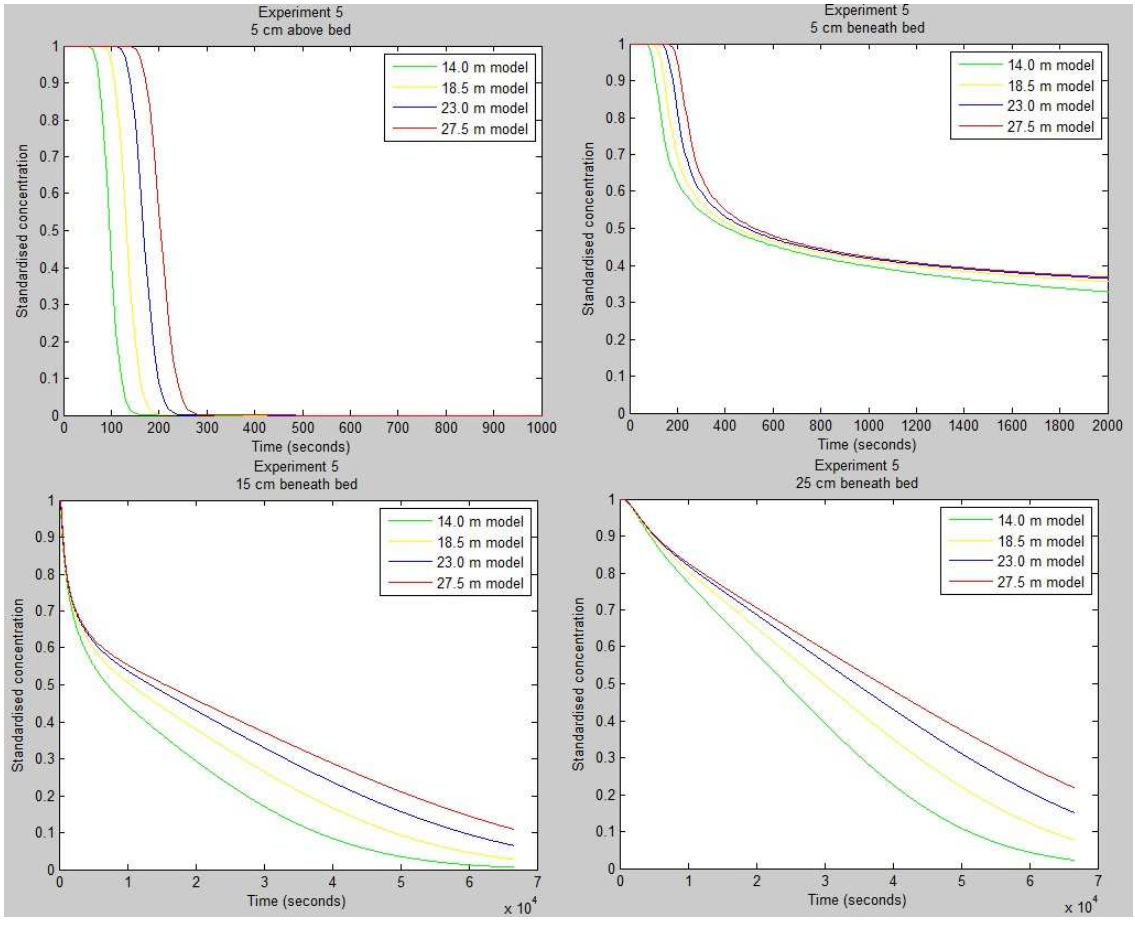

Figure 45, model results of experiment 5, with zeta = 1.0 and beta = 1.0.

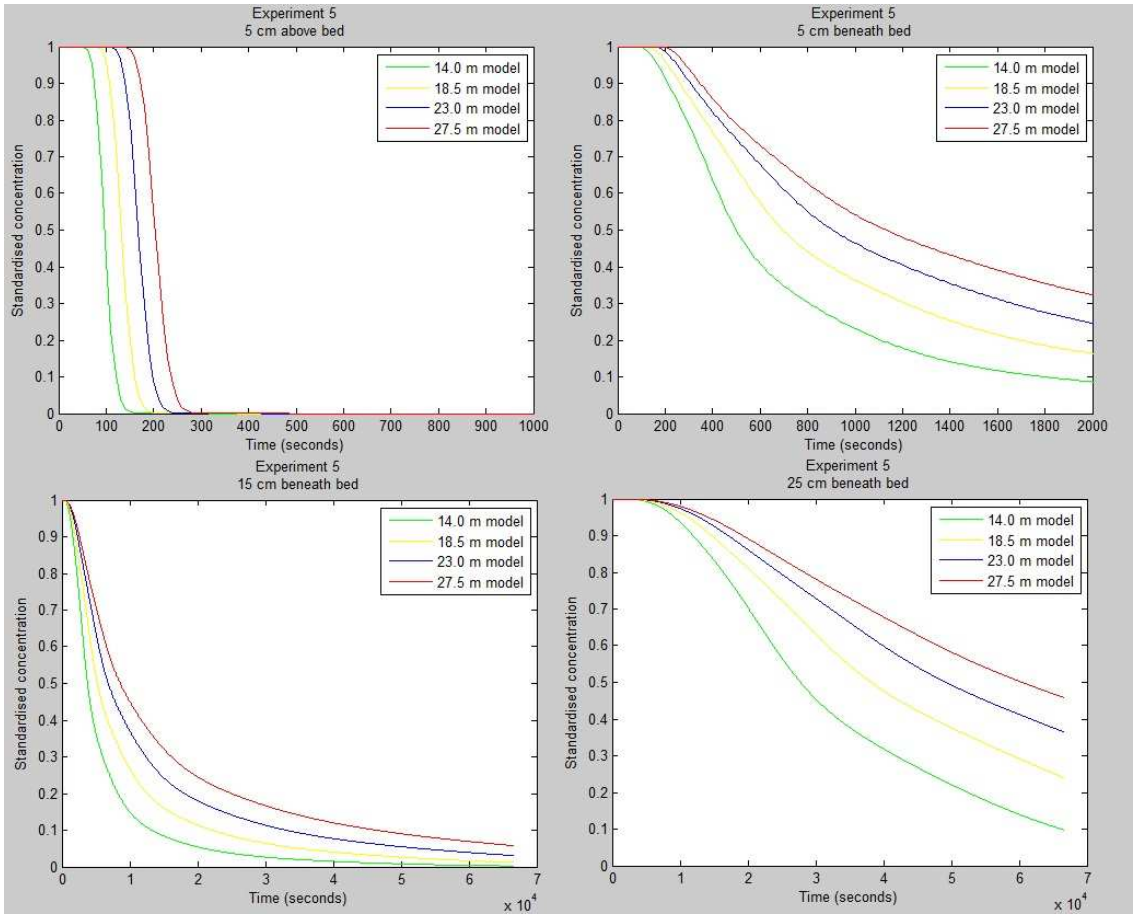

Figure 46, model results of experiment 5, with zeta = 2.0 and beta = 1.0.

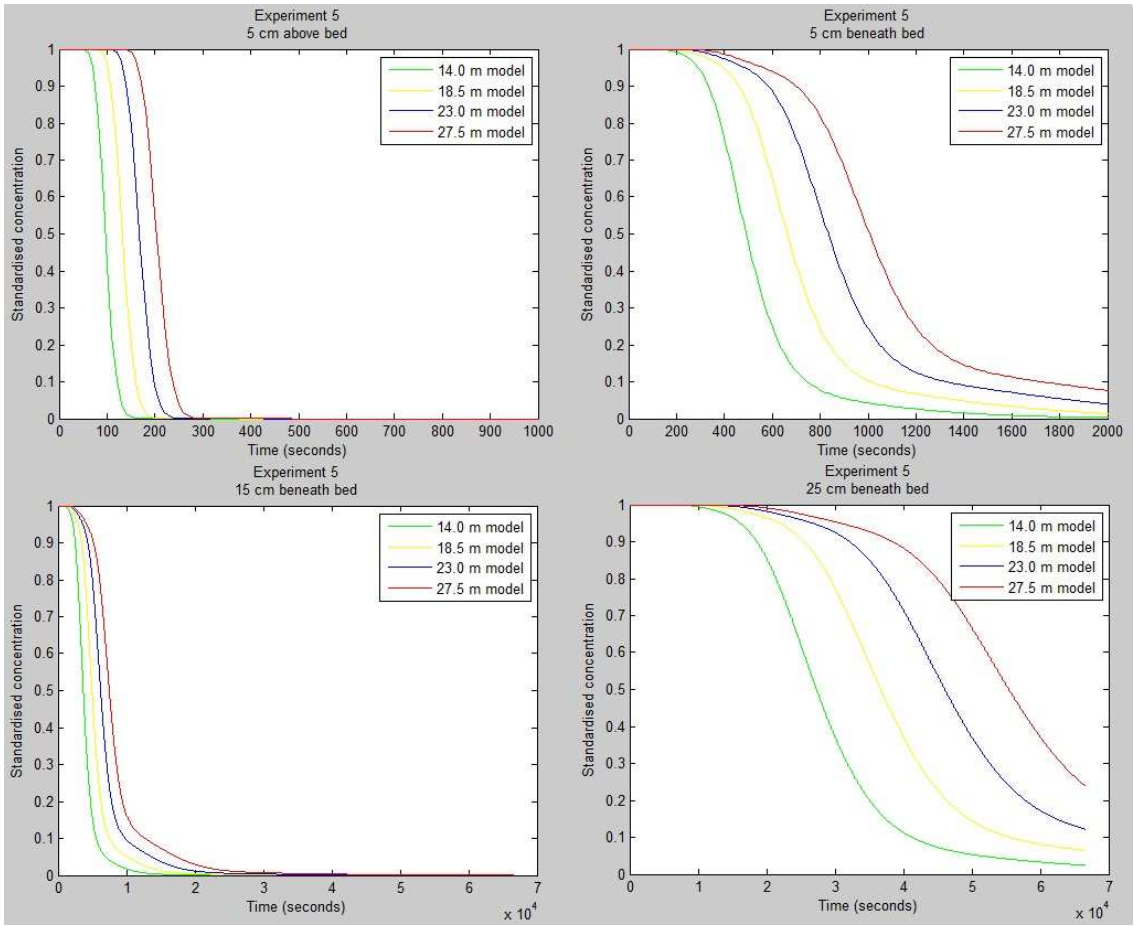

Figure 47, model results of experiment 5, with zeta = 3.0 and beta = 1.0.

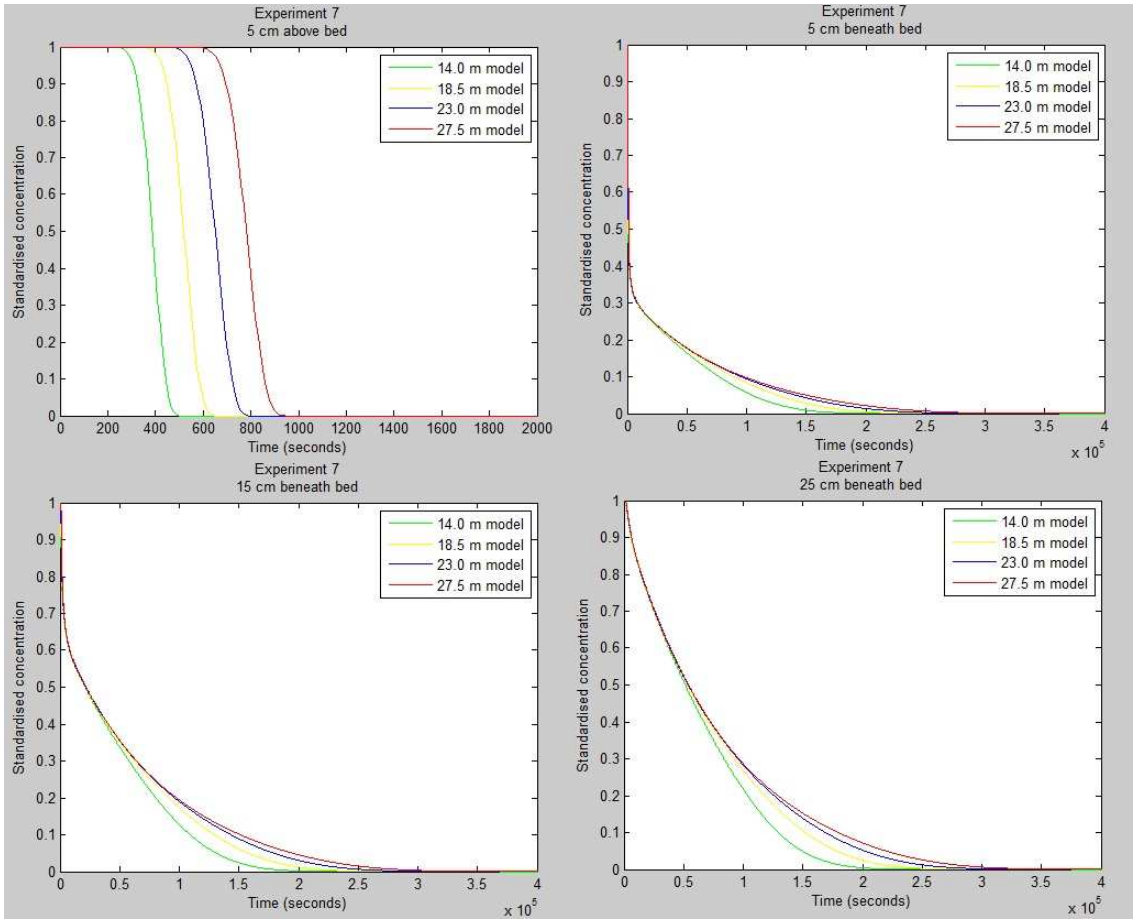

Figure 48, model results of experiment 7, with zeta = 1.0 and beta = 1.0.

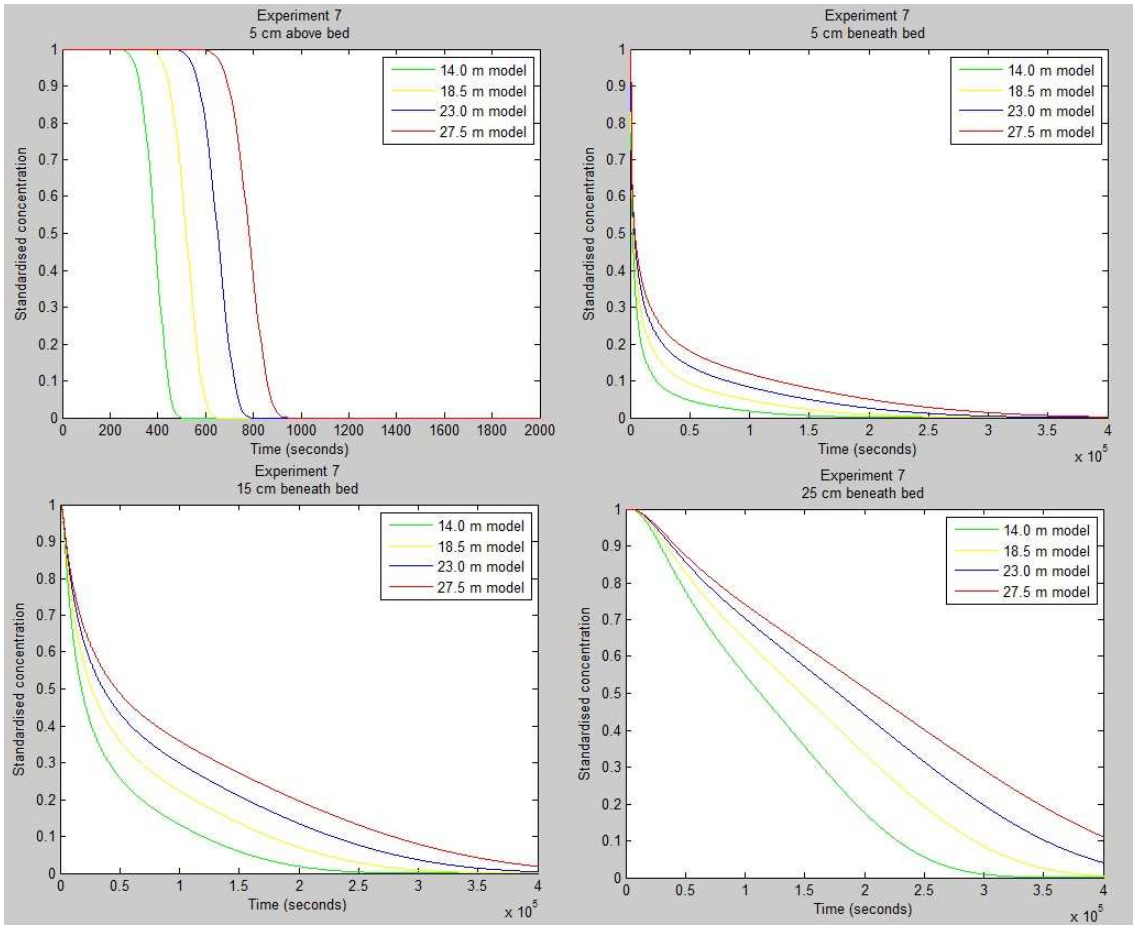

Figure 49, model results of experiment 7, with zeta = 2.0 and beta = 1.0.

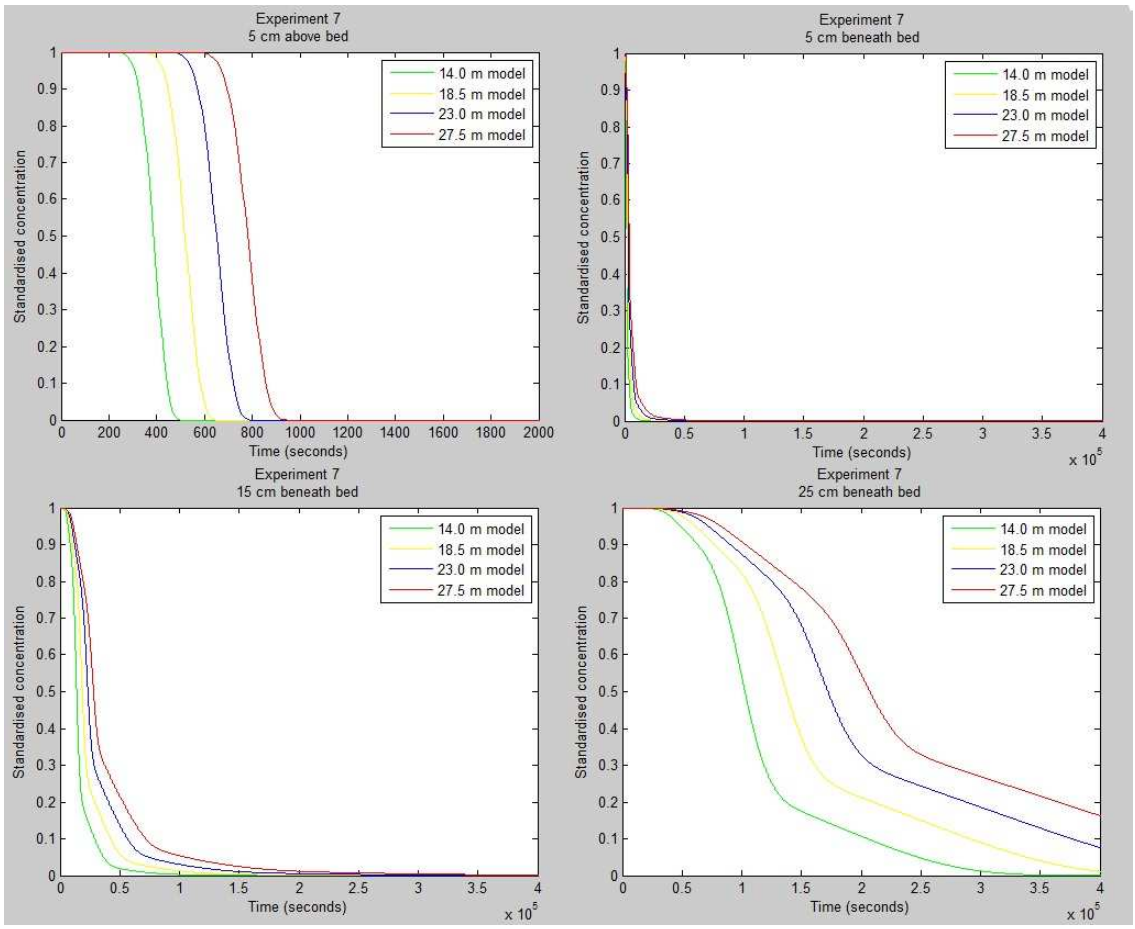

Figure 50, model results of experiment 7, with zeta = 3.0 and beta = 1.0.

Beta

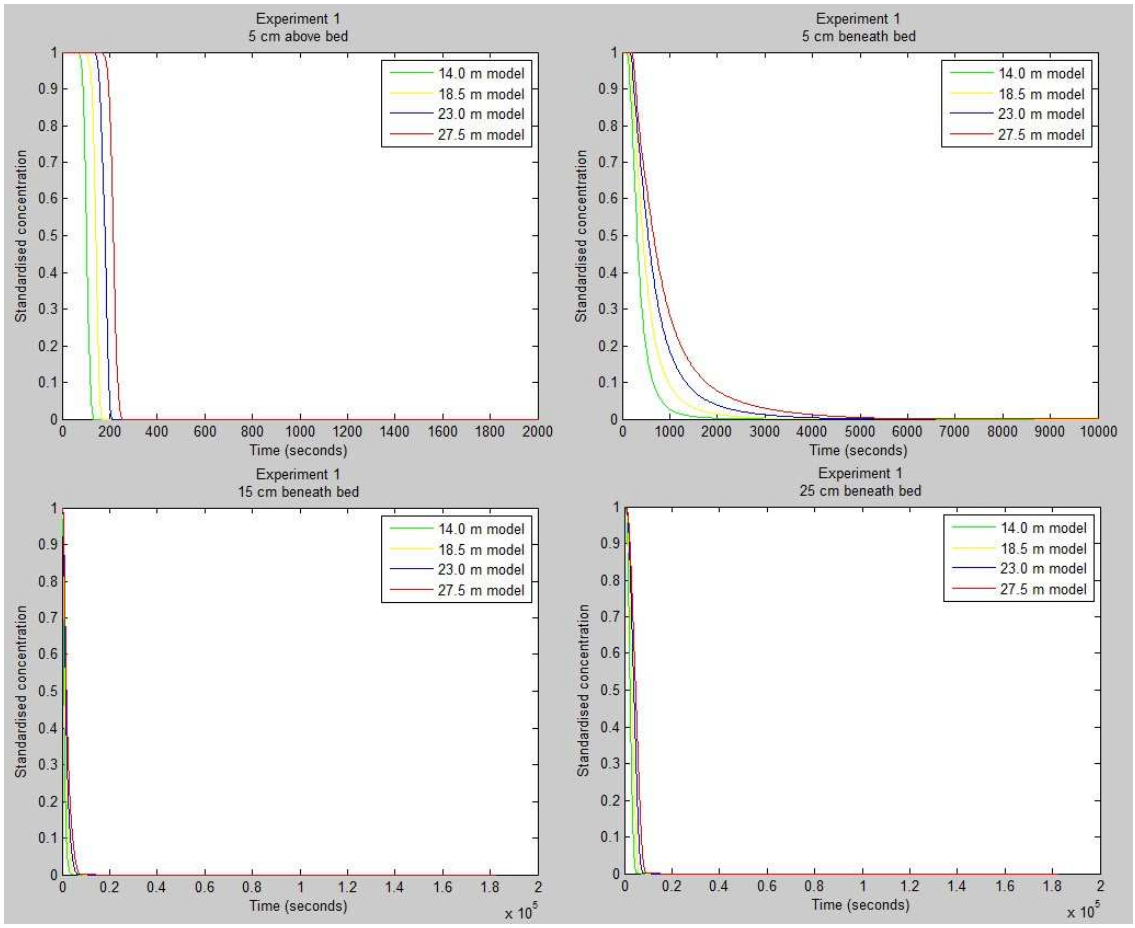

Figure 51, model results of experiment 1, with zeta = 2.0 and beta = 0.5.

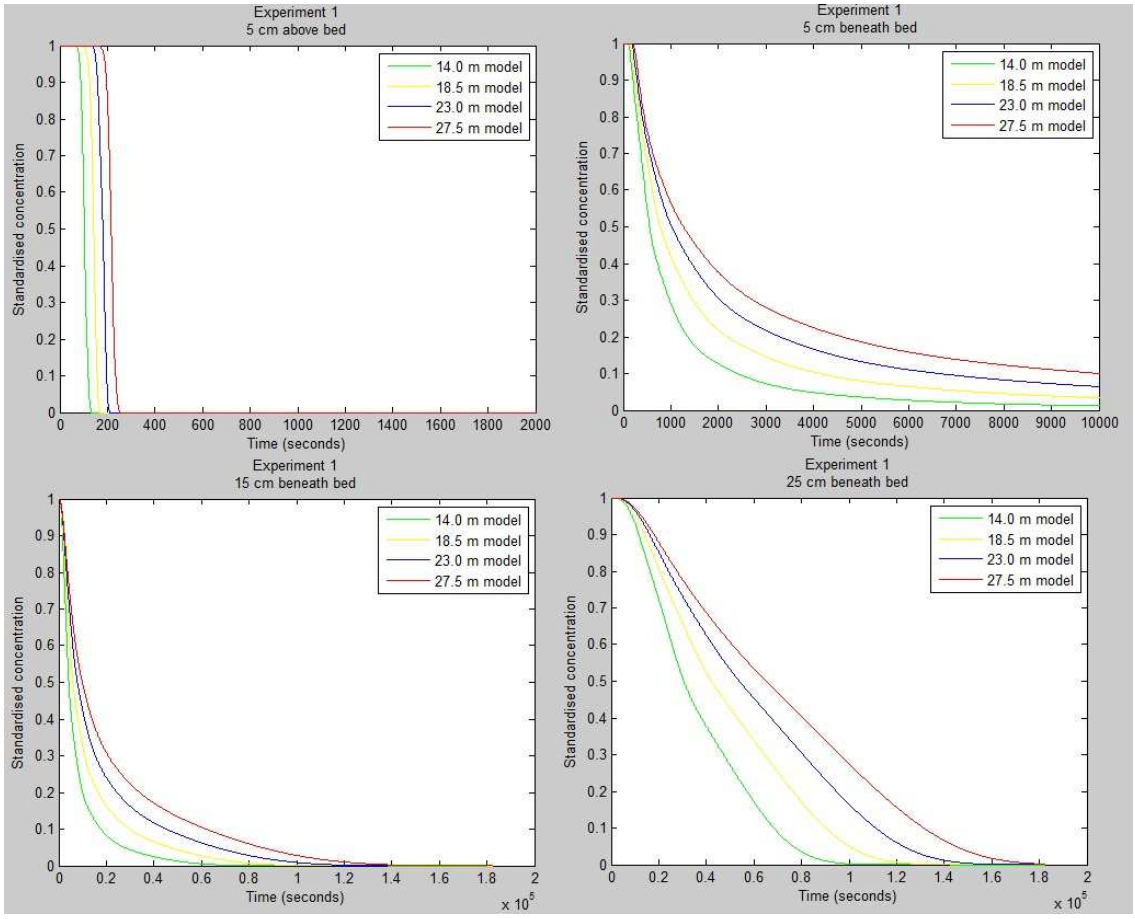

Figure 52, model results of experiment 1, with zeta = 2.0 and beta = 1.0.

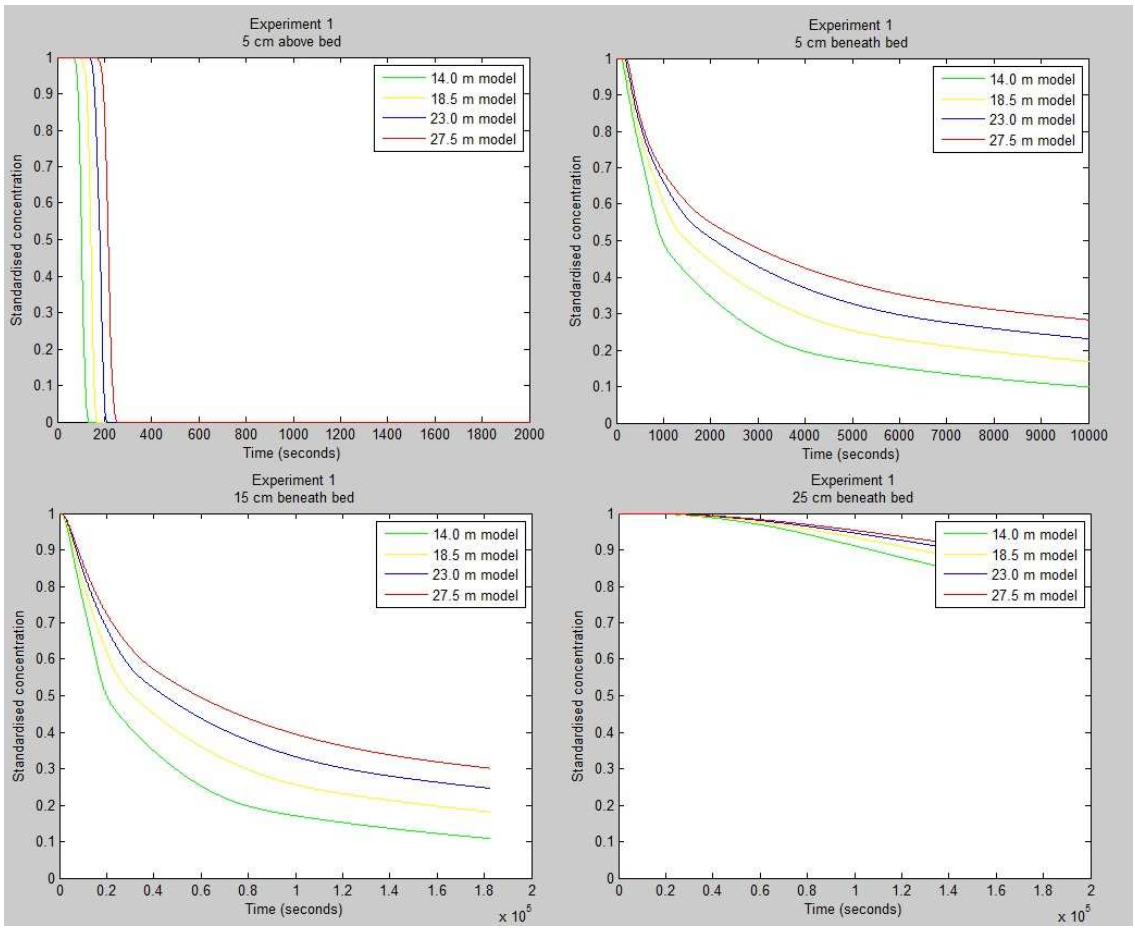

Figure 53, model results of experiment 1, with zeta = 2.0 and beta = 1.5.

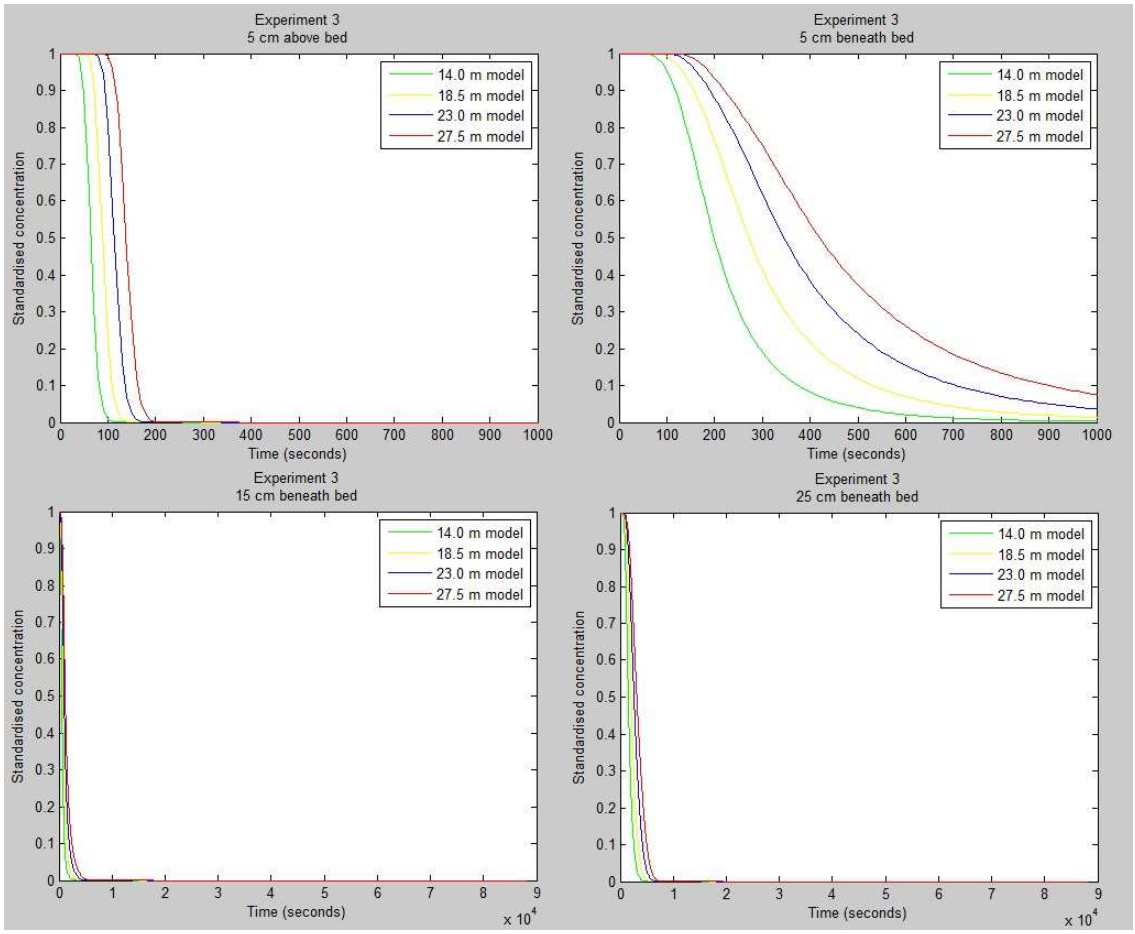

Figure 54, model results of experiment 3, with zeta = 2.0 and beta = 0.5.

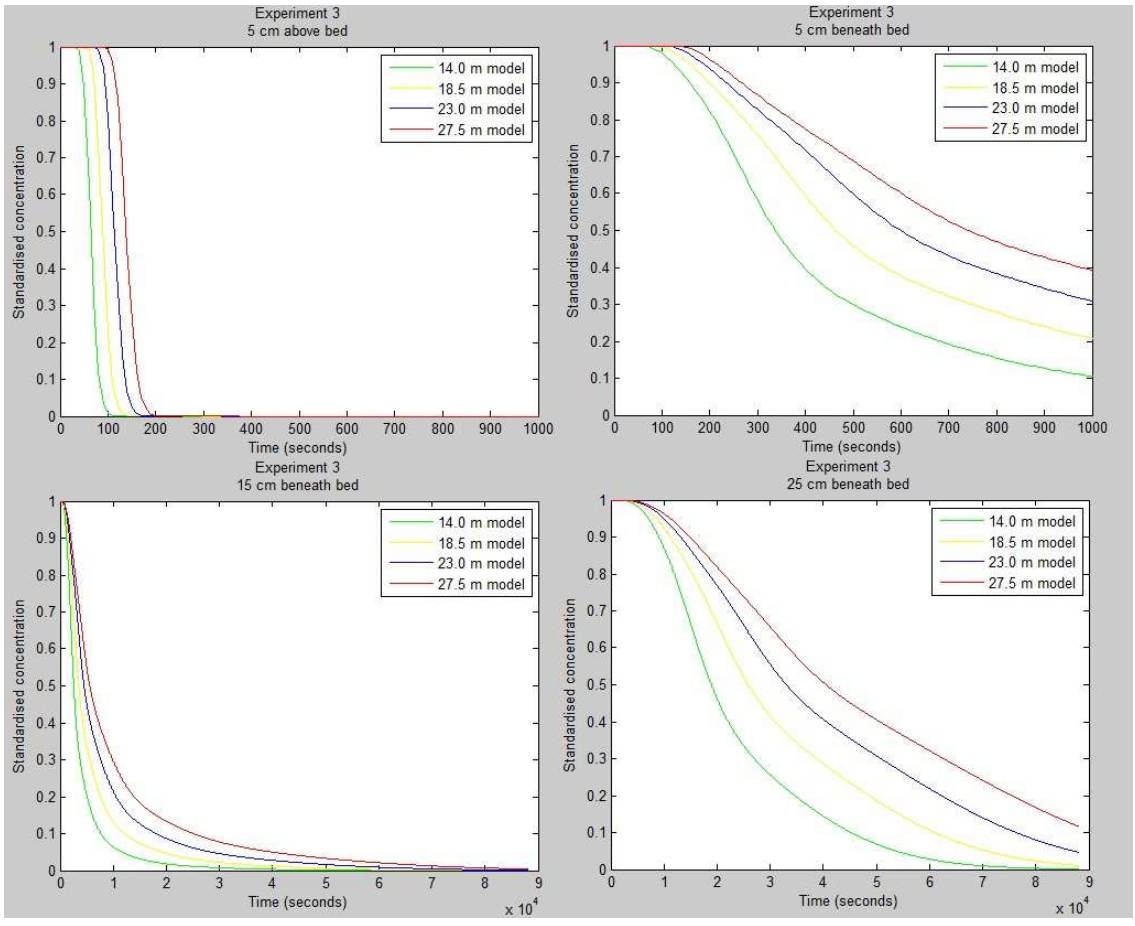

Figure 55, model results of experiment 3, with zeta = 2.0 and beta = 1.0.

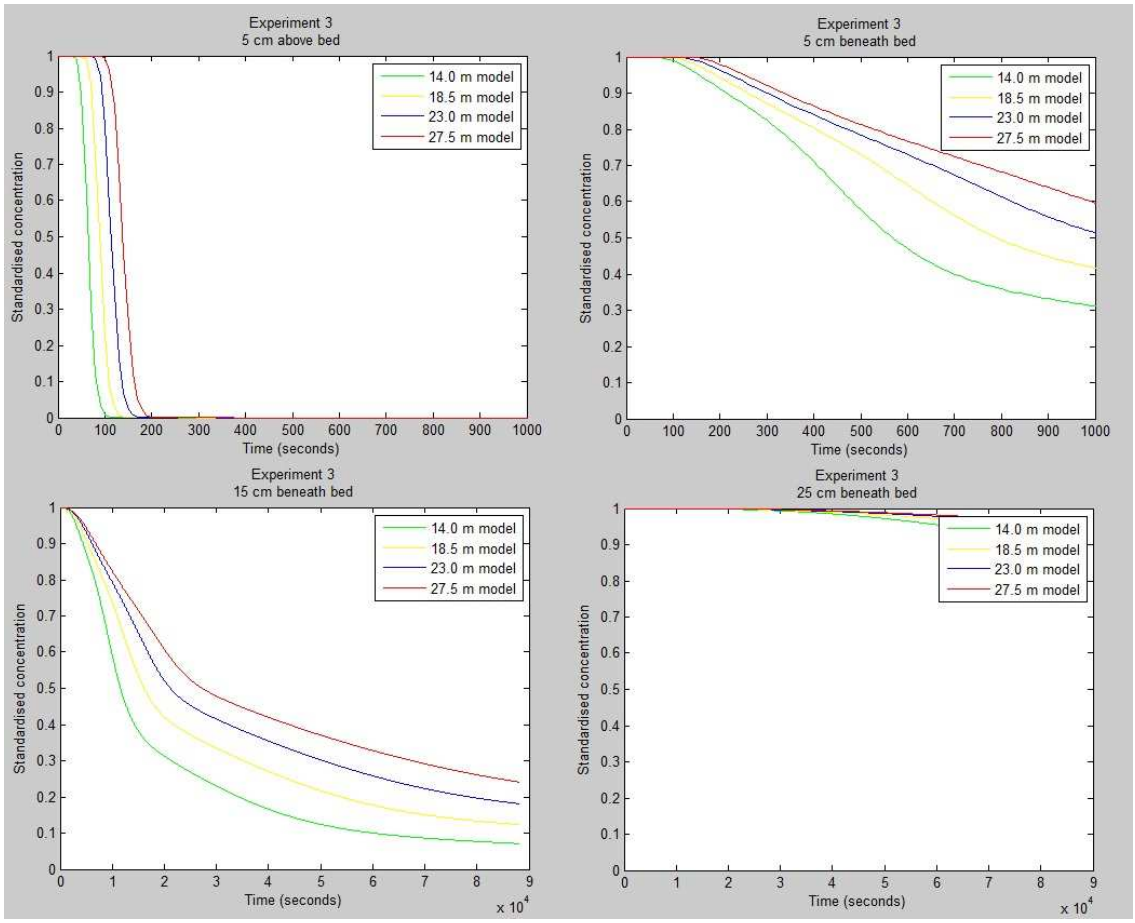

Figure 56, model results of experiment 3, with zeta = 2.0 and beta = 1.5.

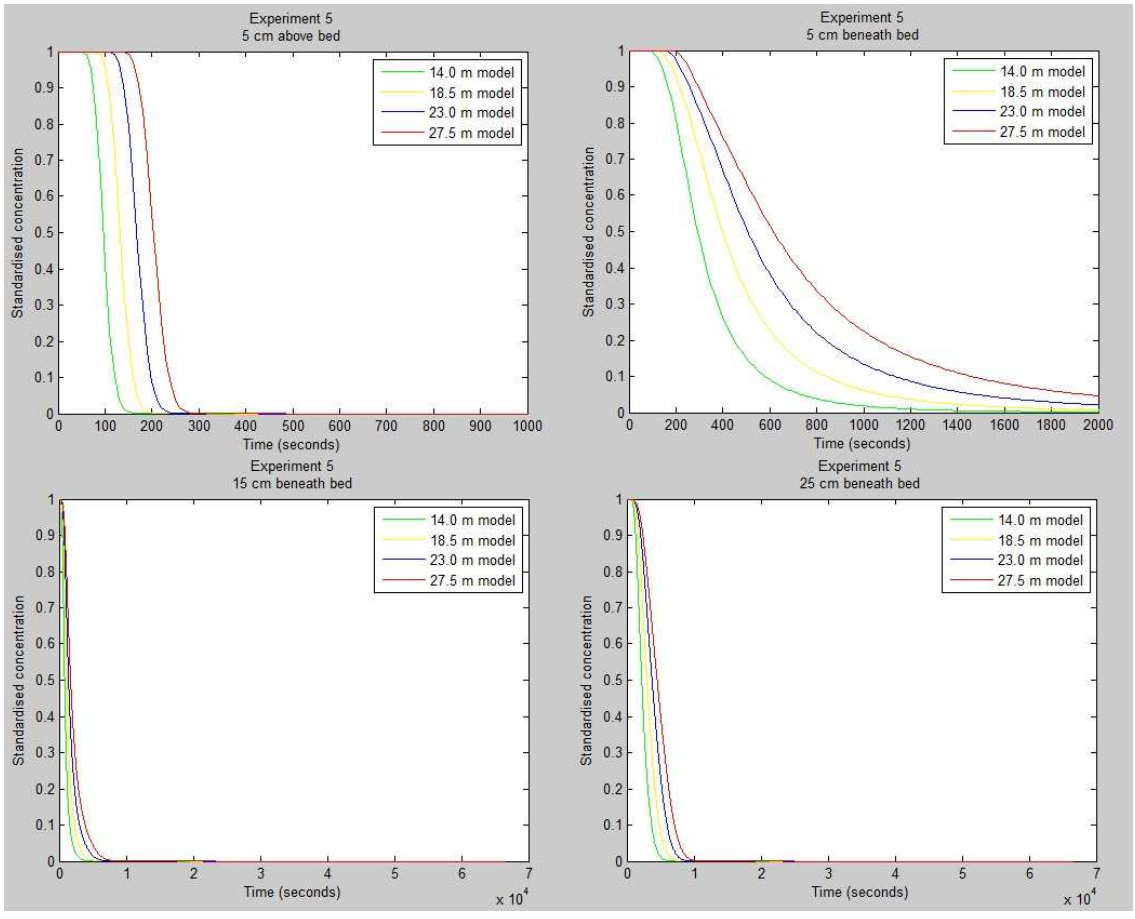

Figure 57, model results of experiment 5, with zeta = 2.0 and beta = 0.5.

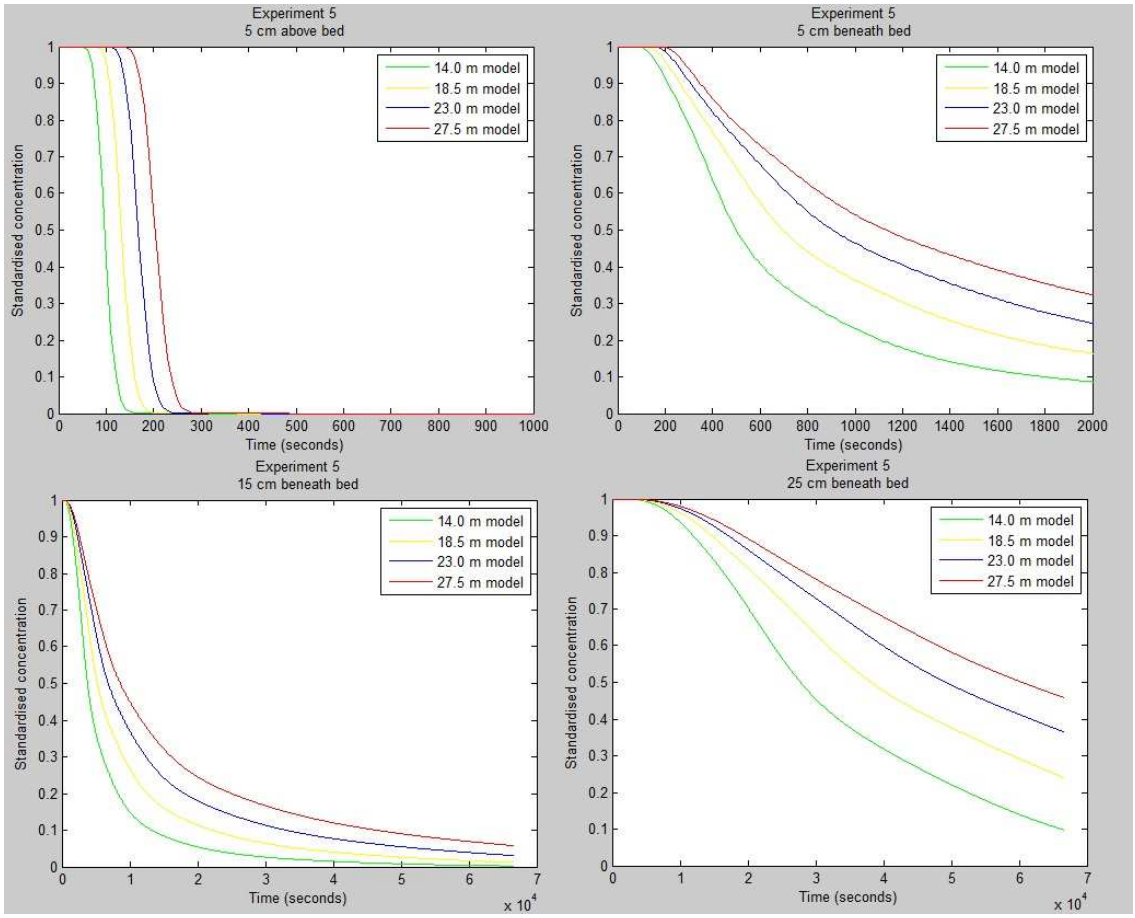

Figure 58, model results of experiment 5, with zeta = 2.0 and beta = 1.0.

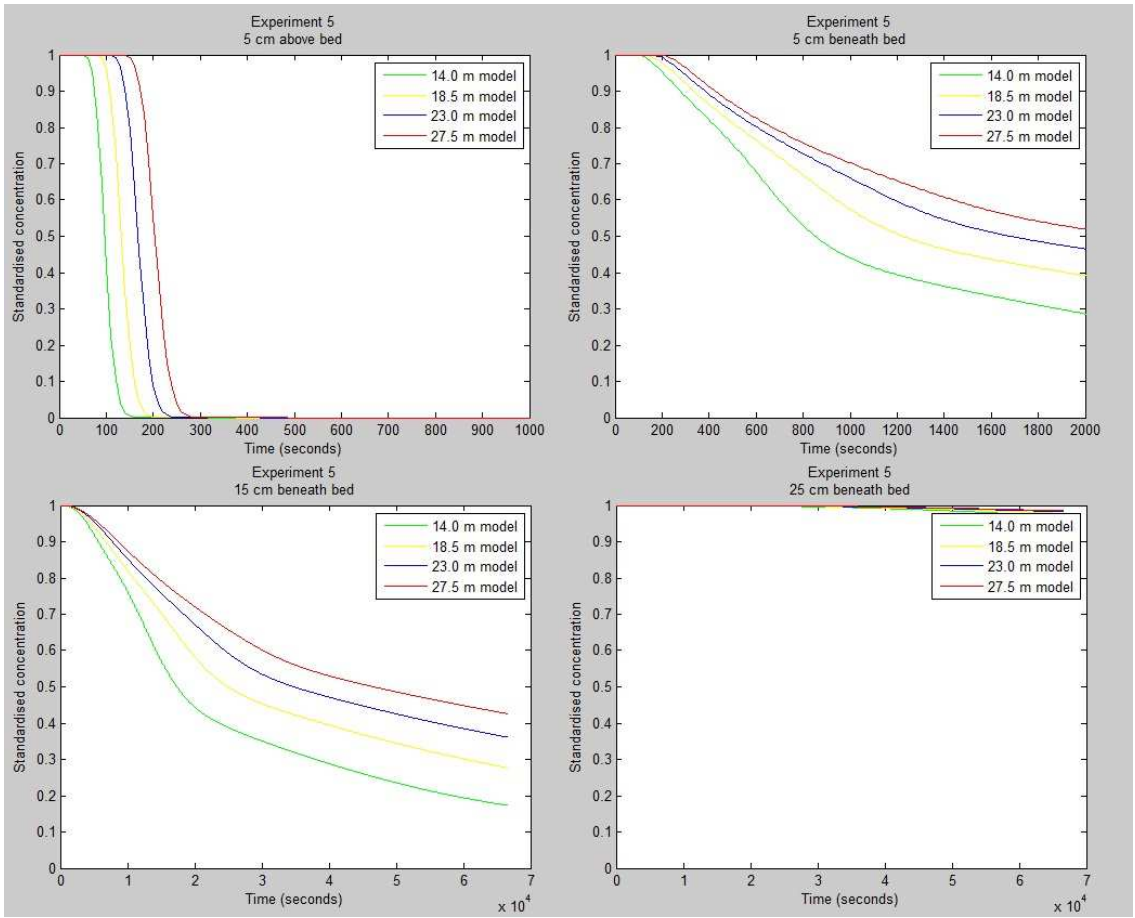

Figure 59, model results of experiment 5, with zeta = 2.0 and beta = 1.5.

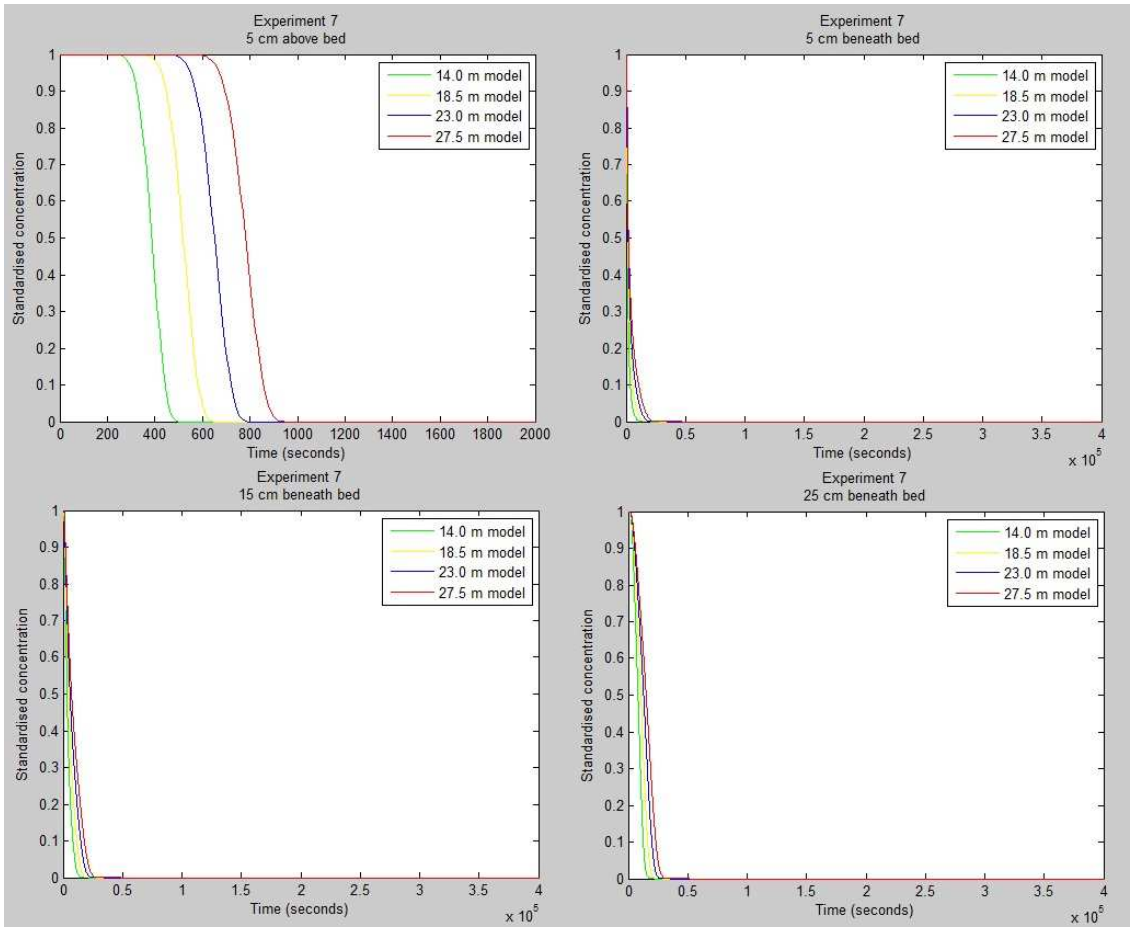

Figure 60, model results of experiment 7, with zeta = 2.0 and beta = 0.5.

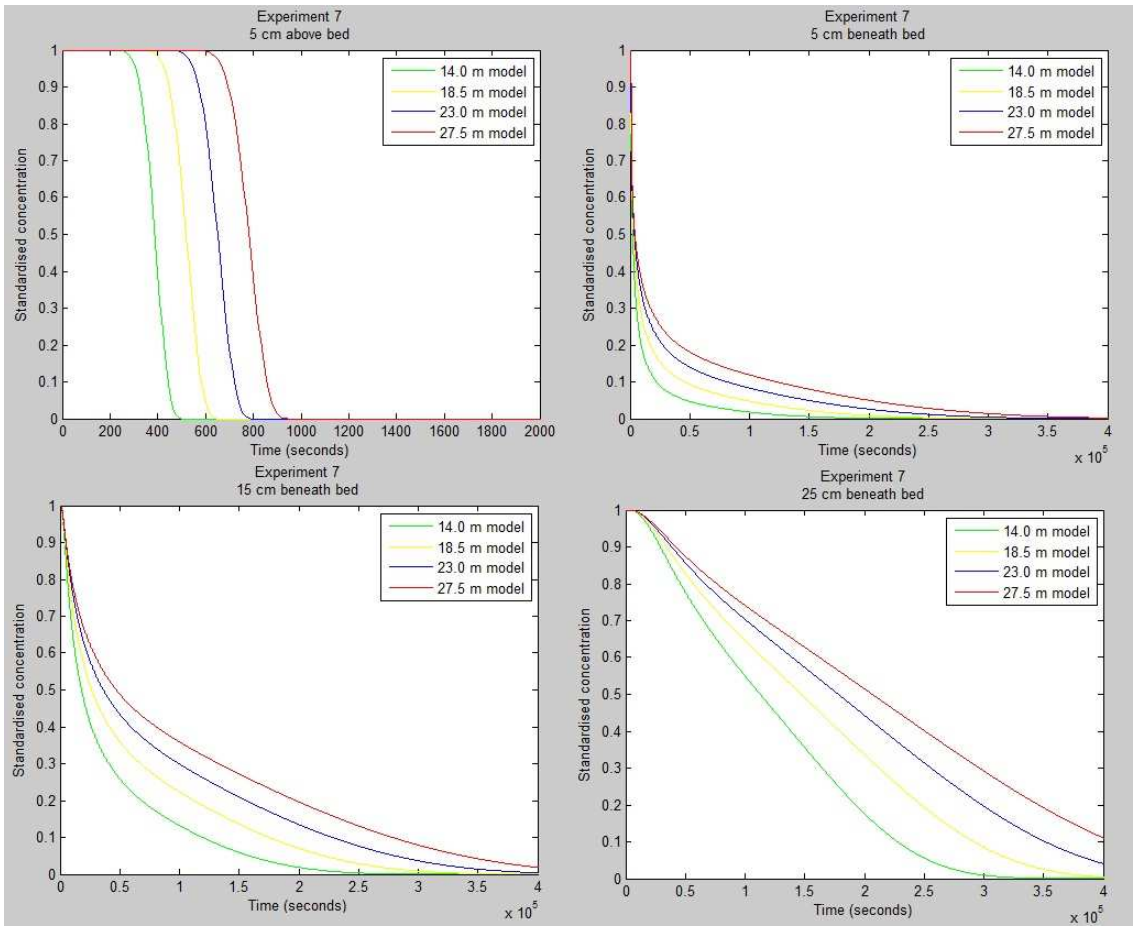

Figure 61, model results of experiment 7, with zeta = 2.0 and beta = 1.0.

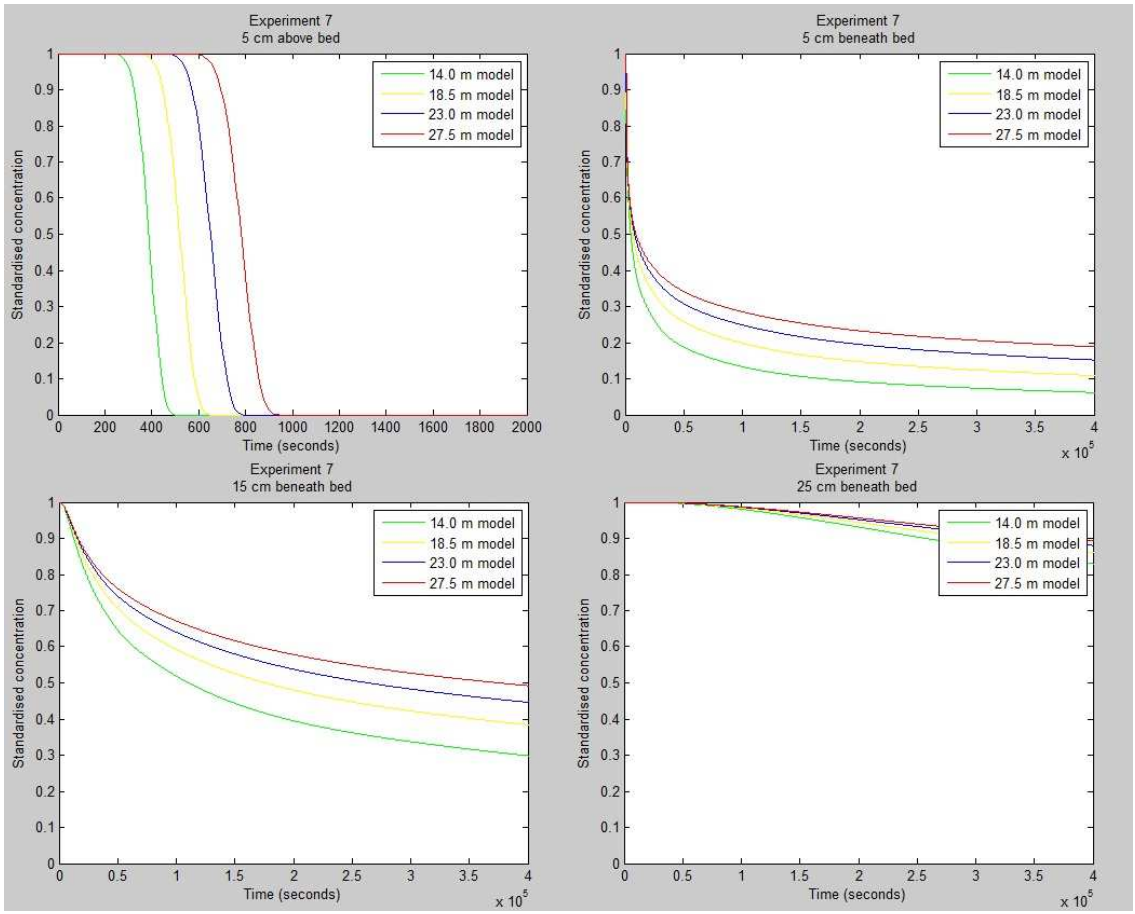

Figure 62, model results of experiment 7, with zeta = 2.0 and beta = 1.5.

Appendix 3 : Experiment 7 as example of model script

```
% Script voor het inlezen van alle ruwe data
% Alle ruwe data is 39 breed [Als T(x,y) dan is y 39)
% T(x,1) = de verstreken tijd in seconden (elke 10 seconden 1 meting)
% T(x,2) = de datum
% T(x,3) = de tijd in seconden
% T(x,4) T(x,13) T(x,22) T(x,31) = nummering van Black Boxes 1 tot 4
% T(x,5) T(x,14) T(x,23) T(x,32) = EC node 1
% T(x,6) T(x,15) T(x,24) T(x,33) = Temp node 1
% T(x,7) T(x,16) T(x,25) T(x,34) = EC node 2
% T(x,8) T(x,17) T(x,26) T(x,35) = Temp node 2
% T(x,9) T(x,18) T(x,27) T(x,36) = EC node 3
% T(x,10) T(x,19) T(x,28) T(x,37) = Temp node 3
% T(x,11) T(x,20) T(x,29) T(x,38) = EC node 4
% T(x,12) T(x,21) T(x,30) T(x,39) = Temp node 4
%
clear all
clc
%
%
% Input variabelen
%
beta = 1.13;
zeta = 1.8;
phi = 0.5625;
arno = 1.0; % vermenigvuldiging met avg flow velo
gamma = 1.0; % standaard is 1.0 maar +-50% mogelijk, dus gamma range = 0.5-
1.5
timestep = 1.0; % timestep van berekening (10/timestep moet een heel getal
zijn!! (10/1 = goed || 10/5 = goed || 10/3 = fout))
ctmt = 10/timestep; %conversion to measured timestep van modelwaarden voor
omrekenen naar een reeks gelijkwaardig als de reeks van gemeten waarden
%
%
% importeren ruwe data
%
A = importdata('Exp1En2Op21Tot23Aug.txt');
B = importdata('Exp3En4Op25Tot26Aug.txt');
C = importdata('Exp5En6Op27Tot28Aug.txt');
D = importdata('Exp7En8Op28AugTot4Sept.txt');
%
% Removing 99.9 and 0 from the data (these are unmeasured points)
%
%
% Experiment 7 en 8
%
h = find(D == 99.9);
j = find(D == 0);
D(h) = NaN;
D(j) = NaN;
D(1,1) = 0;
xmaxD = 57371;
Exp7en8 = IndepEC(D, xmaxD);
MaxExp7(1,1) = NaN;
MaxExp7(1,2) = NaN;
MaxExp7(1,3) = NaN;
MaxExp7(1,4) = NaN;
MaxExp7(1,5) = max(Exp7en8(:,5));
```

```
MaxExp7(1,6) = max(Exp7en8(:,6));
MaxExp7(1,7) = max(Exp7en8(:,7));
MaxExp7(1,8) = max(Exp7en8(:,8));
MaxExp7(1,9) = NaN;
MaxExp7(1,10) = max(Exp7en8(:,10));
MaxExp7(1,11) = max(Exp7en8(:,11));
MaxExp7(1,12) = max(Exp7en8(:,12));
MaxExp7(1,13) = max(Exp7en8(:,13));
MaxExp7(1,14) = NaN;
MaxExp7(1,15) = max(Exp7en8(:,15));
MaxExp7(1,16) = max(Exp7en8(:,16));
MaxExp7(1,17) = max(Exp7en8(:,17));
MaxExp7(1,18) = max(Exp7en8(:,18));
MaxExp7(1,19) = NaN;
MaxExp7(1,20) = max(Exp7en8(:,20));
MaxExp7(1,21) = max(Exp7en8(:,21));
MaxExp7(1,22) = max(Exp7en8(:,22));
MaxExp7(1,23) = max(Exp7en8(:,23));
MinExp7(1,1) = NaN;
MinExp7(1,2) = NaN;
MinExp7(1,3) = NaN;
MinExp7(1,4) = NaN;
MinExp7(1,5) = min(Exp7en8(:,5));
MinExp7(1,6) = min(Exp7en8(:,6));
MinExp7(1,7) = min(Exp7en8(:,7));
MinExp7(1,8) = min(Exp7en8(:,8));
MinExp7(1,9) = NaN;
MinExp7(1,10) = min(Exp7en8(:,10));
MinExp7(1,11) = min(Exp7en8(:,11));
MinExp7(1,12) = min(Exp7en8(:,12));
MinExp7(1,13) = min(Exp7en8(:,13));
MinExp7(1,14) = NaN;
MinExp7(1,15) = min(Exp7en8(:,15));
MinExp7(1,16) = min(Exp7en8(:,16));
MinExp7(1,17) = min(Exp7en8(:,17));
MinExp7(1,18) = min(Exp7en8(:,18));
MinExp7(1,19) = NaN;
MinExp7(1,20) = min(Exp7en8(:,20));
MinExp7(1,21) = min(Exp7en8(:,21));
MinExp7(1,22) = min(Exp7en8(:,22));
MinExp7(1,23) = min(Exp7en8(:,23));
%
Exp7en8Standardised = zeros(57371,23);
for n = 1:23;
    Exp7en8Standardised(:,n) = (Exp7en8(:,n)-MinExp7(1,n))/(MaxExp7(1,n)-
MinExp7(1,n));
end
Exp7en8Standardised(:,1) = Exp7en8(:,1);
Exp7en8Standardised(:,2) = Exp7en8(:,2);
Exp7en8Standardised(:,3) = Exp7en8(:,3);
Exp7en8Standardised(:,4) = Exp7en8(:,4);
Exp7en8Standardised(:,9) = Exp7en8(:,9);
Exp7en8Standardised(:,14) = Exp7en8(:,14);
Exp7en8Standardised(:,19) = Exp7en8(:,19);
%
% eperiment 7 modelled
%
flowvelo = arno*0.034393; %average flow velo determined with bucket filling
(might be overestimation, since water depth was purely measured from
sediment till water surface, if this was higher due to the water in the
bed, the average flow velocity would be a bit lower)
```

```
width = 2.005;
gravaccel = 9.81;
waterdepth = 0.14;
gradient = 0.01;
shearvelo = (gravaccel*waterdepth*gradient)^0.5; %(Perk, 2003)
longdispcoeffwaterestimate =
0.011*flowvelo^2.0*width^2.0/(waterdepth*shearvelo); %<---  +-50%!!! The
initial estimate of the longitudinal dispersion Fischer et al. [1979]
%gamma = 1.0; %adjusting factor for changing initial estimate of
longitudinal dispersion coefficient
longdispcoeffwater = gamma*longdispcoeffwaterestimate;
porosity = 0.40324074;
vertdispwater = 0.0;
vertdisp0 = 10^(-zeta)*0.067*0.3*shearvelo*0.5;

% defining grid
xmin=0.0; xmax=30.0; xnum=61;
xstp=(xmax-xmin)/(xnum-1);
ymin=0.0; ymax=0.605; ynum=13;
ystp=(ymax-ymin)/(ynum-1);

vertdispcoeff = zeros(1,7);
for yn = 1:7
    vertdispcoeff(yn) = vertdisp0*(exp(-beta*(7-yn))); %[Zhou and
Mendoza,1993; Habel et al., 2002]
end

sedflowvelo0 = phi*0.034393;

sedflowvelo = zeros(1,7);
for yn = 1:7
    sedflowvelo(yn) = sedflowvelo0*(exp(-beta*(7-yn)));
end

longdispcoeff = zeros(1,7);
for yn = 1:7
    longdispcoeff(yn) = longdispcoeffwater*(exp(-beta*(7-yn)));
end

% Defining Initial Concentration structure
concwatermax=1.0;
concwatermin=0.0;

concwaterT0 = zeros(xnum,ynum);
for xn=1:xnum
    for yn=1:ynum
        concwaterT0(xn,yn)= concwatermax;
    end
end

% Defining number of cycles for a simulation
maxcycle = 57371;
concwaterT1 = zeros(xnum, ynum);
ModelledExp7 = zeros(57371,23);
for k = 1:maxcycle
    for xn = 1:xnum
        for yn = 1:ynum
            % Boundary nodes:
            if (xn==1)
                concwaterT1(xn,yn)=concwatermin;
```

```
            elseif (xn==xnum)
                if yn==1
                    kappaX=longdispcoeff(yn);
                    kappaY=vertdispcoeff(yn);
                    if concwaterT0(xn,yn)==0.0;
                       concwaterT1(xn,yn)=0.0;
                    else

concwaterT1(xn,yn)=concwaterT0(xn,yn)+timestep*kappaX*(concwaterT0(xn-
1,yn)-concwaterT0(xn,yn))/(xstp*xstp); %x contribution

concwaterT1(xn,yn)=concwaterT1(xn,yn)+timestep*kappaY*(-
concwaterT0(xn,yn)+concwaterT0(xn,yn+1))/(ystp*ystp); %y contribution
                        %And now we add the advection in time with a
standard Finite Difference scheme:
                        if
0.5*sedflowvelo(yn)*timestep/xstp*(concwaterT0(xn,yn)-concwaterT0(xn-
1,yn))>=concwaterT1(xn,yn);
                            concwaterT1(xn,yn)=0.0;
                        else
                            concwaterT1(xn,yn)=concwaterT1(xn,yn)-
0.5*sedflowvelo(yn)*timestep/xstp*(concwaterT0(xn,yn)-concwaterT0(xn-
1,yn));
                        end
                    end
                elseif (yn==ynum)
                    kappaX=longdispcoeffwater;
                    kappaY=vertdispwater;
                    if concwaterT0(xn,yn)==0.0;
                        concwaterT1(xn,yn)=0.0;
                    else

concwaterT1(xn,yn)=concwaterT0(xn,yn)+timestep*kappaX*(concwaterT0(xn-
1,yn)-concwaterT0(xn,yn))/(xstp*xstp); %x contribution

concwaterT1(xn,yn)=concwaterT1(xn,yn)+timestep*kappaY*(concwaterT0(xn,yn-
1)-concwaterT0(xn,yn))/(ystp*ystp); %y contribution
                        %And now we add the advection in time with a
standard Finite Difference scheme:
                        if 0.5*flowvelo*timestep/xstp*(concwaterT0(xn,yn)-
concwaterT0(xn-1,yn))>=concwaterT1(xn,yn);
                            concwaterT1(xn,yn)=0.0;
                        else
                            concwaterT1(xn,yn)=concwaterT1(xn,yn)-
0.5*flowvelo*timestep/xstp*(concwaterT0(xn,yn)-concwaterT0(xn-1,yn));
                        end
                    end
                elseif (yn < 8)
                    kappaX=longdispcoeff(yn);
                    kappaY=vertdispcoeff(yn);
                    if concwaterT0(xn,yn)==0.0;
                        concwaterT1(xn,yn)=0.0;
                    else

concwaterT1(xn,yn)=concwaterT0(xn,yn)+timestep*kappaX*(concwaterT0(xn-
1,yn)-concwaterT0(xn,yn))/(xstp*xstp); %x contribution

concwaterT1(xn,yn)=concwaterT1(xn,yn)+timestep*kappaY*(concwaterT0(xn,yn-
1)-2.0*concwaterT0(xn,yn)+concwaterT0(xn,yn+1))/(ystp*ystp); %y
contribution
```

```
                        %And now we add the advection in time with a
standard Finite Difference scheme:
                        if
0.5*sedflowvelo(yn)*timestep/xstp*(concwaterT0(xn,yn)-concwaterT0(xn-
1,yn))>=concwaterT1(xn,yn);
                            concwaterT1(xn,yn)=0.0;
                        else
                            concwaterT1(xn,yn)=concwaterT1(xn,yn)-
0.5*sedflowvelo(yn)*timestep/xstp*(concwaterT0(xn,yn)-concwaterT0(xn-
1,yn));
                        end
                    end
                else
                    kappaX=longdispcoeffwater;
                    kappaY=vertdispwater;
                    if concwaterT0(xn,yn)==0.0;
                            concwaterT1(xn,yn)=0.0;
                    else

concwaterT1(xn,yn)=concwaterT0(xn,yn)+timestep*kappaX*(concwaterT0(xn-
1,yn)-concwaterT0(xn,yn))/(xstp*xstp); %x contribution

concwaterT1(xn,yn)=concwaterT1(xn,yn)+timestep*kappaY*(concwaterT0(xn,yn-
1)-2.0*concwaterT0(xn,yn)+concwaterT0(xn,yn+1))/(ystp*ystp); %y
contribution
                        %And now we add the advection in time with a
standard Finite Difference scheme:
                        if 0.5*flowvelo*timestep/xstp*(concwaterT0(xn,yn)-
concwaterT0(xn-1,yn))>=concwaterT1(xn,yn);
                            concwaterT1(xn,yn)=0.0;
                        else
                            concwaterT1(xn,yn)=concwaterT1(xn,yn)-
0.5*flowvelo*timestep/xstp*(concwaterT0(xn,yn)-concwaterT0(xn-1,yn));
                        end
                    end
                end
            elseif (yn==1)
                kappaX=longdispcoeff(yn);
                kappaY=vertdispcoeff(yn);
                if concwaterT0(xn,yn)==0.0;
                    concwaterT1(xn,yn)=0.0;
                else

concwaterT1(xn,yn)=concwaterT0(xn,yn)+timestep*kappaX*(concwaterT0(xn-
1,yn)-2.0*concwaterT0(xn,yn)+concwaterT0(xn+1,yn))/(xstp*xstp); %x
contribution

concwaterT1(xn,yn)=concwaterT1(xn,yn)+timestep*kappaY*(-
concwaterT0(xn,yn)+concwaterT0(xn,yn+1))/(ystp*ystp); %y contribution
                    %And now we add the advection in time with a standard
Finite Difference scheme:
                    if
0.5*sedflowvelo(yn)*timestep/xstp*(concwaterT0(xn,yn)-concwaterT0(xn-
1,yn))-0.5*sedflowvelo(yn)*timestep/xstp*(concwaterT0(xn+1,yn)-
concwaterT0(xn,yn))>=concwaterT1(xn,yn);
                        concwaterT1(xn,yn)=0.0;
                    else
                        concwaterT1(xn,yn)=concwaterT1(xn,yn)-
0.5*sedflowvelo(yn)*timestep/xstp*(concwaterT0(xn,yn)-concwaterT0(xn-
1,yn))-0.5*sedflowvelo(yn)*timestep/xstp*(concwaterT0(xn+1,yn)-
concwaterT0(xn,yn));
```

```
                end
            end
        elseif (yn==ynum)
            kappaX=longdispcoeffwater;
            kappaY=vertdispwater;
            if concwaterT0(xn,yn)==0.0;
                concwaterT1(xn,yn)=0.0;
            else

concwaterT1(xn,yn)=concwaterT0(xn,yn)+timestep*kappaX*(concwaterT0(xn-
1,yn)-2.0*concwaterT0(xn,yn)+concwaterT0(xn+1,yn))/(xstp*xstp); %x
contribution

concwaterT1(xn,yn)=concwaterT1(xn,yn)+timestep*kappaY*(concwaterT0(xn,yn-
1)-concwaterT0(xn,yn))/(ystp*ystp); %y contribution
                %And now we add the advection in time with a standard
Finite Difference scheme:
                if 0.5*flowvelo*timestep/xstp*(concwaterT0(xn,yn)-
concwaterT0(xn-1,yn))-0.5*flowvelo*timestep/xstp*(concwaterT0(xn+1,yn)-
concwaterT0(xn,yn))>=concwaterT1(xn,yn);
                    concwaterT1(xn,yn)=0.0;
                else
                    concwaterT1(xn,yn)=concwaterT1(xn,yn)-
0.5*flowvelo*timestep/xstp*(concwaterT0(xn,yn)-concwaterT0(xn-1,yn))-
0.5*flowvelo*timestep/xstp*(concwaterT0(xn+1,yn)-concwaterT0(xn,yn));
                end
            end
        elseif (yn < 8)
            kappaX=longdispcoeff(yn);
            kappaY=vertdispcoeff(yn);
            if concwaterT0(xn,yn)==0.0;
                concwaterT1(xn,yn)=0.0;
            else

concwaterT1(xn,yn)=concwaterT0(xn,yn)+timestep*kappaX*(concwaterT0(xn-
1,yn)-2.0*concwaterT0(xn,yn)+concwaterT0(xn+1,yn))/(xstp*xstp); %x
contribution

concwaterT1(xn,yn)=concwaterT1(xn,yn)+timestep*kappaY*(concwaterT0(xn,yn-
1)-2.0*concwaterT0(xn,yn)+concwaterT0(xn,yn+1))/(ystp*ystp); %y
contribution
                %And now we add the advection in time with a standard
Finite Difference scheme:
                if
0.5*sedflowvelo(yn)*timestep/xstp*(concwaterT0(xn,yn)-concwaterT0(xn-
1,yn))-0.5*sedflowvelo(yn)*timestep/xstp*(concwaterT0(xn+1,yn)-
concwaterT0(xn,yn))>=concwaterT1(xn,yn);
                    concwaterT1(xn,yn)=0.0;
                else
                    concwaterT1(xn,yn)=concwaterT1(xn,yn)-
0.5*sedflowvelo(yn)*timestep/xstp*(concwaterT0(xn,yn)-concwaterT0(xn-
1,yn))-0.5*sedflowvelo(yn)*timestep/xstp*(concwaterT0(xn+1,yn)-
concwaterT0(xn,yn));
                end
            end
        else
            kappaX=longdispcoeffwater;
            kappaY=vertdispwater;
            if concwaterT0(xn,yn)==0.0;
                    concwaterT1(xn,yn)=0.0;
            else
```

```
concwaterT1(xn,yn)=concwaterT0(xn,yn)+timestep*kappaX*(concwaterT0(xn-
1,yn)-2.0*concwaterT0(xn,yn)+concwaterT0(xn+1,yn))/(xstp*xstp); %x
contribution

concwaterT1(xn,yn)=concwaterT1(xn,yn)+timestep*kappaY*(concwaterT0(xn,yn-
1)-2.0*concwaterT0(xn,yn)+concwaterT0(xn,yn+1))/(ystp*ystp); %y
contribution
                    %And now we add the advection in time with a standard
Finite Difference scheme:
                    if 0.5*flowvelo*timestep/xstp*(concwaterT0(xn,yn)-
concwaterT0(xn-1,yn))-0.5*flowvelo*timestep/xstp*(concwaterT0(xn+1,yn)-
concwaterT0(xn,yn))>=concwaterT1(xn,yn);
                        concwaterT1(xn,yn)=0.0;
                    else
                        concwaterT1(xn,yn)=concwaterT1(xn,yn)-
0.5*flowvelo*timestep/xstp*(concwaterT0(xn,yn)-concwaterT0(xn-1,yn))-
0.5*flowvelo*timestep/xstp*(concwaterT0(xn+1,yn)-concwaterT0(xn,yn));
                    end
                end
            end
            concflum = concwaterT1;
        end
    end
    concwaterT0=concwaterT1;% Reloading solutions to concwaterT0
    if k == start
        ModelledExp7(k/ctmt,1) = Exp7en8(k/ctmt,1);
        ModelledExp7(k/ctmt,2) = Exp7en8(k/ctmt,2);
        ModelledExp7(k/ctmt,3) = Exp7en8(k/ctmt,3);
        ModelledExp7(k/ctmt,4) = Exp7en8(k/ctmt,4);
        ModelledExp7(k/ctmt,5) = concflum(55,8);
        ModelledExp7(k/ctmt,6) = concflum(55,6);
        ModelledExp7(k/ctmt,7) = concflum(55,4);
        ModelledExp7(k/ctmt,8) = concflum(55,2);
        ModelledExp7(k/ctmt,9) = Exp7en8(k/ctmt,9);
        ModelledExp7(k/ctmt,10) = concflum(28,8);
        ModelledExp7(k/ctmt,11) = concflum(28,6);
        ModelledExp7(k/ctmt,12) = concflum(28,4);
        ModelledExp7(k/ctmt,13) = concflum(28,2);
        ModelledExp7(k/ctmt,14) = Exp7en8(k/ctmt,14);
        ModelledExp7(k/ctmt,15) = concflum(46,8);
        ModelledExp7(k/ctmt,16) = concflum(46,6);
        ModelledExp7(k/ctmt,17) = concflum(46,4);
        ModelledExp7(k/ctmt,18) = concflum(46,2);
        ModelledExp7(k/ctmt,19) = Exp7en8(k/ctmt,19);
        ModelledExp7(k/ctmt,20) = concflum(37,8);
        ModelledExp7(k/ctmt,21) = concflum(37,6);
        ModelledExp7(k/ctmt,22) = concflum(37,4);
        ModelledExp7(k/ctmt,23) = concflum(37,2);
        start = start+ctmt;
    end
end
%
%
% Least squares fit
%
LsfExp7 = (ModelledExp7-Exp7en8Standardised).^2.0;
%
% NaN verwijderen zodat som geen NaN wordt
%
z = isnan(LsfExp7);
```

```
LsfExp7(z) = 0.0;
%
% Som van fout
%
LsfSumExp7 = sum(LsfExp7);
%
% Plotting Figures
%
%
% Experiment 7
%
figure
plot(Exp7en8Standardised(:,1),Exp7en8Standardised(:,10), 'g')
hold on
plot(Exp7en8Standardised(:,1),Exp7en8Standardised(:,20), 'y')
hold on
plot(Exp7en8Standardised(:,1),Exp7en8Standardised(:,15), 'b')
hold on
plot(Exp7en8Standardised(:,1),Exp7en8Standardised(:,5), 'r')
hold on
plot(ModelledExp7(:,1),ModelledExp7(:,10), 'g')
hold on
plot(ModelledExp7(:,1),ModelledExp7(:,20), 'y')
hold on
plot(ModelledExp7(:,1),ModelledExp7(:,15), 'b')
hold on
plot(ModelledExp7(:,1),ModelledExp7(:,5), 'r')
title({'Experiment 7' ; '5 cm above bed'})
xlabel('Time (seconds)')
ylabel('Standardised concentration')
axis([0 0.02*10^5 0 1])
legend('14.0 m','18.5 m','23.0 m','27.5 m')
figure
plot(Exp7en8Standardised(:,1),Exp7en8Standardised(:,11), 'g')
hold on
plot(Exp7en8Standardised(:,1),Exp7en8Standardised(:,21), 'y')
hold on
plot(Exp7en8Standardised(:,1),Exp7en8Standardised(:,16), 'b')
hold on
plot(Exp7en8Standardised(:,1),Exp7en8Standardised(:,6), 'r')
hold on
plot(ModelledExp7(:,1),ModelledExp7(:,11), 'g')
hold on
plot(ModelledExp7(:,1),ModelledExp7(:,21), 'y')
hold on
plot(ModelledExp7(:,1),ModelledExp7(:,16), 'b')
hold on
plot(ModelledExp7(:,1),ModelledExp7(:,6), 'r')
title({'Experiment 7' ; '5 cm beneath bed'})
xlabel('Time (seconds)')
ylabel('Standardised concentration')
axis([0 4.0*10^5 0 1])
legend('14.0 m','18.5 m','23.0 m','27.5 m')
figure
plot(Exp7en8Standardised(:,1),Exp7en8Standardised(:,12), 'g')
hold on
plot(Exp7en8Standardised(:,1),Exp7en8Standardised(:,22), 'y')
hold on
plot(Exp7en8Standardised(:,1),Exp7en8Standardised(:,17), 'b')
hold on
plot(Exp7en8Standardised(:,1),Exp7en8Standardised(:,7), 'r')
```

```
hold on
plot(ModelledExp7(:,1),ModelledExp7(:,12), 'g')
hold on
plot(ModelledExp7(:,1),ModelledExp7(:,22), 'y')
hold on
plot(ModelledExp7(:,1),ModelledExp7(:,17), 'b')
hold on
plot(ModelledExp7(:,1),ModelledExp7(:,7), 'r')
title({'Experiment 7' ; '15 cm beneath bed'})
xlabel('Time (seconds)')
ylabel('Standardised concentration')
axis([0 4.0*10^5 0 1])
legend('14.0 m','18.5 m','23.0 m','27.5 m')
figure
plot(Exp7en8Standardised(:,1),Exp7en8Standardised(:,13), 'g')
hold on
plot(Exp7en8Standardised(:,1),Exp7en8Standardised(:,23), 'y')
hold on
plot(Exp7en8Standardised(:,1),Exp7en8Standardised(:,18), 'b')
hold on
plot(Exp7en8Standardised(:,1),Exp7en8Standardised(:,8), 'r')
hold on
plot(ModelledExp7(:,1),ModelledExp7(:,13), 'g')
hold on
plot(ModelledExp7(:,1),ModelledExp7(:,23), 'y')
hold on
plot(ModelledExp7(:,1),ModelledExp7(:,18), 'b')
hold on
plot(ModelledExp7(:,1),ModelledExp7(:,8), 'r')
title({'Experiment 7' ; '25 cm beneath bed'})
xlabel('Time (seconds)')
ylabel('Standardised concentration')
axis([0 4.0*10^5 0 1])
legend('14.0 m','18.5 m','23.0 m','27.5 m')
```